UCSF

UC San Francisco Electronic Theses and Dissertations

Title
Parasites Reprogram the Intestinal Crypt

Permalink
https://escholarship.org/uc/item/11x6v3rx

Author
Nusse, Ysbrand M

Publication Date
2018

Supplemental Material
https://escholarship.org/uc/item/11x6v3rx#supplemental

Peer reviewed|Thesis/dissertation

Parasites Reprogram the Intestinal Crypt

by

Ysbrand Michael Nusse

DISSERTATION

Submitted in partial satisfaction of the requirements for the degree of

DOCTOR OF PHILOSOPHY

in

Biomedical Sciences

in the

GRADUATE DIVISION

of the

UNIVERSITY OF CALIFORNIA, SAN FRANCISCO

Dedication and Acknowledgements

I'm very lucky to have many important people to thank for their support during my PhD. I have had many excellent mentors in and out of the lab, and any success that I've had is directly attributable to them. I've also had invaluable support from my friends and family – I couldn't have gotten through the past years without you.

First, I would like to thank my graduate advisor, Ophir Klein. Ophir is one of the kindest people I've met, and I'm very grateful for his unwavering support and enthusiasm for my project. Ophir has always been a great advocate for me, especially as I struggled in and out of the lab. Thank you for encouraging me, Ophir. Despite all my doubts, your perspective and cheer were very important in my decisions about my future. You're a great role model of kindness and support, and I hope I can do the same one day.

I also thank the members of my thesis committee: Richard Locksley, Averil Ma, and Todd Nystul. I always enjoyed our meetings and looked forward to discussing science and my career plans with all of you. Thank you very much for your reassurance and advice.

I'd especially thank Rich for welcoming me in to his lab as part of our ongoing collaboration during this project. I always enjoyed coming down to your lab – it's a great group of people. I learned a lot from your and your lab. Collaboration is my favorite part of science, and I'm so glad I got to work with you. Thank you so much for supporting our weird project.

A special thanks goes to Adam Savage, my collaborator in Rich's lab throughout this project. Adam and I spent most of the past five years working side by side. Adam, I'm proud of what we did, but more so how we did it. I learned more from you than anyone else during my

time here, especially how to be careful, diligent, and calm. You're a fantastic scientist and an invaluable mentor and collaborator. Working with you was the best part of my PhD.

Several other people directly contributed to our project. Pauline Marangoni was instrumental in analyzing the incredibly complex single cell RNAseq data. Pauline, I'm sure we made those months of your life very difficult, but you saved us. Thank you. Axel and Ty completed internships with me and helped conduct experiments. I've had great mentors, and I've always wanted to pay it forward and mentor younger students as well. I hope you two had a good time in the lab. Working with you made me realize just how fortunate I was to have the teachers I had. It's really hard to do a good job mentoring while also doing your own work. I learned a lot from you. Thanks for all your hard work, and best of luck in the future.

I'd also like to thank Fred de Sauvage for his contributions to the project, but also for the ongoing collaboration between his and Ophir's labs. It's an impressive place with great people doing really good work. I always really enjoyed visiting his group at Genentech. I hope we will stay in touch.

Beyond the people who directly worked on the project, I'd like to thank members of the Klein and Locksley laboratories. In the Klein lab, many people over the years have worked alongside me and contributed advice and company. Thank you in particular to Adriane Joo, Amnon Sharir, Andrew Jheon, Brad Youngblood, David Castillo-Asofeifa, Haim Belinson, Jimmy Hu, Julia Farache, Kara McKinley, Kerstin Seidel, Kyle Jones, Laura Weichselbaum, Roy Nattiv, Saunders Ching, and Tomas Wald for your feedback, advice, and company. Thank you as well to the many other lab members who made the Klein Lab a nice place to spend my PhD. I'd also like to acknowledge the tireless work of the technical staff in the Klein lab that greatly facilitate our ability to focus on our projects. Thank you to Nick Wang, Rebecca D'Urso,

Sarah Alto, and Asoka Rathnayake. I, and everyone else in the lab, really appreciate what you do for us.

I also thank the members of the Locksley lab who welcomed me into your space and were always so friendly. It was a pleasure to get to know all of you. You're an impressive group of scientists, I learned a lot from you.

The administrative staff of the BMS program was great. Thank you for helping all the BMS cohorts and me during our graduate school experiences. Everyone in the BMS program is very grateful for your work.

I was lucky to work in a few labs at Stanford before I came to UCSF, and the mentorship and training I received there really helped me start working independently right at the start of my thesis. A big thanks goes to Mike Clarke, who offered me a "technician" job after college. I say "technician" because I was really a student who did no true technical work. Mike was extremely generous to let me work with Mike Rothenberg, a postdoc in his lab, rather than just generally support the lab, which is what a real technician does. I didn't realize it at the time, but this was incredibly kind. Thank you, Mike. The training I got in your lab was so important in my PhD. I learned how to ask a good question, and how to try to answer it with an appropriate amount of skepticism, which is a core part of science. I also had a great time, which made me enthusiastic about going to graduate school.

Mike Rothenberg, who I worked with in the Clarke lab, was, and still is, an invaluable mentor. Mike taught me so much in two years, and was unfailingly enthusiastic, friendly, and patient. I've learned that it takes a lot of time to train someone, and Mike was so generous to let me work on his project. Mike, thank you so much for your mentoring and friendship. I attribute a

lot of my success to your teaching. You're a great role model and scientist, and it's always so great to see you. Thank you.

Before coming to the Clarke lab, Jill Helms, Philipp Leucht, and Pat Brown gave me early experiences in the lab. They were a lot of fun, and I learned a lot. You all were very kind to have me in your labs, and spend time training me. Thank you.

Many people were equally important outside of the lab. I had a lot of fun in graduate school. I'd like to thank the new friends I made while living in San Francisco, and my many old friends. I'd especially like to thank the people who became mentors for me in rock climbing. You opened up a world that has become very important to me. Thank you to Simon Moore, Stephen Nayfach, Robert Schiemann, and Dylan Stewart, as well as my other climbing partners through the years. Climbing kept me sane throughout graduate school – thank you all.

Lastly, I'd like to thank my family – my wife Jessica, my brothers Jamie and Ben, and my parents Betsy and Roel. This is just my thesis, and what you've contributed to my life far exceeds what I can write here. I will just thank my Dad in particular. It's funny that we've ended up working on similar things, and with similar interests. It's hard to say why that is, but it doesn't matter. Thank you for sharing with me, it's been very meaningful to me to learn from you and about you through science.

Contributions

This thesis includes previously published material. I wrote Chapters 1 and 4 independently.

Chapter 2 is adapted from a brief literature review that was published in *Cell Stem Cell* in 2013, with the citation: Nusse, Y. M. & Klein, O. D. If a stem cell dies in the crypt, and no one is around to see it... *Cell Stem Cell* **12,** 389–390 (2013).

Ophir Klein is a co-author on this review and jointly wrote the manuscript with me.

Chapter 3 is adapted from a manuscript that was published in *Nature* in 2018, with citation: Nusse, Y.M., Savage, A.K., Marangoni, P., Rosendahl-Huber, A.K.M., Landman, T.A., de Sauvage, F.J., Locksley, R.M., and Klein, O.D. Parasitic helminths induce fetal-like reversion in the intestinal stem cell niche. *Nature* **559,** 109–113 (2018)

The co-authors for this study are Adam K. Savage, Pauline Marangoni, Axel K. M. Rosendahl-Huber, Tyler A. Landman, Frederic J. de Sauvage, Richard M. Locksley, and Ophir D. Klein.

Adam Savage and I have equal contribution towards this study. Adam and I jointly conceived, designed, performed and interpreted histology, cytometry, transcriptomic, and culture experiments.

Pauline Marangoni performed computational analysis of the single-cell transcriptomic experiment. Axel Rosendahl-Huber and Tyler Landman assisted the study by performing and interpreting histological experiments. Frederic de Sauvage contributed essential mouse reagents. Ophir Klein and Richard Locksley oversaw the study.

Adam Savage, Richard Locksley, Ophir Klein, and I jointly wrote the manuscript that Chapter 3 is based on.

Science is an increasingly collaborative and multi-disciplinary endeavor, and is especially exemplified in this joint project between a developmental biology and immunology lab. As such, this work fulfills all standards and requirements for a PhD thesis.

Competing interest statement

Fred J. de Sauvage is an employee of Genentech and owns shares in Roche. No author authors declare any conflict of interest.

List of Acronyms Used

BMP – Bone morphogenetic protein

CBC – Crypt Base Columnar Cell

cDNA - complementary DNA

DAMP – Damage associated molecular pattern

DNA – Deoxyribonucleic acid

DT – Diphtheria Toxin

EdU - 5-ethynyl-2'-deoxyuridine

EGF – Epidermal growth factor

FACS – Fluorescence-activated cell sorting

GC – Granuloma crypt

GVHD – Graft-versus-host disease

Hp – Heligmosomoides polygyrus

HSC – Hematopoietic stem cell

IBD – Inflammatory bowel disease

IFN - Interferon

IGF – Insulin-like growth factor

iNKT - Invariant natural killer T

ISC – Intestinal stem cell

Nb - Nippostrongylus brasiliensis

NICD – Notch intracellular domain

PCR – Polymerase chain reaction

qPCR - Quantitative polymerase chain reaction

RNA – Ribonucleic acid

RNAseq - RNA sequencing

TA – Transit amplifying

TAZ - Transcriptional coactivator with PDZ-binding motif

TCR – T-cell receptor

TNF – Tumor-necrosis factor

YAP – Yes-associated protein

Abstract

Parasites Reprogram the Intestinal Crypt

Ysbrand Nusse

Damage to mammalian organs elicits an inflammatory response and is repaired by tissue remodeling and cell proliferation. Healing therefore requires a complex interplay between immune cells and tissue resident progenitor cells. In the intestine, the epithelial surface must be repaired after breaches to the barrier caused by injury or infection. However, how intestinal stem and progenitor cells sense and respond to damage is relatively unknown. Here, we examined how epithelial crypt progenitors respond to damage driven by the natural parasite, *Heligmosomoides polygyrus* (Hp). Damage to the epithelial barrier by Hp larvae induced an inflammatory granulomatous reaction and a local regenerative response in epithelial crypt progenitors. Paradoxically, markers of homeostatic intestinal stem cells, including *Lgr5*, were absent in granuloma-associated crypts. Concurrently, immune cells responding to Hp infection drove the expression of Sca-1 on regenerative epithelium through IFNγ cytokines. Several other non-infectious models of intestinal damage induced similar responses in the crypt, suggesting that Hp elicited a conserved response to injury. In Hp infections, regenerative Sca-1$^+$ cells formed undifferentiated fetal-like spheroids in *in vitro* culture, which were distinct from adult organoids stemming from unaffected crypts from the same mice. Furthermore, regenerative crypts adapted a transcriptional signature resembling the developing fetal intestine, and a subset of Sca-1$^+$ cells were undifferentiated and enriched for fetal markers. Together, our functional and transcriptional analysis suggested that regenerative Sca-1$^+$ crypt cells were developmentally reprogrammed to a fetal-like state. We speculate that fetal reprogramming is a critical mechanism for maintaining

intestinal integrity after injury. By recapitulating aspects of fetal development, the intestinal epithelium may unlock proliferative capacity silenced during homeostasis.

Table of Contents

List of Tables

List of Figures

Chapter 4

Chapter 1: Introduction and Background

1.1 Injuries involve progenitors and immunity

Biological organisms must dynamically respond to changing environments and perturbations to maintain homeostasis. Throughout the lifespan of an organism, tissues cope with insults and new systemic needs that require a switch from a homeostatic maintenance program to a new program responsive to novel tissue demands.

One particularly striking example of the need for a dynamic tissue response is injury. Damage is repaired through production of new tissue, such as the growth of new skin after a traumatic wound[1,2]. In order to repair tissue damage, complex processes involving multiple cell types must be coordinated. First, the presence of damage must be sensed[3]. After detection, a response must be mounted which instructs the tissue to change from a homeostatic program to a tissue repair program. Once completed, this repair program must be switched off to return to a homeostatic state[4]. This process necessitates the interaction of multiple cellular compartments within the tissue, coordinating a complex response across diverse cell types. The cells involved in this process must include cells responsible for sensing and initiating repair processes, as well as the cells responsible for generating new cells within that tissue. In this study, I explored how this is accomplished in the intestine, in collaboration with other members of the Klein and Locksley laboratories at UCSF. We probed how the immune system and tissue resident progenitor cells cooperate during injury repair by making use of a natural model of intestinal injury, parasitic infection.

1.2 Stem cells

Many tissues in mammals are maintained by cellular turnover, particularly epithelial barrier surfaces exposed to the outside world, such as the skin[5]. Dead or damaged cells are replaced by new cells, which are the result of cell division. In many tissues though, the grand majority of cells are not capable of dividing. Rather, cell division is restricted to a small subset of tissue resident progenitor cells. Progenitor cells divide and produce new cells, which differentiate into the adult cells that make up the bulk of the tissue. However, most proliferative cells only go through a limited number of cell divisions before terminally differentiating. In contrast, a rare subgroup of cells has long-term growth potential. These cells are dubbed "stem cells" and are distinguished from other progenitors by their functional capabilities to differentiate and self-renew[6]. The capacity to differentiate indicates that stem cells are capable of producing clones (a group of cells arising from the same cell) that contribute to adult cell types within that tissue. Self-renewal is the cellular ability to undergo seemingly limitless numbers of cell divisions while maintaining the original growth capacity of the cell. Self-renewal is thought to be restricted only to stem cells, in contrast to other proliferative progenitors. Non-self-renewing progenitors, sometimes referred to as Transit Amplifying (TA) cells, go through a limited number of cell divisions before differentiating. TA cells are often the immediate daughter cells of stem cells and expand the clonal output of the stem cell (**Fig. 1.1**).

Several mammalian tissues are maintained by stem cells, notably the blood, skin, and intestine. The intestine is a particularly apt tissue for studying stem cell biology, as the epithelial lining of the intestinal tract is replaced every few days. Furthermore, the architecture and spatial restriction of the progenitor zone has made intestinal stem cells (ISCs) easily identifiable, and in

recent years much has been learned about where these cells are located, their function, and how they are controlled.

1.3 Tools for tracking stem cells

Stem cells are defined by their two central functions, differentiation and self-renewal. As such, to prove that a candidate cell is a stem cell, one must use experimental techniques to show that the cell is capable of differentiation and self-renewal through analysis of cell clones arising from that population. Several key techniques are used in the field of stem cell biology to define stem cells.

1.3.1 Label retention

Label retention is a method that was used in attempts to locate tissue resident stem cells for many years before more advanced functional techniques were developed[7,8]. This method arose from the theory that stem cells are quiescent, or non-dividing, a notion based on early characterization of hematopoietic stem cells[9,10]. Label-retention utilizes various methods to mark cells in a non-heritable way, followed by a chase period to identify slowly dividing cells. It is important that the label is not refreshed by daughter cells, such that the marker is diluted out over cell divisions. Quickly dividing cells rapidly lose the label, while slowly dividing cells retain the marker. Label retaining cells, which divide less rapidly than other progenitors, such as TA cells, were therefore proposed to be stem cells based on their relative quiescence compared to their highly proliferative cousins.

Several methods to label cells exist, such as loading cells with tagged DNA nucleosides integrated into newly synthesized DNA during S-phase, or the controllable expression of fluorescently labeled histones. While these techniques do effectively identify infrequently

dividing cells, they can be misleading when used to define stem cells. Quiescence is not a strict property of many stem cell populations, some of which divide relatively rapidly compared to hematopoietic stem cells[11,12]. Furthermore, infrequently dividing cells are not necessarily stem cells. Some populations of cells that are definitively not stem cells divide infrequently, such as tissue resident macrophages. Lastly, label retention provides little to no information about the functional capacity of the labeled cell. It is impossible to use label retention to prove that a cell can self-renew, a key feature of tissue stem cells. While label retention can identify a candidate cell population for further experimentation, or characterize the proliferation kinetics of progenitor cells, it cannot be used in isolation to prove stemness.

1.3.2 Colony formation

A functional test of cellular growth capacity is assaying the ability of an isolated cell to form long-lived clonal colonies *in vitro*. As stem cells can self-renew, they should be able to sustain proliferation *in vitro* indefinitely in optimal growth conditions. Combined with fluorescence activated cell sorting (FACS) to isolate specific cell populations of interest, *in vitro* culture systems enable the assessment of long term growth capacity of cells. These techniques have been used in the nervous system to show that rare populations of neural cells were capable of producing clonal colonies of proliferative cells[13]. When plated in differentiation conditions, these colonies were able to form both neurons and glial cells, suggesting the colony-forming cell was multipotent. Stem cell-derived cultures have been established from many different tissues, including the hematopoietic system, epidermis, intestine, and others[14–16]. While culture conditions vary for stem cells from different tissues, they often rely on supplementation with growth factors that are critical for stem cell maintenance and growth *in vivo*. As such, the

experimental process in the development of these systems has led to the discovery of critical regulators of stem cell growth *in vivo*, including components of the stem cell niche, as detailed below in **Section 1.6**

An important caveat of *in vitro* colony formation is that the experiments are inherently non-physiologic. Culture systems provide very high concentrations of growth factors to encourage growth, which do not strictly mimic the *in vivo* environment. *In vitro* studies prove what a cell is *capable* of but do not necessarily reflect their typical behavior *in vivo*. It has sometimes proven difficult to find the *in vivo* correlate of colony forming cells[17]. Nevertheless, *in vitro* systems can be extremely useful in the study of stem cells, as their reductive nature allows precise interrogation of cell behavior and growth.

1.3.3 Transplantation

In vivo transplantation provides a more physiologic assay for stem cell growth than cell culture. Similar to *in vitro* colony formation assays, transplantation assays isolate a target donor population of interest, often by FACS, followed by engraftment into a recipient host[18]. The host tissue must be often be damaged in some way to accept the graft; otherwise the donor cells will usually be outcompeted by the host tissue. These systems have been used extensively in the study of hematopoietic stem cells, where a single transplanted HSC can reconstitute the entire blood system of a lethally irradiated host[19], and in the mammary system, in which mammary stem cells can regenerate the mammary gland in a cleared fat pad[20,21].

However, while they seem more physiologic than *in vitro* assays, transplantation suffers many of the same caveats and shortcomings. In order to successfully engraft stem cells, the donor tissue is often "cleared" first, which clearly alters the host environment such that it is no

longer in a normal state. For example, the bone marrow of a lethally irradiated mouse is clearly not in homeostasis, and thus engraftment may not represent a donor cell's normal growth potential[22,23]. An example of this discrepancy is in mammary stem cell biology, in which mammary stem cells were shown to engraft and give rise to clones that contained both luminal and myoepithelial cells, yet these results were not always recapitulated using lineage tracing[24]. *In vivo* genetic lineage-tracing analysis using different markers suggested that mammary stem cells were uni-potent, only making one cell type in homeostasis[25]. While the discrepancy between these observations may be explained by the particular markers used, it does suggests that the conditions the cells were engrafted in perhaps triggered an expansion of differentiation capacity, or perhaps the very act of isolating the cell from its niche was enough to re-program the cell into a more un-differentiated state than its homeostatic state[26]. In total, while both colony formation and transplantation can provide useful information regarding what a cell can do in certain contexts, they may not always reflect true *in vivo* behavior.

1.3.4 Genetic fate mapping

Currently, the gold standard technique to define stem cells is by *in vivo* genetic inducible fate mapping, or lineage tracing[27,28]. This technique makes use of permanent and heritable labeling of cells of interest, allowing the assessment of the clonal output of single cells within intact and un-manipulated tissues. In mice, genetic fate mapping is often done utilizing a *Cre-loxP* system, in which an inducible Cre recombinase, such as Cre fused to a modified human estrogen receptor molecule (ER^{T2}), is genetically engineered under the control of a cell type specific promotor. This allele can then be crossed to a ubiquitously expressed reporter under control of a *loxP-STOP-loxP* sequence. In the resulting animals, administration of the activating

ligands, such as Tamoxifen, causes the translocation of the Cre-ER molecule to the nucleus, where it recombines the loxP sites flanking the STOP codon. This triggers expression of a ubiquitous reporter that labels the cell with a visualizable marker, such as tdTomato fluorescence. Importantly, the ubiquitous expression of the marker is inherited by daughter cells, such that the cell daughter of a single labeled cell will also be labeled, and the resulting cell clone can be tracked over time.

Lineage tracing can be used to prove that a cell population of interest is a stem cell if the clone arising from a candidate population is maintained over a long period of time (indicating self-renewal) and gives rise to mature cell types (indicating differentiation potential). The use of this technique has defined bona fide stem cells in several tissues, such as the intestine, skin, and liver[29–31]. However, a caveat of lineage tracing is that it is highly reliant on specific expression of single marker genes to label candidate cells. If a marker gene is expressed in more than one cell population, or is broadly expressed, it becomes problematic to interpret the long-term lineage tracing capacity of a specific cell type of interest[32]. The lack of specific marker genes has hampered the use of genetic lineage tracing in certain tissue, for instance the hematopoietic system in which the expression of a single gene cannot yet define hematopoietic stem cells[33]. More advanced lineage-tracing techniques, such as the use of split Cre systems which only recombine when both fragments are present, can address this problem[34,35]. Furthermore, as with transplantation and colony formation, it is critically important that the techniques used to assess a cell's functional capacity to not alter the behavior of the system[27]. While lineage tracing is thought to be non-invasive, the chemicals used to trigger lineage tracing may have biologically relevant side effects that confound studies[36] (See **Chapter 2**).

1.4 The intestinal epithelium

The intestine is a fascinating organ. Its main function is to absorb nutrients and water from ingested food, and in order to complete this task it must contend with trillions of potentially pathogenic bacteria, which outnumber mammalian cells in the human body ten to one[37]. Mammals rely on commensal microbes in the intestinal lumen to help break down macromolecules during digestion, and these bacteria are normally tolerated by their host. However, intestinal microbes can cause opportunistic infections if not properly sequestered in the lumen. As such, the intestinal epithelium is a critical tissue in maintaining whole organismal homeostasis for both its functions in nutrient absorption and as a component of the immune system as a physical barrier to infection.

To contend with the harsh environment of the intestinal lumen, the entire intestinal epithelium is rapidly replaced. Almost every intestinal epithelial cell is replaced every 3 to 5 days. Compounded with the large surface area of the intestine, it is estimated that one hundred billion intestinal epithelial cells are replaced every day in humans[38].

1.4.1 Architecture and components of the intestinal epithelium.

The lining of the small intestine is composed of epithelium organized into two discrete domains – the villi and the crypts[39] (**Fig. 1.2**). The villi are finger-like projections into the intestinal lumen that facilitate nutrient absorption. The villi are populated with a number of different epithelial cells. Most common are enterocytes, which are absorptive cells that take up nutrients and other luminal contents. Goblet cells are less numerous, but serve an important role in secreting a protective mucus layer which helps separate and protect the epithelium from pathogens and bacteria in the intestinal lumen. More rare villus epithelial cell populations

8

include tuft cells and enteroendocrine cells. Tuft cell function has long been a mystery, although they have been recently described to be involved in coordinating immune responses to intestinal pathogens[40–42]. Tuft cells may have a sensory role and secrete cytokines to initiate and amplify intestinal immune responses. Enteroendocrine cells are secretory cells involved in hormone secretion and digestion[43]. These cells constantly move toward the villus tip, where they undergo programmed cell death and are shed in to the lumen. New cells migrate up the villus from the underlying crypt to replace dying villus cells.

The glandular crypt invaginates into the sub-mucosal layer of the intestinal wall and is the location of epithelial proliferation. It is also the location of another type of epithelial cell, the Paneth cell, which unlike its cousins on the villus has a relatively long life and remains embedded deep in the crypt base[44]. Paneth cells secrete anti-microbial peptides into the crypt lumen[45–47], which is thought to help create a sterile environment in the crypt base to protect epithelial progenitor cells from pathogens. Importantly, Paneth cells are also a central cellular component of the stem cell niche, as detailed below in **Section 1.6**.

The colon, or large intestine, is structured similarly to the small intestine, but it lacks villi. Colonic crypts are deeper than small intestinal crypts, are heavily populated with goblet cells, and lack Paneth cells. Notably, the colon contains many more intestinal bacteria than the small intestine. The colon also exhibits a slower rate of cell turnover than the small intestine, but it still proliferates rapidly. Most cellular behaviors and critical cellular mediators are conserved between the small intestine and colon, with some exceptions.

1.4.2 Development of the intestine

The intestinal epithelium is derived from the endoderm, one of the three germ layers produced during gastrulation (add reference). At gestational stage E9.0 in mice, the primitive gut tube is formed, which proliferates as a single layer epithelium until E14.5. At this time, the epithelium begins to differentiate, and primitive villi begin to evaginate into the intestinal lumen, a process which is dependent on Bmp and Hedgehog signaling as well as mechanical forces from mesenchymal smooth muscle[48–51]. The regions between villi later invaginate to form crypts, which is driven by mechanical forces within the epithelium[52]. Wnt signaling is especially critical in intestinal epithelial specification, as abrogation of the Wnt pathway results in failure of intestinal development[53]. Cell differentiation begins shortly after villi are specified, with goblet cells, enterocytes, and enteroendocrine cells appearing at E16.5. Paneth cells emerge later, at postnatal day 14 in mice, concurrent with weaning and crypt formation[54].

1.5 Intestinal stem cells

During adult homeostasis, the major source of epithelial proliferation and cell turnover occurs in the crypt. Transit amplifying cells sit in the mid-crypt, just above the Paneth cell zone. Transit amplifying cells proliferate extremely rapidly, before differentiating and migrating on to the villus. It is thought that the fate decision between secretory cells (Paneth, goblet, tuft, and enteroendocrine cells) and absorptive cells (enterocytes) occurs within the transit amplifying pool and is controlled by Notch signaling[55–59]. However, it remains an open question whether differentiation decisions are exclusively made within TA cells, or if ISCs may play a role in linage specification.

ISCs are located in the deep crypt base near the Paneth cells. It has been postulated for many years that stem cells reside within the deep crypt[32,60–63], but technology allowing functional testing of specific cell types precluded ISC identification. The advent of genetic lineage tracing tools allowed precise *in vivo* interrogation of stemness, which identified ISCs using molecular markers.

1.5.1 *Lgr5*^{+} crypt base columnar cells

In 2007, the lab of Hans Clevers proved that crypt base columnar cells (CBCs) located at the bottom of the crypt were intestinal stem cells. The CBCs could be distinguished by their expression of the G-protein receptor molecule *Lgr5*[29]. Clevers and colleagues showed that multiple *Lgr5*^{+} ISCs existed in each crypt and, by genetic lineage tracing with an *Lgr5*[GFP-IRES-creERT2/+] knock-in allele, that single *Lgr5*^{+} stem cells were capable of giving rise to every other known cell type in the intestinal epithelium in a ribbon-like pattern. Importantly, they also showed that *Lgr5*^{+} cells gave rise to long-lived clones of cells, demonstrating that the cells were capable of self-renewal, thus fulfilling the defining properties of adult tissue stem cells. This work provided strong evidence that the CBCs, marked by *Lgr5* expression, were ISCs.

Beyond proving their self-renewal capacity *in vivo*, the Clevers lab went on to show that *Lgr5*^{+} cells could self-renew *in vitro*. Single *Lgr5*^{+} stem cells could be isolated and grown in a 3-dimensional culture containing the critical growth factors Rspondin, EGF and Noggin[16]. When grown in these conditions, *Lgr5*^{+} ISCs formed colonies that resembled the intestinal epithelium in cell composition and architecture, and that could be cultured indefinitely. These intestinal-like colonies were named "organoids", and their ability to grow indefinitely in culture further demonstrated the self-renewal capacity of *Lgr5*^{+} cells[64,65]. The simple nature of these cultures

was also useful in probing the necessity for certain growth factors, which helped identify critical components of the ISC niche.

In subsequent work, much has been learned about the molecular characteristics, proliferative kinetics, and control of *Lgr5*^{+} ISCs. The Clevers lab showed that *Olfm4* was expressed in *Lgr5*^{+} ISCs, which due to its extremely high transcription level enabled the localization and tracking of ISCs using *in situ* hybridization[66,67], and also went on to compile a comprehensive dataset of the gene and protein expression signature of *Lgr5*^{+} cells relative to their immediate daughter cells[68]. More recently, new RNA sequencing technology has allowed the total gene expression analysis of thousands of single cells within a tissue[69–73]. These single cell RNAseq datasets have further refined the molecular signatures of *Lgr5*^{+} ISCs, while also elucidating the unique gene signatures of their differentiated daughter cells. The identification of the molecular signatures of intestinal cell types, in combination with transgenic reporter mice expressing fluorescent markers, has enabled the precise tracking and lineage tracing of ISCs.

1.5.2 Alternative stem cells

The identification of intestinal stem cells has not been without controversy. As discussed above, a longstanding theory in stem cell biology was that stem cells were both rare and quiescent[6,74–76]. These theories arose from studies done with hematopoietic stem cells, which were shown to be an extremely rare and dormant cell type[77,78]. It was assumed that adult stem cells in other systems would behave similarly, yet CBCs were relatively common and divided frequently. Furthermore, early studies demonstrated that intestinal crypts were clonal, that is, ultimately derived from a single cell[79]. This was seemingly incongruous with the observation that there were multiple CBCs per crypt.

Before the identification of *Lgr5*^{+} CBCs as stem cells, early studies predicted that ISCs were located above the Paneth cells, on average at position +4 in the crypt. In the late 1970s, Chris Potten and colleagues showed that +4 cells were label retaining cells and highly sensitive to damage by irradiation[80]. Radio-sensitivity was thought to be a beneficial property of tissue stem cells to avoid accumulation of mutations. It was thought that each crypt contained a single rarely-dividing +4 stem cell, agreeing with the consensus models that stem cells were both rare and quiescent. The clonal nature of crypts would therefore also be explained by the presence of just one stem cell per crypt. Later, multiple genetic lineage tracing studies suggested that these cells could be labeled by various molecular markers, such as expression of *Bmi1*, *Lrig1*, *mTert*, and *HopX*[81–84]. Many of these cells were shown to have long-term lineage tracing capacity, suggesting that they may in fact be stem cells.

However, in subsequent work, the labeling fidelity of these molecular markers was shown to be unspecific. Many proposed alternative ISC markers are actually widely expressed, including within *Lgr5*^{+} cells or in definitively differentiated cell types[32,68,85]. Recent single cell RNAseq studies have been unable to identify a distinct population of alternative ISCs within the crypt[70,72,86]. The lack of discrete markers for alternative ISCs makes the definitive proof of the existence of these cells challenging. Furthermore, new theories explaining how a large population of dividing cells can eventually generate a pattern of monoclonality have dispelled the notion that only one cell per crypt maintains epithelial turnover. These studies are detailed below in **Section 1.7.3**.

In summary, while definitive proof of their existence may still come to light, the concept of alternative ISCs remains nebulous and of uncertain significance. As such, in this study we mainly focused on the role of *Lgr5+* ISCs in injury repair.

1.6 The intestinal stem cell niche

Like other stem cell systems, *Lgr5+* ISCs are thought to depend on their niche for signals and growth factors to proliferate and self-renew[5,87,88]. The niche is composed of the immediate cell neighbors, matrix components, and growth factors (**Fig. 1.3**). These components act in concert to maintain stem cells and also direct their behavior. While the stem cell niche has not been completely defined, it has been shown that Paneth cells in the small intestine, which are immediately adjacent to *Lgr5*^{+} ISCs in the deep crypt, secrete growth factors that signal to the neighboring stem cells[89]. Similarly, in the colon, which does not have Paneth cells, deep crypt goblet cells serve a similar function[90,91]. The ISCs are also maintained by stromal cells, such as myo-fibroblasts and other non-epithelial cells[92–96]. These cells secrete growth factors that maintain ISC self-renewal, and direct differentiation patterns. Several growth factors and signaling pathways are important in this process[97].

1.6.1 Wnts and Rspondins

An especially important regulator of ISCs is Wnt signaling. The Wnt pathway is a critical signaling pathway that controls many processes, including early embryogenesis, cell proliferation, stem cell self-renewal, and cancer, amongst others[98]. The Wnt pathway is activated when Wnt ligands, which are locally acting signaling molecules meditating signaling between cell neighbors, bind the Frizzled/LRP receptor complex. This results in a molecular cascade activating intracellular signaling proteins leading to the ultimate phosphorylation of β-catenin and transcription of Wnt target genes via Tcf transcription factors.

Wnt activation is critical for maintenance of *Lgr5*^{+} ISCs and crypt proliferation. Loss of critical Wnt signaling effector molecules, such as the Tcf4 transcription factor or β-catenin,

14

causes a complete loss of intestinal crypts[99,100], while over-activation of the Wnt pathway in intestinal epithelium causes crypt metaplasia and eventually, cancer[101–105]. Wnt ligands are secreted from both Paneth cells and stromal niche cells, and these are critical for maintenance of ISCs and the crypt[44,89,94,106–108]. *Lgr5*^{+} ISCs are especially sensitive to Wnt signaling, as Wnt activity is highest in CBCs and perturbations to Wnt levels modulate ISC activity[66,109].

Lgr5 itself is a Wnt target gene as well as an important member of the Wnt signaling pathway. *Lgr5*, and its family members *Lgr4* and *Lgr6*, are receptors for various Rspondin family members[29,110–113]. Rspondins are Wnt agonists that modulate Wnt activity through interactions between Lgr4-6, Rnf43, and Znrf receptor complexes[112,114,115]. Rspondin is critical in maintaining intestinal organoids[16,116,117], and over-expression of Rspondin *in vivo* leads to intestinal overgrowth[118]. Rspondins regulate the number of *Lgr5*^{+} ISCs[119,120], while mice deficient for both the *Lgr4* and *Lgr5* receptors are not viable and feature a loss of intestinal crypts[121]. Rspondins are thought to be secreted by the intestinal stroma[122,123], but their precise source remains unclear.

1.6.2 Notch

Another key pathway important in both ISC maintenance and differentiation decisions is the Notch signaling pathway[55,57,124]. The Notch pathway is activated when Notch ligands tethered to neighboring cells ligate with Notch receptors on the cell surface. Binding of Notch ligands, such as the Delta-like and Jagged family members, results in the proteolytic cleavage of the Notch intracellular domain (NICD) by γ-secretase. NICD then translocates to the nucleus where it mediates target gene expression through its interaction with the CSL transcription factor.

The Notch pathway has been shown to be important in several aspects of crypt biology. Genetic or pharmacologic inhibition of the Notch pathway results in a conversion of proliferative cells to secretory goblet cells[56,59], indicating that Notch plays a key role in the major differentiation decision between intestinal cell lineages. Conversely, hyperactivation of the Notch pathway by driving expression of NICD results in increased numbers of absorptive enterocytes[58,125].

Notch signaling regulates the decision between secretory and absorptive fates through a simple mechanism of lateral inhibition, which specifies a uniform field of equipotent cells to adopt different fates. Through stochastic interactions between cells signaling to each other bi-directionally, feedback mechanisms amplify small differences in signaling activity and eventually result in uni-directional signaling. In the intestine, this process is thought to occur in the TA compartment, such that subgroups of cells within the equipotent TA pool stochastically up-regulate Delta-like ligands, specifying their neighboring cells to become absorptive cells. The Delta-like expressing cells are then fated to become secretory[126,127].

Within the ISC niche, *Lgr5*^{+} cells are directly regulated by Notch signaling. The Notch ligands Dll1 and 4 are expressed by Paneth cells, which signal to neighboring *Lgr5*^{+} ISCs through Notch receptors[89]. *Lgr5*^{+} ISCs are sensitive to Notch inhibition[128], and the ISC marker gene *Olfm4* is a direct target of Notch[129–131]. Additionally, the addition of Notch ligands is required to grow single *Lgr5*^{+} ISCs in *in vitro* organoid cultures[16,132]. Notch signaling heavily interacts with the Wnt pathway as well to maintain ISCs and intestinal fate decisions[133,134].

1.6.3 Other pathways

Several other pathways have been shown to be important regulators of the niche. Epidermal growth factor (EGF) is a niche factor secreted by Paneth cells and is a necessary supplement in organoid cultures, suggesting it is required for growth of intestinal crypt cells[16,89,116]. *In vivo* treatment with EGF supplements results in overgrowth of the intestinal epithelium[135]. Mice that are deficient for the EGF receptor EGFR die soon after birth due to failed development of several epithelial tissues, including the intestine[136].

While not directly acting on stem cells, Bone morphogenetic proteins (BMPs) control intestinal differentiation and must be inhibited to maintain *Lgr5*^{+} ISCs[137,138]. BMP ligands are expressed in the stroma of villi, which specify epithelial differentiation[139]. BMP inhibitors are present near the intestinal crypt, preventing premature differentiation of intestinal precursors[140]. As such, the BMP inhibitor Noggin is an essential supplement in organoid growth[16]. Bmp signaling directly represses expression of the *Lgr5*^{+} signature[138].

Finally, a relatively new described signaling pathway has been revealed to play important roles in intestinal crypt maintenance, but especially regeneration[141]. The Hippo pathway is a key regulator of growth in many organs and acts as a mediator between mechanical stimuli, growth factors, and cellular behavior[142–144]. The mechanisms that activate the Hippo pathway are not yet completely worked out but include external mechanical forces, which results in a signaling cascade ultimately modulating the localization of the effectors YAP and TAZ. YAP and TAZ are co-factors for TEAD transcription factors, so that when the Hippo pathway is activated, Hippo target genes are silenced. While the Hippo pathway is important in homeostasis of several organs, and YAP is localized to the nucleus of crypt cells in homeostasis, it appears dispensable in the intestine, as conditional YAP/TAZ double knockouts have no overt phenotype in the

intestine[145,146]. However, YAP/TAZ and the Hippo pathway do play important roles in injury repair, and are notably required for regeneration after intestinal injuries[145,147,148]. This is further discussed in **Section 1.10.2**.

1.7 Plasticity in the crypt

It has become increasingly apparent that the lineage hierarchy within the intestinal crypt is not as rigid as was once assumed. While it was previously thought that differentiation occurred in a linear path - that adult cells were terminally differentiated with no ability to regain abilities of progenitor cells - this model has been challenged by several observations.

1.7.1 ISC ablation

In 2011, an intriguing paper was published, demonstrating that $Lgr5^+$ cells could be ablated with little to no consequence on the tissue[149]. The expression of a diphtheria toxin receptor by the $Lgr5$ promotor allowed the specific depletion of $Lgr5^+$ cells in $Lgr5^{DTRGFP/+}$ mice by administration of diphtheria toxin. Despite clear evidence that $Lgr5^+$ cells were *bona fide* stem cells and contributed to epithelial turnover, paradoxically there was little to no phenotype when the $Lgr5^+$ cells were ablated. During a week of continuous $Lgr5^+$ cell ablation, epithelial turnover, proliferation, differentiation, villus morphology were maintained, and no inflammation occurred. In the days after diphtheria toxin administration was stopped, $Lgr5^+$ cells re-emerged. These results seemed to indicate that an alternative stem cell was re-activated in this context, which was able to repopulate the $Lgr5^+$ pool. While a plausible explanation, this argument was complicated by the lack of specific genetic markers of alternative stem cells, making it difficult to prove that a discrete population of "reserve" stem cells existed in the crypt[32,68]. As such, alternative hypotheses of how the loss of $Lgr5^+$ cells is compensated for have been proposed.

1.7.2 De-differentiation

It first seemed unthinkable that the loss of the intestinal stem population could have largely no effect on intestinal homeostasis. The dispensability of the *Lgr5*^{+} ISCs seemed to argue for the existence of an *Lgr5*-negative ISC that could be activated in conditions of *Lgr5*^{+} loss. However, while it was possible that *Lgr5*-negative ISCs were activated when *Lgr5*^{+} cells were lost, a novel concept emerged: that certain populations of non-stem cells might acquire stem cell properties when the stem pool was damaged or lost.

This was driven by observations that TA cells could give rise to long-lived cell clones in non-homeostatic conditions. *Dll1*^{+} secretory progenitor cells, normally fated for differentiation and unable to give rise to long lived cell clones in homeostasis, gave rise to stem cell like lineage tracing ribbons after irradiation, which is known to induce crypt damage and ISC loss[127]. This was bolstered when label-retaining Paneth cell precursor cells were shown to behave similarly, expanding their generative potential after irradiation[150]. Furthermore, *Alpi*[+] absorptive progenitors, again typically restricted to generating short term enterocyte-specific clones, could give rise to long lived cell clones and regenerated the *Lgr5*^{+} cell pool after DT-mediated *Lgr5*^{+} cell ablation[151].These observations have been corroborated with enteroendocrine cells[86,152], and in intestinal tumors, in which *Lgr5*^{+} cancer stem cells, which drive tumor expansion, could be ablated, and then regenerated by *Lgr5*-negative tumor cells[153]. Furthermore, it was shown that intestinal tumor initiation could be driven by de-differentiation of non-stem cells into stem cells[154].

While it was clear that in certain contexts non-stem populations could reacquire ISC growth capacity, the mechanism by which this occurred was unclear. Some argued that perhaps the ISCs were not intrinsically important, but rather that extrinsic signals endowed stemness.

Perhaps the niche specified stem cells, and when *Lgr5*^{+} ISCs were lost, other cells could fill the vacant niche space to become an ISC. An *in vivo* live-imaging study of crypt cell behavior hinted that non- *Lgr5*^{+} cells above the Paneth-ISC zone could regenerate *Lgr5*^{+} ISCs in the niche after *Lgr5*^{+} cell ablation[69].

These studies suggested that the lineage hierarchy within the crypt is not necessarily fixed, and that cells can interconvert between various states of differentiation, perhaps depending on the presence of ISCs in the niche. However, a precise mechanistic understanding of crypt plasticity remains unclear. We still do not know how cellular plasticity is accomplished – which signals govern de-differentiation, and in which precise contexts it happens.

1.7.3 Population dynamics of ISCs

It remained an open question why crypts were monoclonal, when approximately 15 *Lgr5*^{+} cells resided within each crypt[29,79]. It was difficult to reconcile the comparatively large pool of *Lgr5*^{+} cells with crypt monoclonality, which could suggest that a quiescent stem cell above *Lgr5*^{+} cells in the lineage hierarchy was responsible for crypt turnover. However, drawing from new ideas in the study of skin and testes[11,155,156], a novel idea was introduced to the ISC community – the population asymmetry or neutral drift model, which resolved this discrepancy[157,158].

Previously, it was thought that tissue stem cells divide strictly asymmetrically to produce one differentiated daughter and one self-renewing stem cell. By this pattern, lineage hierarchy is maintained through retention of "stemness" within one daughter cell fated to remain in the stem cell niche[159]. This theory is called the invariant asymmetry model, and was thought to govern the behavior of stem cell in many tissues in mammals, including the intestine.

In contrast to the strict asymmetric cell divisions proposed in the invariant asymmetry model, the population asymmetry models suggests that stem cells can divide in three ways – giving rise to two stem cells, or one stem cell and one differentiated daughter, or two differentiated daughters. The decision between these three fates is stochastic (random), yet the frequency of each decision is balanced such that the number of self-renewing stem cells is maintained within the entire population by the competition between stem cells and their clonal daughters[160,161].

These two models could be resolved by a quantification of the number and size of clones arising from stem cells[12]. The invariant asymmetry model implied that clones arising from a stem cell would reach a fixed size over time and be maintained indefinitely, as each individual stem cell was conserved within its niche. If stem cells followed the population asymmetry model however, over time their clones would expand in size, yet the number of clones would shrink, as stem cells were randomly lost through stochastic competition during cell division.

Through extensive quantification fitted to mathematical models, the population asymmetry model was proven to govern stem cell division patterns in the testes and epidermis[11,156]. In the intestine, extensive quantification of the frequency and size of cellular clones arising from ISCs found that, over time, crypts gradually drift towards monoclonality in a pattern that statistically fit with the population asymmetry model rather than the invariant asymmetry model[157,158]. Over a long timecourse, most clones arising from ISCs were lost, while others expanded in size, giving rise to monoclonal crypts.

These studies proved that ISCs compete with each other during cell division as predicted by the population asymmetry model. They also reconciled why crypts appeared to be ultimately clonal despite harboring multiple ISCs per crypt. This showed that it was feasible to derive a

monoclonal crypt from multiple equipotent stem cells, rather than strictly from one quiescent stem cell higher in the lineage hierarchy from $Lgr5^+$ ISCs.

1.7.4 Plasticity summary

Between the cell plasticity in the crypt, and the population asymmetry governing stem cell behavior, it has become apparent that the relationships between the crypt cells is much more fluid than previously thought[97]. ISCs compete with each other, and are constantly lost and gained through stochastic mechanisms. TA and progenitor cells can act as stem cells in certain contexts, perhaps even in homeostasis. As such, the strict rules governing lineage relationships between ISCs, TA cells, and their differentiated daughter cells should perhaps be reconsidered.

1.8 Inflammation and injury

Beyond its canonical function to detect and eliminate pathogens, the immune system also plays important roles in maintenance of healthy tissues, such as recycling of old and damaged cells, elimination of tumor cells, and tissue repair. Tissue damage is detected by the innate immune system, resulting in cytokine signaling and recruitment of immune cells that is crucial for proper tissue repair. Several immune pathways are of special importance in this process.

1.8.1 Detection of damage

Tissue damage results in non-apoptotic cell death and the release of signaling molecules which instigate an immune response[162,163]. However, unlike "non-self" signals, such as bacterial components that result in anti-pathogenic immune responses, sterile tissue damage is detected by endogenous "self" molecules. These endogenous signals, which are not released during normal cell apoptosis, are classified into alarmins and damage-associated molecular patterns

22

(DAMPs)[164]. Alarmins are intracellular proteins that can serve as cytokines when released by damaged cells. Alarmins, such as IL-1α, IL-33, and HMGB1, signal through dedicated cytokine receptors. DAMPs are "self" molecules, hidden from detection in homeostasis, but upon non-apoptotic cell death are detected by immune sentinels through pattern recognition receptors (PRRs). DAMPs include ATP, histones, mitochondrial DNA, and several other molecules[165]. DAMPs activate responses through PRRs, which also have important roles in pathogen detection[166]. There are several classes of PRRs, which are located in different cellular compartments, such as Toll-like receptors (TLRs), NOD-like receptors (NLRs), and others[167]. Upon ligand binding to PRRs, signaling cascades through NF-kb, mitogen-activated protein kinase (MAPK) and type I interferon pathways ultimately result in a pro-inflammatory response. Both alarmin and PRR signaling result in release of cytokines and chemo-attractants that result in the recruitment of additional immune cells such as macrophages and neutrophils, and further inflammation.

1.8.2 Interferon signaling

An important pathway in many early immune responses is interferon (IFN) signaling. IFN cytokines are produced in response to diverse stimuli, such as viruses, bacteria, parasites, and cell damage, and play important roles in controlling and modulating the immune response[168]. IFN cytokines, of which there are several members organized intro three classes, bind to membrane bound receptors and activate the JAK-STAT pathway, resulting in the transcription of interferon stimulated genes (ISGs)[169]. The type 1 interferons are composed of IFNα, IFNβ, and others, and signal through the receptors IFNAR1 and IFNAR2. There is only one type 2 interferon, IFNγ, which signals through the IFNγ receptor complex. IFNγ is produced only by

immune cells, although most cell types express the IFNγ receptor[170]. Type 3 interferons have been discovered more recently and signal through the IFN lambda receptor and IL-10 receptor 2. All classes of IFN utilize STATs to mediate signaling downstream of their receptors[171]. Upon pathway activation, STATs are phosphorylated and translocate to the nucleus, where they can act as transcriptional activators of ISGs. IFN activation results in up-regulation of heightened immune sensing and inflammatory signaling capacity[172], as well as expression of genes that directly target pathogens. IFN signaling is classically described in viral immunity, and many ISGs have anti-viral roles, such as targeting pathways required for viral entry and replication.

Beyond activation of immune cells and targeting of pathogens, IFNs have been shown to target stromal cells within tissues. IFNs activate quiescent HSCs, leading to their proliferation, which may help the hematopoietic system dynamically respond to infection[173,174]. Interferons increase epithelial proliferation turnover in multiple tissues after viral and parasitic infections, suggesting that interferons target tissue progenitor activity to expel pathogens[175,176].

1.9 Injury repair

Injuries are repaired through a complex process of inflammation and regeneration[1,2]. Several organ systems have demonstrated that inflammatory processes are necessary for proper repair after injury, and that these immune reactions mobilize tissue resident progenitor cells during regeneration.

1.9.1 Muscle regeneration

A relatively well understood demonstration of immune influence on stem cells after injury occurs in the skeletal muscle[177]. During homeostasis, skeletal muscle fibers do not turn over like the skin or intestine, but are repaired after injury through the activity of a dedicated

population of tissue resident stem cells – the satellite cells[178]. Satellite cells are rare and quiescent cells closely associated with muscle fibers[179]. After damage, *Pax7*$^+$ satellite cells escape quiescence and proliferate to expand their numbers. During resolution, new daughter muscle progenitor cells lose expression of *Pax7* and begin expressing the specification factors *MyoD* and *MyoG* before fusing together to form new myotubes. Critically, *Pax7*$^+$ satellite cells are required for proper regeneration, as their deletion prevents regeneration of the myotubes[180,181].

Multiple models of skeletal muscle injury demonstrate that an acute and dynamic immune response occurs after damage and that the immune response is critical for proper repair[177,182]. Damage causes recruitment of a diverse pool of immune cells, notably neutrophils, macrophages, and T-cells. Proper recruitment depends on the chemo-attractant signaling molecule *Ccl2,* which signals from local macrophages to recruit neutrophils. Resident T-cells also secrete *d* to recruit macrophages. Importantly, perturbation of immune processes, such as loss of *Ccl2* or inhibition of macrophage phenotype switching, slows the growth of new muscle fibers[183–186], suggesting that inflammation is critical in establishing a reparative environment for satellite cell mediated regeneration.

An important question is whether immune cells directly influence the behavior of satellite cells in injury repair, or whether this is a secondary to other immune processes, such as debris clearance. One clue to this effect is that both TNFα and IFNγ signaling from immune cells to muscle cells are essential for the prevention of premature progenitor cell differentiation[187–189]. Additionally, IGF1 secretion from myeloid cells promotes proliferation of muscle progenitors[190], while amphiregulin produced by regulatory T-cells also acts on muscle cells to promote repair[191].

Taken together, this suggests that immune derived signaling factors are important in the expansion of regenerative muscle precursors.

1.9.2 Liver repair

Another organ showing interactions between immune cells and tissue progenitor cells is the liver. The liver performs multiple important metabolic processes, which are accomplished by two main cell populations - hepatocytes, which make up the large majority of liver cells, and the less frequent biliary ductal cells. Like the muscle, the liver does not exhibit significant cellular replacement during homeostasis, and hepatocytes can have an average lifespan of hundreds of days[192]. Despite this, evidence for the slow replacement of hepatocytes has pointed to several potential progenitor pools. Mature hepatocytes themselves are a somewhat unique cell in mammalian tissues in that they possess self-replication abilities, and can massively expand after injury to repair the liver[193]. Biliary cells are able to give rise to hepatocytes when transplanted[194,195], but it remains unclear if biliary cells contribute to hepatocytes in vivo[196,197]. Rare sub-populations of hepatocytes labeled by *Axin2* or *mTert* expression can give rise to new hepatocytes in homeostasis, suggesting that dedicated pools of hepatic progenitor cells may well contribute to liver turnover[31,198].

While the precise identity of liver stem cells remains currently unclear, the liver does possess extraordinary abilities to repair after damage. Liver damage, either through surgical resection, chemical damage, or cell ablation, is repaired with remarkable efficiency through the proliferation of existing hepatocytes or progenitor cells[192,199–201]. Depending on the damage agent used, new hepatocytes are produced through the proliferation of adult hepatocytes, hepatocyte

precursor cells, or trans-differentiation of biliary cells during the "ductal reaction"[202]. Adult hepatocytes may also de-differentiate during injury to contribute to the ductal reaction[203].

Again, as in the muscle, the immune response is important in proper repair after damage[204,205]. Soon after damage, an immune response is mounted, characterized by the rapid recruitment of platelets, neutrophils, macrophages, and other cell types. Innate cells recognize DAMPs through Toll-like receptors, eliciting the activation of the inflammasome and secretion of cytokines such as IL-1β and Ccl2 to recruit additional immune cells[206,207]. Disruption of inflammation through the depletion of inflammatory cells or abrogation of immune signaling inhibits repair[208–212].

Several findings point to a specific role for immune cells directing liver repair. In a chronic chemical model of damage, macrophages exposed to debris from cellular damage expressed *Wnt3a*, which was important in proper specification of new hepatocytes arising from liver progenitors[213]. After partial liver resection or toxin injury, eosinophils recruited to the liver induced proliferation of hepatocytes through IL-4 signaling via the IL-4 receptor on hepatocytes, pointing to a direct role for immune-derived cytokine signaling in regeneration[214]. Additionally, iNKT cells responding to DAMPs co-localized with hepatocytes after sterile injury and secreted IL-4 to induce hepatocyte proliferation[215]. These observations suggest that, as in the muscle, immune reactions to liver damage specifically target tissue resident progenitor cells to initiate a pro-proliferative program towards completing tissue repair.

1.10 Injury repair in the intestine

In the intestine, investigation into injuries has largely focused on models attempting to recreate conditions relevant to human patients, such as inflammatory bowel disease (IBD) and

mucositis arising from chemotherapy or irradiation treatments for cancer. These studies have given some insight into how the intestine copes in injuries, including which epithelial cells are mobilized, and how inflammation plays a role.

1.10.1 Intestinal irradiation

Exposure to radiation models injuries experienced by human patients during cancer treatments or in military conflicts. Intestinal epithelial cells are damaged by high doses of irradiation, causing epithelial cell death, inflammation, and diarrhea, but the epithelium can recover after moderate doses of irradiation if hematopoietic system failures are avoided[216,217]. After radiation exposure, there is extensive P53-dependent apoptosis[218–220], followed by a regenerative response featuring extensive proliferation and crypt fission. ISCs and other progenitor cells are known to be sensitive to irradiation[80,221]. *Lgr5*^{+} ISCs are lost soon after irradiation, yet re-appear five to seven days after injury[222,223]. The early regenerative response does not feature the presence of *Lgr5*^{+} cells, suggesting that an *Lgr5*-negative cell population drives the early period of regeneration[222–224]. Committed progenitor cells can acquire stem cell like lineage capacity after irradiation, which may be a mechanism to sustain intestinal function after stem cell damage[86,127,150]. Paradoxically though, *Lgr5*^{+} cells are required for regeneration after irradiation injury, as ablation of *Lgr5*^{+} with irradiation results in epithelial failure[224]. It is difficult to reconcile these observations, as the de-differentiation of committed progenitor cells would seem to preclude the requirement for *Lgr5*^{+} cells in regeneration. It is plausible that there is a requirement to transition though a *Lgr5*^{+} state during de-differentiation, or that additional damage by *Lgr5*^{+} ablation reaches a critical threshold resulting in epithelial failure.

28

1.10.2 Colitis models

Perhaps the most frequently used model of intestinal injury is colitis driven by administration of chemicals. While targeting the colon rather than the small intestine, administration of Dextran Sodium Sulfate (DSS) is a widely used model of IBD. Human patients with IBD, which includes Crohn's disease (affecting the entire intestinal tract) and Ulcerative colitis, which is restricted to the colon, have chronic disease which leads to damage to the colonic epithelium, resulting in chronic diarrhea, weight loss, abdominal pain, and other symptoms[225,226]. DSS treatments attempt to recreate the pathology of IBD in mice, although the model may not entirely recapitulate human disease. Other IBD models have been developed, such administration of trinitrobenzene sulfonic acid (TNBS) and oxazolone, or adoptive T-cell transfer (detailed below in **Section 1.10.3**), or genetic models such as IL-10 deficient mice which spontaneously develop colitis[227–229].

Standard DSS regimens feature administration of 2.5-5% DSS in drinking water for five days to trigger colonic injury, followed by a recovery period. Depending on the DSS dose, DSS treatment causes a complete loss of crypts in the distal colon, and extensive inflammation. In the recovery period, epithelial restitution occurs, featuring an expansion of epithelium over lesions, re-emergence of proliferative crypts and crypt fission, followed by re-establishment of differentiation and homeostatic cell behaviors. Much has been learned about DSS inflammatory responses, which demonstrates that innate immune cells are the primary drivers of inflammation, as mice deficient for adaptive immune cells still exhibit extensive inflammation after DSS[230]. As in liver and muscle, the inflammatory response is important in proper wound healing after DSS injuries. TLR signaling deficient mice exhibit increased damage after DSS, as TLR signaling can promote epithelial proliferation and barrier repair[231–235]. Inhibition of macrophage phenotype

switching also can inhibit repair processes[236,237]. IL-6 signaling has also been implicated in colonic wound repair, intriguingly linked to YAP activity. IL-6 is expressed after wounding by multiple immune cell types, and inhibition of IL-6 prevents epithelial proliferation after injury[238]. Gp130 is a co-receptor for IL-6, and simulation of gp130 results in epithelial proliferation and YAP activity[148]. Activation of gp130-YAP pathway confers resistance to DSS colitis, suggesting that IL-6 activity may mediate YAP activity to influence repair. Furthermore, during mucosal healing, proliferative epithelium migrates over wound beds, before invaginating into the wound to form new crypts. This process depends on *Wnt5a* expressing mesenchymal cells, pointing to novel role for non-epithelial cells in directing wound repair[239].

Within the stem cell compartment, *Lgr5*^{+} cells are quickly lost after DSS administration and re-appear in the recovery period[240]. The re-emergence of *Lgr5*^{+} cells likely is the result of cellular plasticity as in irradiation, although this has not been extensively studied.

1.10.3 Graft versus host disease

A clear link between immune reactions and *Lgr5*^{+} ISC mediated regeneration is found in graft versus host disease (GVHD). During allogeneic bone marrow transplant, grafted donor T-cells can be activated causing acute inflammation and attacking recipient tissues, including in the intestine where it results in epithelial damage[241]. In mouse models of GVHD, treatment with Rspondin1 ameliorates damage from GVHD by protecting *Lgr5*^{+} ISCs, suggesting that intestinal stem cells are important in regeneration[242]. Indeed, *Lgr5*^{+} ISCs are lost in GVHD models[243]. Immune derived IL-22 is protective in GVHD and prevents additional tissue damage. IL-22 is produced by innate lymphoid type 3 cells (ILC3s) and T helper cells[244–246], while the IL-22 receptor is expressed on non immune cells, notably the intestinal epithelium and *Lgr5*^{+} ISCs[247].

Treating intestinal organoids with IL-22 increased the growth of intestinal organoids directly through $Lgr5^+$ ISCs, while systemic administration with IL-22 increased $Lgr5^+$ ISC recovery after GVHD. These observations indicate that the immune derived factors can play a significant role in directed targeting ISCs and mediating recovery from injury.

1.11 Parasites as a model for injury

Most established intestinal injury models heavily rely on non-physiologic stimuli, such as administration of chemicals or irradiation. These un-natural perturbations do not necessarily elicit evolutionarily adapted responses in tissues, and may not faithfully recapitulate endogenous repair processes. A relatively unexplored model in the study of injury that avoids this caveat is damage caused by natural pathogens. Most pathogens, whether viral, bacterial, fungal, or parasitic, cause tissue damage during colonization of their host organisms. These infections elicit host responses that are the result of millennia of co-evolution between the host and the pathogen.

1.11.1 *Heligmosomoides polygyrus*

Helminthes are co-evolved natural parasites of mammals, which establish chronic infections, and can modulate the host immune response[248–250]. *Heligmosomoides polygyrus* (Hp) is nematode which is a natural helminth of mice[251]. Most laboratory strains of mice are susceptible to Hp infection and do not clear the worms. However, upon secondary infection after anti-helminthic drug clearance, most mice are able to develop immunity and expel the parasite. Immunity to Hp is heavily reliant on Th2 type immune responses, which can be suppressed by Hp in primary infections to facilitate host colonization. Hp infections elicit stereotypical responses exemplified by the induction of IL-4, IL-5, IL-13 and other type 2 cytokines[252]. These

cytokines drive the recruitment and differentiation of immune cells which attempt to expel the worm by altering the host environment and releasing anti-helminthic agents[253,254].

Immune responses to Hp infections, like other helminths, have strong effects on the intestinal epithelium[255]. The expansion of mucus secreting goblet cells is striking[256,257]. Goblet cell hyperplasia results in increased mucus production, which assists in worm expulsion, but also secretion of anti-helminth products such as RELM-β[258,259]. Besides goblet cells, tuft cells are also highly expanded in worm infections and assist in initiating anti-worm immunity[40,41]. Mast cells increase permeability of the intestine by breakdown of epithelial tight junctions, which may alter the niche for worms[260]. Interestingly, in *Trichuris muris* infections, worm expulsion is strongly correlated with an increase in epithelial proliferation and turnover, which is dependent on IL-13[261]. This intriguing observation suggests that the immune system may target epithelial progenitor cell activity to drive the worm out of its niche. All of these epithelial responses depend on immune derived cytokine signaling, indicating that the intestinal epithelium is a primary effector for Hp immunity[262].

1.11.2 Life cycle of Hp and granulomas

Hp has a life cycle in which L3 stage larval parasites are ingested (or orally gavaged in the laboratory) and penetrate the proximal duodenum mucosal barrier within 24 hours (**Fig. 1.4**)[263]. Within the sub-mucosa, the larval parasites grow and molt twice, before re-emerging into the lumen of the duodenum as adults. Adult worms establish long term infections in the duodenal lumen, where they mate and lay eggs that are excreted with the feces.

An interesting facet of Hp infections is the formation of granulomas around sites of worm invasion. Granulomas are large aggregations of immune cells surrounding the larval parasite.

Granulomas are composed largely of innate cell types such as neutrophils, macrophages, and eosinophils, but adaptive cells such as T-cells are also present in granulomas[264,265]. Macrophages within granulomas are heavily skewed to a Type 2 "alternatively activated" phenotype[253,266]. These immune reactions do not usually kill the developing worm in primary infections, but may prevent excess tissue damage by preventing worm migration through the tissue[267].

1.12 Outline of Study

In this study, in collaboration with members of the Klein and Locksley labs, I examined how ISCs respond to tissue disruption caused by Hp infection. We attempted to answer several questions in this regard.

1. How do ISCs behave after damage caused by Hp transiting through the epithelium?

2. What signals and/or biological processes mediate the damage response?

3. Is the epithelial response to Hp unique or do other perturbations behave similarly?

4. How do crypts regenerate after Hp damage?

I chose to examine Hp as a model of intestinal injury for several reasons. First, Hp elicits endogenous biological responses from the tissues it inhabits. As a natural helminth of mice, these responses are the result of millions of years of co-evolution between mice and the parasite, so unlike other laboratory models of intestinal injury, such as chemical administration or irradiation, the damage caused by Hp in repaired through processes that occur in the wild.

Second, the focal nature of tissue disruption driven by Hp larvae allows the use of internal non-affected tissue controls rather than whole tissue from untreated animals. This is advantageous because it gives greater resolution into the responses to tissue disruption and is not potentially compromised by systemic effects on the animal and the immune system.

33

Third, while Hp has been extensively used in immunological studies, these worms have not yet been leveraged to study stem cells. As such, we may uncover novel injury phenotypes.

Lastly, helminths, and the immune responses to them, induce reparative processes that are relevant for human therapies. Parasitic type 2 immune responses are often referred to as "pro-healing" or "anti-inflammatory", and while these terms may be an over-simplification of parasitic immunity, helminths may have therapeutic use in the clinic for inflammatory bowel disorders. Several ongoing clinical trials are examining the effects of "worm therapy" for Crohn's disease and ulcerative colitis, based on data from animal models that suggests that helminth infection may be protective or curative in IBD[268]. This may be due to the potent immuno-modulatory effects of the worms, but also because they may induce a regenerative response in the epithelium.

Here, we found that immune reactions to Hp larvae have a dramatic effect on crypts in their immediate vicinity. Larvae associated injured crypts became hyper-proliferative and enlarged, yet paradoxically silenced *Lgr5*$^+$ ISCs. Concurrently, immune cells responding to Hp infection drove the expression of Sca-1 on these injured crypts, through immune-epithelial IFNγ signaling. Many other models of epithelial injury and perturbation resulted in similar responses, including *Lgr5*$^+$ cell independent hyper-proliferation, Sca-1 expression, and IFNγ signaling, suggesting that this represents a core response to injury in the intestine. Intriguingly, Sca-1$^+$ cells from Hp infection formed large spheroids in culture, rather than the typical organoids formed by *Lgr5*$^+$ cells. These Sca-1$^+$ spheroids were devoid of differentiated cell types, but featured activation of a fetal like program. *In vivo*, the fetal transcriptional signature was activated within Hp-injured crypts, and a novel population of fetal like cells arose within these crypts. This

34

suggests that the intestinal crypt copes with injury by suppressing the canonical ISC program, and adopting a hyper-proliferative state recapitulating aspects of intestinal development.
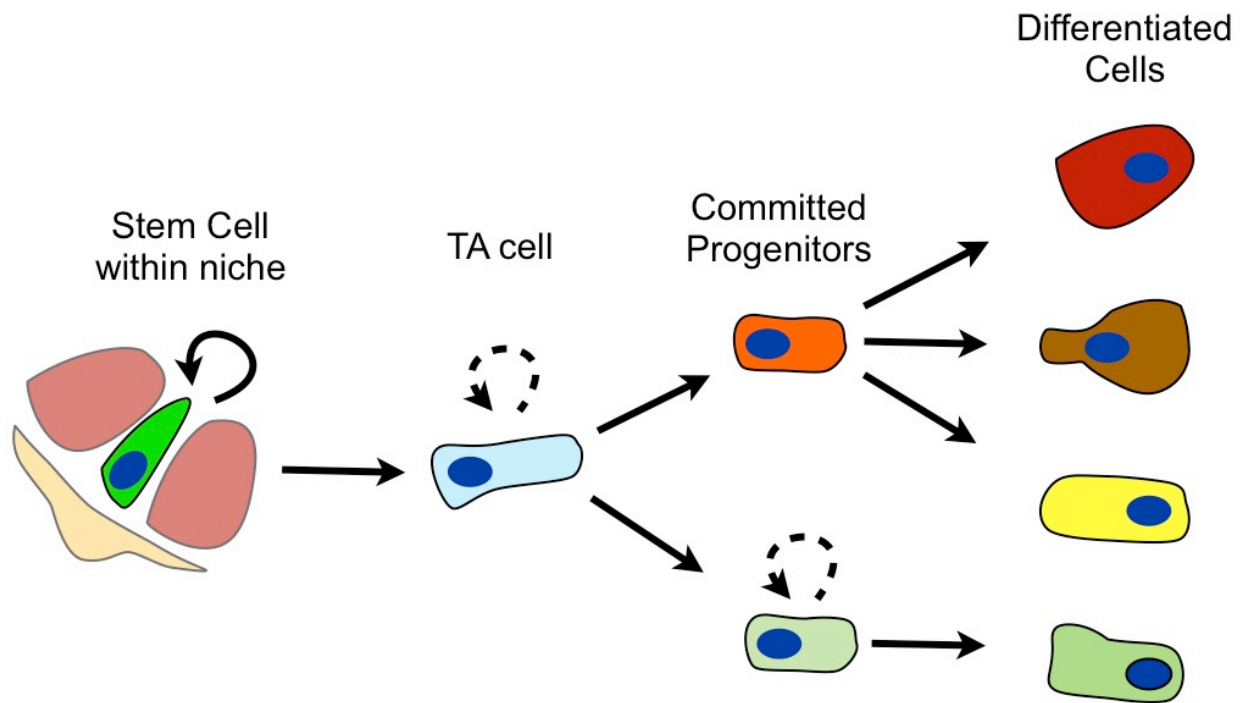
Figure 1.1 | Lineage hierarchy of self renewing tissues

Within self-renewing tissues such as the skin and intestine, populations of adult stem cells are responsible for long-term cell turnover. Stem cells are the only population of cells endowed with self-renewal, which is thought to be dependant on the stem cell receiving proper signals from the surrounding stem cell niche. Stem cells divide and produce transit-amplifying (TA) cells, which continue to undergo limited rounds of proliferation. Within the TA pool, differentiation decisions are made that drive cells into terminally differentiated cell types, fulfilling adult tissue needs.
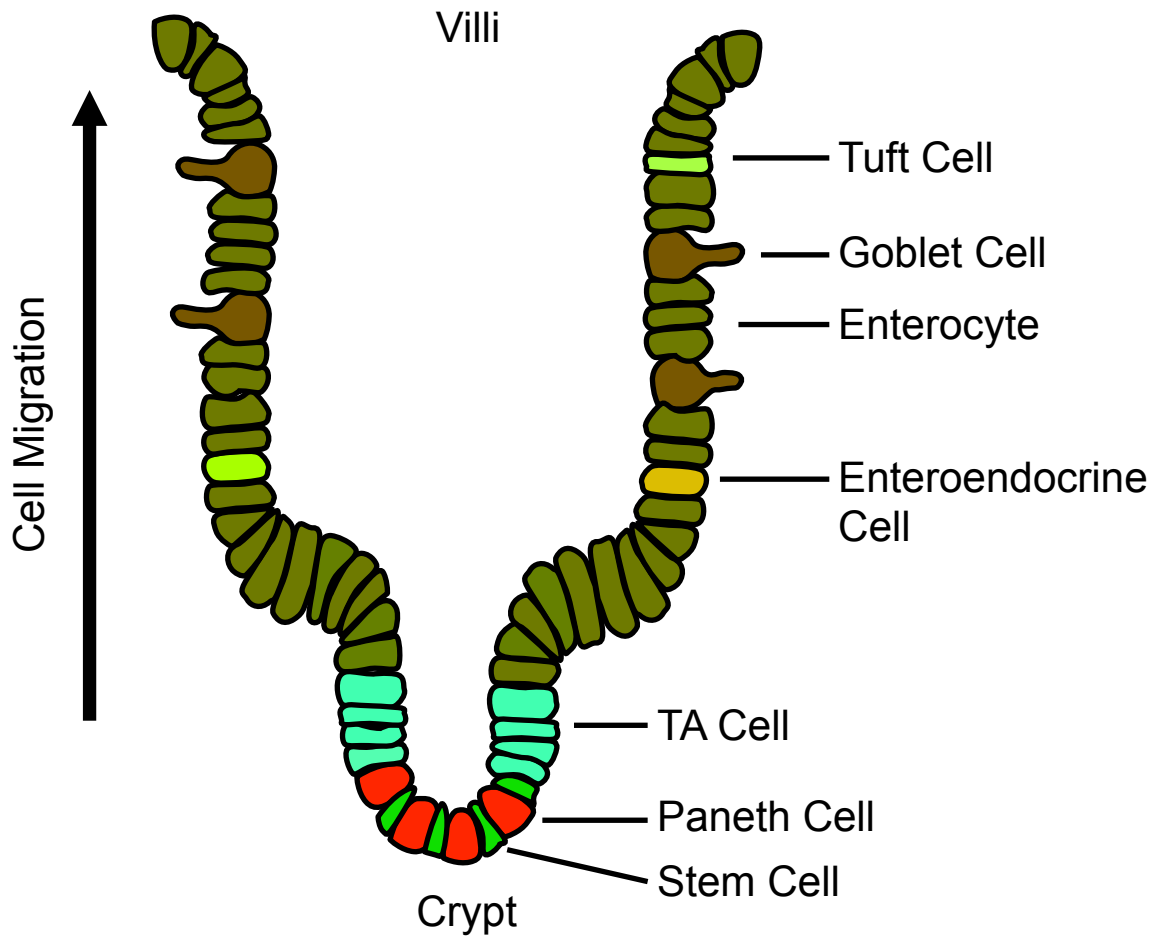
Figure 1.2 | The intestinal lining

The lining of the intestine is covered with a single layer simple epithelium that is organized into repeating units of crypts and villi. Villi are fingerlike protrusions that extend into the intestinal lumen, and facilitate increased surface area for nutrient absorption. The crypt is a glandular invagination in the intestinal wall, which is the site of intestinal cell proliferation and self-renewal. New cells are produced in the intestinal crypt and migrate out of the crypt and on to the villus in a conveyer belt like pattern. Cells at the tip of the villus die and are shed into the lumen. Differentiated cell types populate the villus. Absorptive enterocytes are most common. Tuft cells, goblet cells, and enteroendocrine cells are also present on the villus, and perform

specialized functions. Within the crypt, Paneth cells are present in the deep crypt, and surround intestinal stem cells. Transit amplifying (TA) cells reside just above the Paneth-stem cell zone.
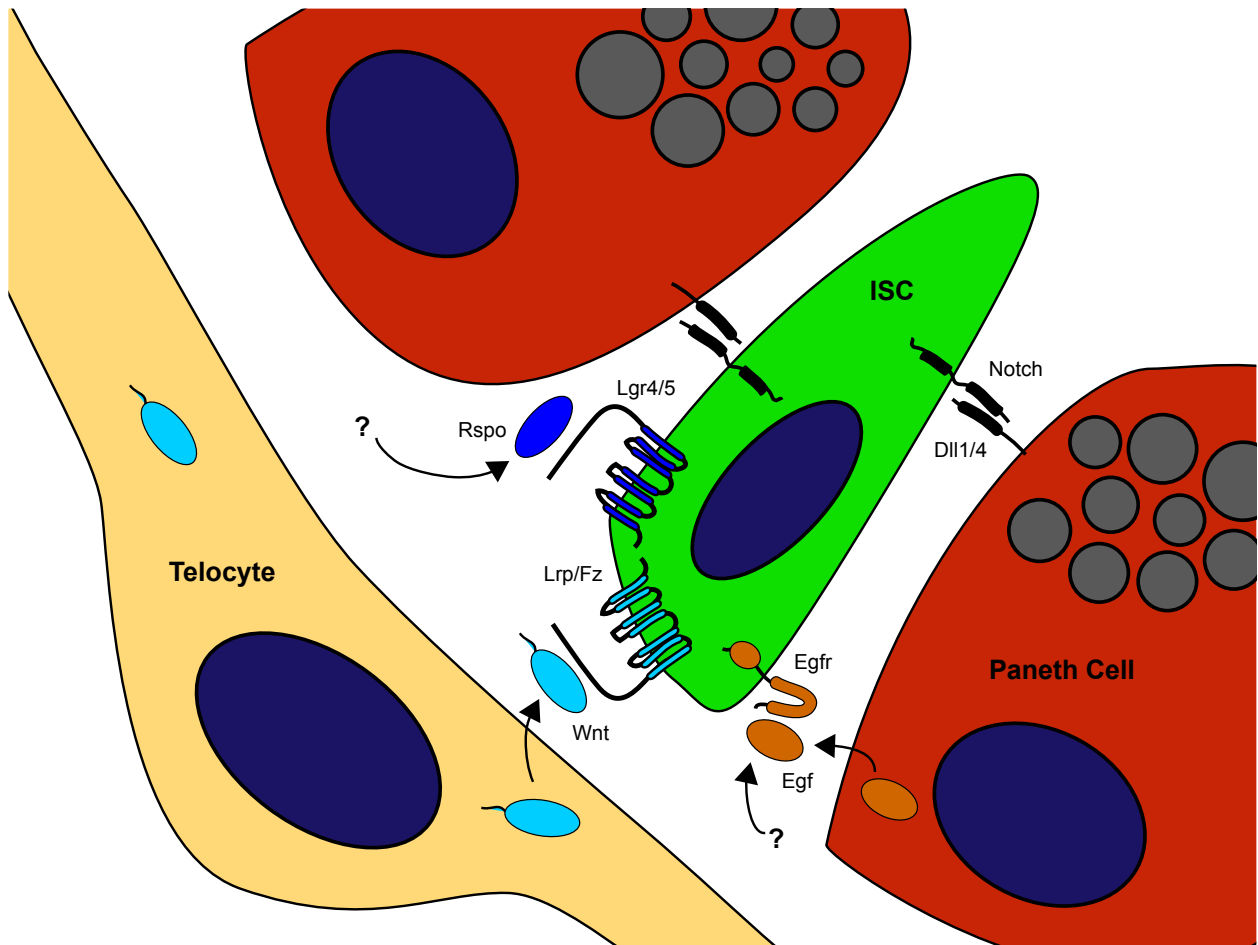
Figure 1.3 | The intestinal stem cell niche

Lgr5[+] ISCs are reliant on their niche to provide the proper growth signals for cell renewal and maintenance. The niche for *Lgr5*^{+} ISCs includes neighboring epithelial cells and stromal cells. Paneth cells immediately adjacent to *Lgr5*^{+} ISCs express the ligands DLL1 and DLL4, which signal to neighboring *Lgr5*^{+} ISCs through Notch receptors expressed by the stem cells. Paneth cells are also thought to secrete EGF ligands. Stromal cells, including sub-epithelial telocytes, supply Wnt ligands. Wnts expressed by stromal niche cells signal through Lrp/Frizzled receptor complexes. Rspondins are also critical, although their precise source is unclear. Rspondins are ligands for Lgr4/5 receptors on ISCs, and are critical for stem cell maintenance and self renewal.

Perturbations to any of these pathways or niche components affects stem cell proliferation and differentiation decisions[94,269].
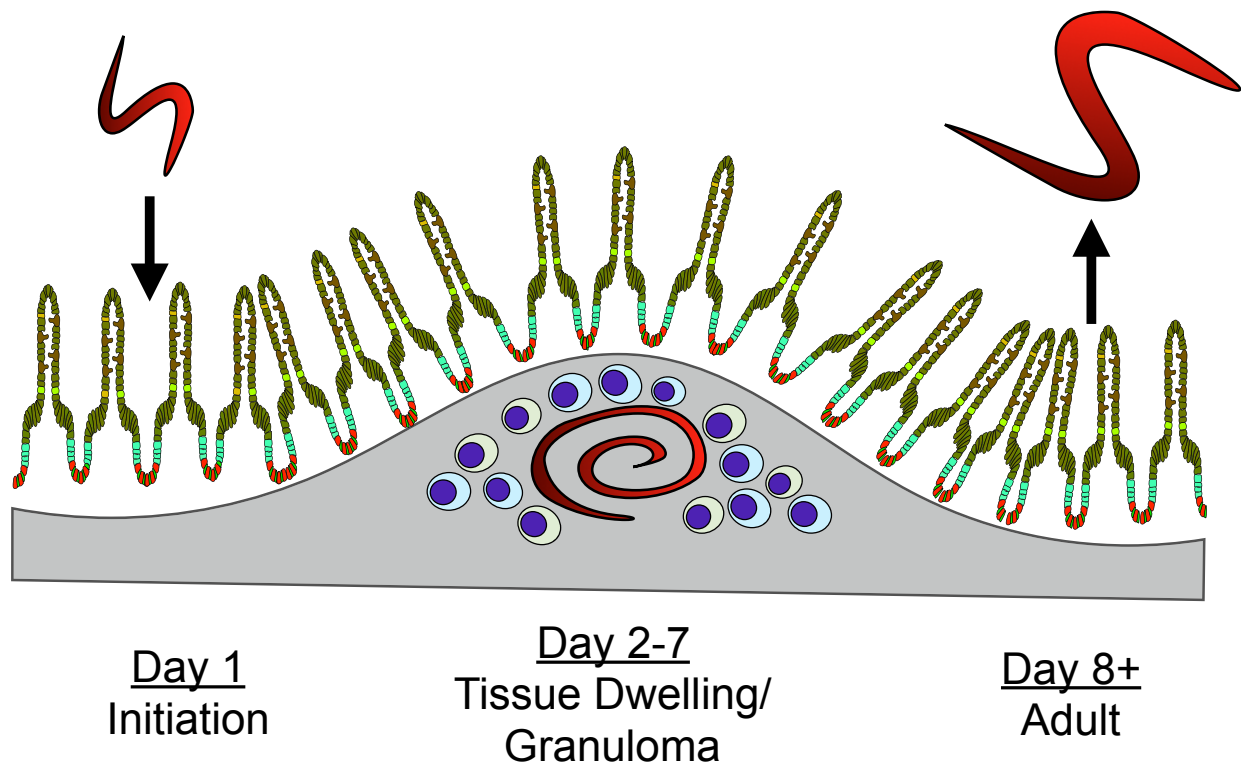
Figure 1.4 | Life cycle of *H. Polygyrus*

L3 stage larval Hp parasites initiate infection of mice after oral gavage into the stomach by migrating to the proximal duodenum. There, they penetrate through the intestinal epithelial barrier, accessing the sub-mucosal space within the first 24 hours of infection. After penetration, the larvae reside beneath the epithelium for approximately one week, while undergoing two molts. During this time, the worms are detected by the host immune system, and an aggregation of immune cells is recruited around the developing worm, forming a granuloma. At approximately the 8th day of infection, the worms leave these sites and cross the epithelial barrier again, gaining entry to the intestinal lumen. Within the proximal intestinal lumen, adult worms feed on luminal contents and lay eggs. The eggs are excreted with host feces.

Chapter 2: If a Stem Cell Dies in the Crypt, and No One Is Around to See It...

Ysbrand M. Nusse[1,2] and Ophir D. Klein[1,2,3]

[1] Biomedical Sciences Graduate Program, Program in Craniofacial and Mesenchymal Biology, University of California, San Francisco, San Francisco, CA 94143, USA

[2] Department of Orofacial Sciences, University of California, San Francisco, San Francisco, CA 94143, USA

[3] Department of Pediatrics and Institute for Human Genetics, University of California, San Francisco, San Francisco, CA 94143, USA

2.1 Abstract

Two recent studies continue the debate regarding lineage and hierarchy in the intestinal epithelium. One reports that quiescent crypt cells are Paneth cell precursors[150]. The second shows that tamoxifen induces apoptosis in crypt cells and that suppressing apoptosis alters lineage tracing patterns[270].

2.1.1 Preview of Buczacki *et al.*, 2013 and Zhu *et al.*, 2013

Epithelial tissues are routinely replenished during homeostasis and require repair after damage. A small number of self-renewing stem cells are the source of new cells in many epithelia. The identification of these stem cells has been the focus of intense investigation, and the principle approach has involved tamoxifen-inducible Cre lineage-tracing systems.

One of the best-understood epithelial stem cell systems is that of the intestine, whose entire lining is replaced every few days. New epithelial cells are born at the crypt base before migrating out of the crypt and differentiating into one of several cell types. Mature cells continue to migrate along the villus and are eventually shed into the gut lumen. The life span of a typical epithelial cell in the small intestine is 3–5 days, although Paneth cells located at the crypt base persist for several weeks.

Lineage tracing and other functional studies, building on decades of earlier work, point to two populations of intestinal stem cells. Crypt base columnar cells (CBCs), interspersed between Paneth cells and marked by the gene *Lgr5*, generate all the cell types of the epithelial crypt in vivo[29]. These cells, of which there are approximately 15 per crypt, can be isolated and grown in vitro to form organoid ''miniguts'' that resemble the intestinal crypt[16]. Alternatively, cells at the +4 position just above the Paneth cell zone have been put forward as stem cells. These cells die

43

from low doses of radiation, which may prevent accumulation of mutations in the stem cell pool[32]. Several genes are reported to mark these rare cells, including *Bmi1*, *mTert*, *Hopx*, and *Lrig1*. These cells are also thought to be quiescent, consistent with the classical notion that stem cells do not frequently cycle.

The debate regarding intestinal stem cell identity has been driven by several conflicting arguments. Crypts are clonal[79], meaning that they are derived from a single cell, a finding that appears to be at odds with the presence of a large number of *Lgr5*-positive stem cells per crypt. This paradox suggests the existence of a ''master'' stem cell hierarchically above the CBCs. In addition, the active proliferation of *Lgr5*-positive cells has vexed those who believe that a defining characteristic of adult tissue stem cells is quiescence. Finally, targeted killing of *Lgr5*-positive cells has no obvious short-term effects on crypt architecture or function, suggesting that these cells are dispensable[149].

Despite these issues, it has become accepted that *Lgr5*-positive cells are bona fide crypt stem cells. Models of neutral drift have countered arguments that the clonality of the crypt is inconsistent with a role for *Lgr5*-positive cells as stem cells[157]. Definitive analysis of +4 cells is challenging because markers of quiescent stem cells are also expressed in Lgr5-positive cells[32]. Finally, cells fated for differentiation and loss can revert to a stem-cell-like state after tissue damage and stem cell death, making plasticity in the crypt one potential explanation for the dispensability of *Lgr5*-positive cells. For example, progenitor cells that express the Notch ligand Dll1, which are normally restricted to a secretory fate, can dedifferentiate after irradiation and contribute to multiple lineages[127].

The argument for plasticity has been strengthened by a new report that a subset of *Lgr5*-positive cells are quiescent and are fated to become Paneth cells[150]. Buczacki and colleagues

developed an ingenious lineage tracing strategy that marks only label-retaining cells in the intestinal epithelium. The authors fused a fragment of Cre recombinase (CreA) to Histone 2B, under the control of a b-naphthoflavone (bNF)-inducible promoter expressed in intestinal epithelial cells. After a pulse of bNF, followed by a chase of several days, only quiescent cells (whose histones had not turned over) retained CreA. Administration of a dimerization agent reunited the histone-fused CreA fragment with its ubiquitously expressed counterpart CreB. This triggered lineage tracing in label-retaining cells through recombination. The authors found that during homeostasis, label-retaining cells were *Lgr5*-positive and were destined to become Paneth cells (**Fig. 2.1A, B**). Much like Dll1-positive progenitor cells, upon crypt damage these differentiated cells reverted to a stem-cell-like state (**Fig. 2.1C**).

These experiments help to reconcile competing notions of clonality, quiescence, hierarchy, and plasticity in the crypt. However, a recent study in *Cell Stem Cell* adds another perspective to the story, suggesting that the very methods used to identify intestinal stem cells may bias those results. Zhu and colleagues showed that intraperitoneal injection of tamoxifen, an agent used extensively to activate the inducible CreER molecules upon which most lineage tracing approaches rely, led to cell death in the crypt base[270]. They found that doses of tamoxifen typically administered in lineage tracing experiments induced apoptosis in both *Lgr5*-positive cells and *Lgr5*-negative cells in the +4 position (**Fig. 2.1E**). Because this phenomenon could substantially affect results garnered from lineage tracing using tamoxifen-induced recombination, the authors asked whether suppression of apoptosis affects lineage tracing. They found that transgenic mice that repressed apoptosis, either through overexpression of *Bcl2* or deletion of *Chk2*, had markedly different lineage tracing patterns compared to their wild-type counterparts. Importantly, they found that suppression of apoptosis led to a decrease in the

number of lineage tracing ribbons from *Lgr5*-positive cells, whereas lineage tracing from *Bmi1*-positive cells was increased (**Fig. 2.1E, F**). Consequently, the authors suggest that apoptosis in one stem cell population confers an advantage to another population of stem cells.

A gut reaction to this study is that many intestinal lineage-tracing experiments have been unintentionally biased due to the undetected death of progenitor cells. However, a number of issues must be addressed before far-reaching conclusions can be drawn. It is possible that the genetic strategies used in this study, such as the overexpression of *Bcl2*, could influence the physiology of the crypt and alter the behavior of stem cell populations. It is unclear why limited cell death has such a broad effect on lineage tracing from *Lgr5*-positive cells, and it is surprising that overexpression of *Bcl2* thoroughly shut down lineage tracing from *Lgr5*-positive cells. It is also possible that environmental factors, or genetic effects such as strain background, can differentially influence progeny production by specific stem cell pools. These questions can be addressed by the development of non-noxious lineage tracing agents.

The work by Zhu et al. raises an important point, which is that the methods used for lineage tracing should be stringently evaluated for unintended side effects and possible biases. As stated in a recent review, ''For any lineage tracer, the key features are that it should not change the properties of the marked cell, its progeny, and its neighbors''[27]. The new studies by Buczacki et al. and Zhu et al. continue the debate about the identity and location of intestinal stem cells, which does not yet appear to be over.
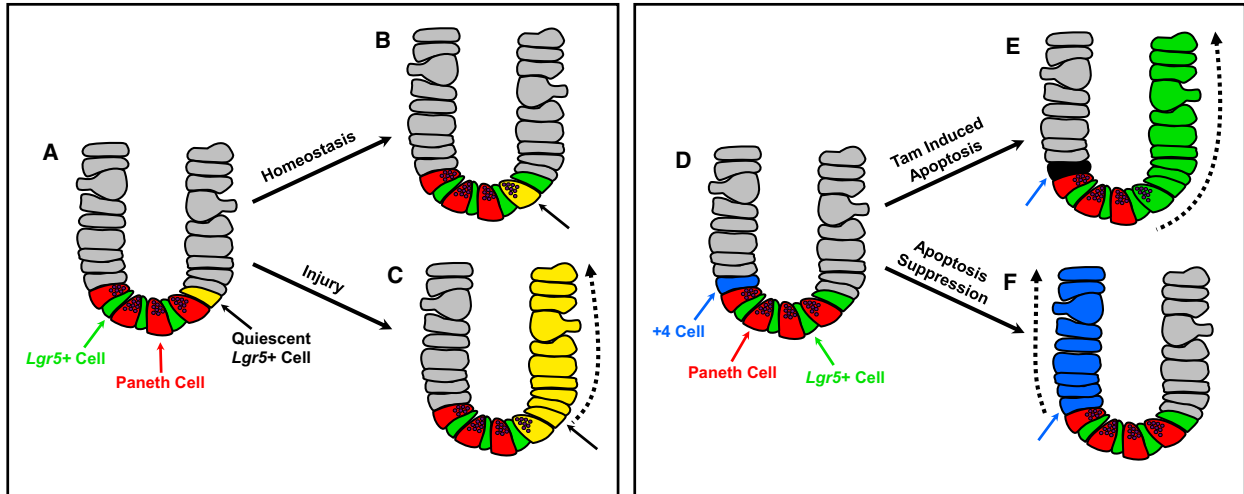
Figure 2.1 | Quiescence and Apoptosis in the Intestinal Crypt

(A) A subset of *Lgr5*-positive cells are quiescent (black arrow) and function as Paneth cell precursors. (B) Under normal conditions, quiescent *Lgr5*-positive cells are destined to become Paneth cells (black arrow). (C) After damage to the crypt, quiescent *Lgr5*-positive Paneth cell precursors (black arrow) can revert to a stem-cell-like state and give rise to lineage tracing clones as shown by Buczacki et al. (2013). (D) *Lgr5*-positive CBCs are interspersed between Paneth cells. +4 cells (blue arrow) reside just outside the CBC/Paneth cell zone. (E) Upon administration of tamoxifen (Tam), a small number of crypt base cells die (black cell with blue arrow), including CBCs and +4 cells. Zhu and colleagues argue that tamoxifen-induced death of +4 cells enhances lineage tracing from *Lgr5*-expressing CBCs. (F) Suppression of apoptosis blocks cell death in the +4 position and promotes lineage tracing from +4 cells. Lineage tracing from *Lgr5*-positive CBCs is severely reduced.

Chapter 3: Parasitic helminthes induce fetal-like reversion in the intestinal stem cell niche

Ysbrand M. Nusse[1,2,*], Adam K. Savage[3,*], Pauline Marangoni[2], Axel K.M. Rosendahl-Huber[2], Tyler A. Landman[2], Frederic J. de Sauvage[4], Richard M. Locksley[3,**], Ophir D. Klein[2,5,**]

[1]Biomedical Sciences Graduate Program, University of California, San Francisco, California 94143, USA

[2]Program in Craniofacial Biology and Department of Orofacial Sciences, University of California, San Francisco, California 94143, USA

[3]Howard Hughes Medical Institute and Departments of Medicine and Microbiology & Immunology, University of California, San Francisco, California 94143, USA

[4]Department of Molecular Oncology, Genentech Inc., South San Francisco, California 94080, USA

[5]Department of Pediatrics and Institute for Human Genetics, University of California, San Francisco, California 94143, USA

*These authors contributed equally to this work and are listed in random order.

**Corresponding authors with equal contribution

3.1 Abstract

Epithelial surfaces form critical barriers to the outside world and are continuously renewed by adult stem cells[2]. Whereas epithelial stem cell dynamics during homeostasis are increasingly well understood, how stem cells are redirected from a tissue-maintenance program to initiate repair after injury remains unclear. Here, we examined infection by *Heligmosomoides polygyrus* (Hp), a co-evolved pathosymbiont of mice, to assess the epithelial response to disruption of the mucosal barrier. Hp disrupts tissue integrity by penetrating the duodenal mucosa, where it develops while surrounded by a multicellular granulomatous infiltrate[263]. Unexpectedly, intestinal stem cell (ISC) markers, including *Lgr5*[29], were lost in crypts overlying larvae-associated granulomas, despite continued epithelial proliferation. Granuloma-associated *Lgr5⁻* crypt epithelia activated an interferon-gamma (IFNγ)-dependent transcriptional program, highlighted by Sca-1 expression, and IFNγ-producing immune cells were found in granulomas. A similar epithelial response accompanied systemic activation of immune cells, intestinal irradiation, or ablation of *Lgr5⁺* ISCs. Granuloma-associated crypt cells generated fetal-like spheroids in culture, and a sub-population of Hp-induced cells activated a fetal-like transcriptional program, demonstrating that adult intestinal tissues can repurpose aspects of fetal development. Thus, re-initiation of the developmental program represents a fundamental mechanism by which the intestinal crypt can remodel to sustain function after injury.

3.2 Methods

3.2.1 Mice

Mice were maintained in the University of California San Francisco (UCSF) specific pathogen-free animal facility in accordance with the guidelines established by the Institutional Animal Care and Use Committee and Laboratory Animal Resource Center. All experimental procedures were approved by the Laboratory Animal Resource Center at UCSF. Male and female mice aged 6–14 weeks were used for all experiments, except those analyzing fetal tissue. $Lgr5^{DTRGFP}$ mice were previously described[149]. Wild-type (C57BL/6J), $Lgr5^{GFP-CreERT2/+}$ (B6.129P2-$Lgr5^{tm1(cre/ERT2)Cle}$/J), $Rosa26^{RFP/+}$ (B6;129S6-$Gt(ROSA)26Sor^{tm14(CAG-tdTomato)Hze}$/J), IFNγ reporter (B6.129S4-$Ifng^{tm3.1Lky}$/J), IFNγ-null (B6.129S7-$Ifng^{tm1Ts}$/J), IFNγ receptor-flox ($Ifngr1^{loxP/loxP}$; C57BL/6N-$Ifngr1^{tm1.1Rds}$/J), and Vil1-Cre (B6.Cg-Tg(Vil1-cre)997Gum/J) mice were from The Jackson Laboratory (Bar Harbor, Maine). For analysis of embryonic tissue, timed matings were established and the morning after plugs were recognized was considered embryonic stage e0.5. Fetal intestine was dissected at the time points indicated.

3.2.2 Helminth infection and treatments

Mice were infected by oral gavage with 200 *H. polygyrus* (Hp) L3 larvae and were killed at the indicated time points. For anti-TCRβ treatment, mice were administered 20 μg per mouse of clone H57 i.p. and analyzed 24 hours later. For irradiation, mice were exposed to 10 gray and analyzed approximately 72 hours later. For ablation of $Lgr5^+$ cells, $Lgr5^{DTRGFP/+}$ mice were administered 50 μg/kg diphtheria toxin i.p. and analyzed at the indicated time points. For determination of cell proliferation, 500 μg of 5-Ethynyl-2′-deoxyuridine (EdU) was administered i.p. 1 hour prior to sacrifice, except as in **Fig. 3.10b**, at 24 hours prior to sacrifice. For lineage

50

tracing experiments, *Lgr5*^{*GFP-CreERT2/+*} *Rosa26*^{*RFP/+*} mice were infected with Hp and injected with 2.5 mg tamoxifen in corn oil i.p. at the indicated time points and analyzed at day 6.

3.2.3 Tissue preparation and flow cytometry

Preparation of intestinal tissue for flow cytometry was modified from previous work[271]. The duodenum was dissected, flushed extensively with cold PBS, and the mesenteric tissue was removed. For whole tissue preps, Peyer's patches were removed and tissue was turned inside-out. For recovery of punch biopsies tissue was fileted open longitudinally. In both cases, tissue was shaken in three changes of 20 ml cold PBS and washed for 20 minutes at 37°C in two changes of 20 ml Ca^{2+}/Mg^{2+}-free HBSS containing 5 mM DTT, 10 mM HEPES, and 2% FCS, followed by 20 ml of Ca^{2+}/Mg^{2+}-replete HBSS containing 10 mM HEPES and 2% FCS. For punch biopsies, granuloma and non-granuloma tissue was dissected with a 1 mm punch tool under low-power magnification. Tissues were digested for 30 minutes at 37°C in 5 ml (whole tissue) or 2 ml (punch biopsies) Ca^{2+}/Mg^{2+}-replete HBSS containing 10 mM HEPES, 2% FCS, 30 mg/ml DNaseI (Roche), and 0.1 Wünsch/ml LibTM (Roche), and whole tissue was homogenized in C tubes using a gentleMACS tissue dissociator (Miltenyi). Homogenate or punch biopsies were passed through a 100 μm filter with assistance of a 3 ml syringe plunger, and enumerated for staining equivalent numbers for flow cytometry or sorting. Fc Block (anti-CD16/32), doublet exclusion, and DAPI exclusion were used in all cases. Data were acquired with a Becton Dickinson Fortessa and analyzed using FlowJo (Tree Star). Cell sorting was performed with a Beckman Coulter MoFlo XDP.

3.2.4 Immunofluorescence and *in situ* hybridization

For tissue staining in section, mice were perfused with cold 4% PFA in PBS. The proximal 10 cm of duodenum was cleaned, flushed with cold 4% PFA, and fixed in 4% PFA for 4 hours at 4°C. The tissue was cryo-protected in 30% sucrose overnight at 4°C. Samples were embedded in OCT and 8 μm sections were prepared for immunofluorescence staining. For immunohistochemistry and *in situ* hybridization, the samples were fixed overnight in 4% PFA, paraffin embedded, and sectioned at 5 μm for immunohistochemistry or 10 μm for *in situ* hybridization. For crypt area quantitation, crypts clearly above distended granuloma tissue containing visible larval worms were called as "gran" and others were called "non-gran". Crypt area was quantitated in ImageJ. For fetal whole mount imaging, fetal intestines were fixed in 4% PFA in PBS for 3 hrs, permeabilized, and blocked for 4 hours at room temperature. Primary and secondary antibodies were incubated at 4°C overnight. Images were acquired and processed with a Leica DM5000 B or a Zeiss Axio Imager 2 and Adobe Photoshop.

3.2.5 *In Situ* Hybridization

An *Olfm4* probe was designed by PCR amplifying an 898 bp sequence from total intestinal cDNA using the primers 5'-AACCTGACGGTCCGAGTAGA-3' (forward) and 5'-TGCTGGCCTCAGTTGCATAA-3' (reverse). *Olfm4* cDNA was cloned into a pGEM-T Easy vector (Promega). *Olfm4* anti-sense probes were prepared and *in situ* hybridization was performed as described[272].

3.2.6 Bulk RNA sequencing

Five wild-type mice were infected with Hp and six days later 1 mm punch biopsies from granuloma and non-granuloma tissue were taken, pooled by tissue, digested, and sorted for

DAPI^{lo} CD45$^-$ EpCAM$^+$ CD44$^+$ crypt epithelium. RNA from six granuloma (30 mice total) and five non-granuloma (25 mice total) sorts was submitted for RNA sequencing. Two granuloma data sets were excluded due to low unique mapping rates and failure to group by tissue in principle components analysis and hierarchical clustering. The remaining data were filtered for a combination of minimum read count, false discovery rate, and fold-change comparison, as indicated in figure legends. Heat maps were generated using Morpheus (https://software.broadinstitute.org/morpheus/) and upstream regulators were determined using Ingenuity Pathways Analysis (Qiagen). Predicted mouse IFN targets were determined using Interferome (http://interferome.its.monash.edu.au/interferome) with default settings. GSEA analysis[273] was done with 1000 permutations by gene set. The expression dataset was generated by filtering out low abundance genes. Hallmark gene sets were obtained from the Broad MSigDB[274]. Additional gene sets were generated from published datasets[68,72,275].

3.2.7 Single cell RNA sequencing

Sca-1$^+$ or Sca-1$^-$ crypt cells were sorted from one mouse infected with Hp for 6 days. The two resulting cell suspensions (~70,000 cells each) were submitted as separate samples to be barcoded for single cell RNAseq using the Chromium Controller (10X Genomics) and the Single Cell 3' Library Kit v2 (PN-120236/37/62). Resulting libraries were sequenced on a HiSeq 4000 (Illumina) using HiSeq 4000 PE Cluster Kit (PN PE-410-1001) with HiSeq 4000 SBS Kit (150 cycles, PN FC-410-1002), with one sample being loaded per sequencing lane. About 20,000 Sca-1$^-$ cells (15,000 reads per cell) and about 7,300 Sca-1$^+$ cells (40,000 reads per cell) were successfully barcoded and their transcriptomes sequenced. Raw sequencing data were processed for initial QC analysis and alignment by our sequencing core (Institute of Human Genetics,

UCSF) using Cell Ranger software. Further analysis of differential gene expression and unsupervised hierarchical clustering were performed using the Seurat package (v2.0)[276,277]. Samples were merged after read depth correction and the combined dataset was filtered to exclude cells expressing less than 200 genes. Additionally, genes detected in less than 10 cells were removed from the analysis. Variable gene expression was assessed in the filtered dataset after correction for mitochondrial gene expression. Linear reduction of the data was performed using principle components analysis, focusing on the first 15 principle components determined to be significant to explain variation in the dataset via a large permutation test. Cells were clustered using the function FindClusters with a resolution parameter of 2.0. Graphical representation was achieved using the t-SNE algorithm, upon which the independently identified clusters were color-coded. Published lists[72,275] of markers for various intestinal crypt cell types were visualized on the clusters with the DoHeatmap function of the Seurat package. For analysis of cluster contribution by Sca-1$^+$ or Sca-1$^-$ crypt cells (**Fig. 3.13a**), cell numbers were first normalized to the total number sequenced for each population. We considered Cluster 19 to be an aberrant cluster due to low cell number (33 of 26,423 total), enrichment for multiple intestinal lineages, and isolation in t-SNE analysis. The mean normalized expression values by cluster and mean normalized expression values presented in the heat maps are available online at https://www.nature.com/articles/s41586-018-0257-1#Sec18. The hypergeometric test for enrichment of the fetal gene program signature within each cluster is available in **Table 3.6**.

3.2.8 Antibodies

The following antibodies (BioLegend) were used for flow cytometry: CD45 (30-F11), CD326/EpCAM (G8.8), CD44 (IM7), Sca-1 (D7), TCRβ (H57), γδTCR (GL3), NK1.1 (PK136),

CD90.2 (53-2.1), CD11b (M1/70), Gr1 (RB6-8C5). For immunofluorescence staining in section, the follow antibodies were used: GFP (GFP-1020, Aves; ab13790, Abcam), Ki67 (Sp6, Thermo Fischer Scientific), E-cadherin (24E10, Cell Signaling Technology), Sca-1 (e13-161.7, Biolegend), Muc2 (SC-15334, Santa Cruz Biotechnology), Mmp7 (AF2967, R&D Systems). EdU was detected using Click-iT Plus EdU Assay Kit (ThermoFisher).

3.2.9 Organoid culture

Cultures from sorted single cells were established as described[132]. Briefly, $CD45^-$ $EpCAM^+$ $CD44^+$ $Sca-1^+$ and $Sca-1^-$ cells were sorted into PBS containing 10% FCS. Cells were re-suspended in GFR, Phenol-free Matrigel (Fisher) supplemented with 500 ng/ml EGF (Sigma-Aldrich), 1 µg/ml Noggin (R&D Systems), 10 µM Jagged-1 peptide (Anaspec), and 10% R-Spondin1 Conditioned Medium (Gift of Noah Shroyer, Baylor College of Medicine). Fifty µl of Matrigel containing cells were plated in a 24-well cell culture plate, and left to set at 37°C for 15 minutes. Pre-warmed 37°C ENR Medium (Advanced DMEM/F12, 10 mM HEPES, 1X GlutaMAX, 1% Pen/Strep, 1X N-2 Supplement, 1X B-27 Supplement, 1 mM N-Acetylcysteine, 100 ng/ml Noggin, 50 ng/ml EGF, 5% R-Spondin1 Conditioned Media) with 2.5 µM CHIR99021, 2.5 µM Thiazovinin, and 1 µM Jagged-1 peptide was overlaid. Cells were cultured at 37°C. After 3 days, the medium was exchanged for ENR medium without CHIR99021, Thiazovinin, or Jagged-1 peptide. Cultures were passaged after 8 days and then every 5-7 days thereafter with growth factor-free Matrigel. Cultures were typically analyzed at the end of the first passage by imaging and qPCR. Some qPCR experiments were conducted on established cultures, such as in **Fig. 3.11c-f**. For *in vitro* IFNγ treatment, wild type organoid lines were prepared from whole crypts and treated 3 days after passage by exchanging the standard

organoid medium with fresh organoid medium containing 5 ng/ml IFNγ (485-MI, R&D Systems). Twenty-four hours later, organoids were harvested by centrifugation, aspirating the media and Matrigel, and lysed using RLT buffer (Qiagen).

3.2.10 Quantitative PCR

RNA from 5 mm whole tissue (after QIAshredder), sorted cells, or organoids was extracted using RNeasy Mini or Micro Kits (Qiagen). cDNA was synthesized with High Capacity cDNA Reverse Transcription Kits (Applied Biosystems). qPCR reactions were performed using Power SYBR Green (Invitrogen) on an Applied Biosystems StepOnePlus for whole tissue, or iTaq Universal SYBR Green Supermix (Bio Rad) in 384-well plates on a QuantStudio 6 Flex Real-Time PCR System (Thermo Fisher Scientific) for sorted cells and organoids. Primers used for qPCR are listed in **Table 3.7**.

3.2.11 Statistics

Except in **Fig. 3.5f**, all data points are biological replicates, randomly assigned without investigator blinding. All experiments were replicated at least twice. No data were excluded, except in the bulk RNAseq experiment, as noted in the Methods. No statistical methods were used to predetermine sample size and differences in intra-sample variances were present. Statistical significance was determined in Prism (GraphPad Software) using an unpaired, two-tailed Mann-Whitney test without multiple comparisons correction, except for the use of unpaired, two-tailed t-tests in **Fig. 3.8e** and **Fig. 3.11c-f**, as noted in the legend. Bar charts indicate the mean of samples and error bars represent ± S.D. of the mean. * $P< 0.05$, ** $P < 0.01$, *** $P < 0.001$, **** $P < 0.0001$. Hypergeometric tests were performed using GeneProf[278].

3.2.12 Data availability

The RNA sequencing data reported in this study are available at the Gene Expression Omnibus under accession codes GSE97405 (bulk) and GSE108233 (single-cell).

3.3 Results

3.3.1 Helminth infection induces an *Lgr5⁻* program in affected crypt epithelium.

To study how intestinal crypts cope with tissue disruption, we infected *Lgr5^{DTRGFP/+}* (Lgr5-GFP) reporter mice[149] with Hp. Six days after infection, larvae resided within the intestinal wall surrounded by an immune infiltrate. Crypts overlying granulomas (granuloma-associated crypts, GCs) were hyper-proliferative and enlarged (**Fig. 3.1a-d**), as previously reported[279]. Strikingly, GCs lost expression of the Lgr5-GFP reporter (**Fig. 3.1a'**), while non-granuloma-associated crypts retained expression of Lgr5-GFP (**Fig. 3.1a''**). *Olfm4*, another ISC marker, was similarly repressed (**Fig. 3.1e**). In addition to loss of *Lgr5* and *Olfm4*, the Paneth cell marker MMP7 often co-stained with the goblet cell marker MUC2 (**Fig. 3.1f-g**), as previously recognized in helminth infections[280] and other perturbations of epithelial lineage commitment[131]. Thus, the epithelium overlying granulomas exhibits loss of ISC markers and disruption of the ISC niche[89].

To assess response pathways within GCs, we purified crypt epithelium from granuloma punch biopsies (**Fig. 3.2a**) and performed RNAseq analysis. We found 277 differentially expressed genes between granuloma and non-granuloma crypt biopsies (**Fig. 3.2b, c, Table 3.1, and Table 3.2**). In addition to *Lgr5* and *Olfm4*, a suite of ISC signature genes[68] was down-regulated in GCs (**Fig. 3.2d, e, Table 3.3**), confirming that Hp infection represses ISCs. Among the genes up-regulated in GCs were an abundance of IFN signaling targets (**Fig. 3.2b**), and pathway analysis revealed an IFN response (**Fig. 3.2f** and **Table 3.4**).

3.3.2 IFNγ mediates the helminth-induced crypt phenotype.

One of the most up-regulated genes was Sca-1 (*Ly6a*), a surface protein associated with proliferative cells, although not present in human. Sca-1 is an interferon target recognized to be induced on epithelia during colitis[281], and immunofluorescence revealed that Sca-1 specifically marked Lgr5-GFP⁻ GCs (**Fig. 3.3a**). Flow cytometry confirmed that Sca-1 was enriched in GC biopsies (**Fig. 3.3b**) and revealed that Sca-1 up-regulation occurred as early as two days after infection (**Fig. 3**.**3c**, **d**). Furthermore, Sca-1 expression was distinct from Lgr5-GFP at all time points examined. As a result of this tight inverse correlation, Sca-1 was a useful marker of crypt cells responding to Hp-driven epithelial disruption. By day 10 post-infection, diminished Sca-1 expression at granuloma remnants (**Fig. 3.3e**) indicated that resolution had commenced. Another intestinal helminth, *Nippostrongylus brasiliensis*, which does not invade intestinal tissue, did not induce Sca-1 expression (**Fig. 3.3f**), suggesting a requirement for crypt disruption.

Although helminthes are typically associated with allergic immunity[249], our data pointed to a role for IFN. We focused on IFNγ, because elevated transcripts of this gene were found in granulomas of infected mice (**Fig. 3.4a**), and there was no induction of Type I and Type III IFN transcripts in GCs (**Table 3.5**). We also found large numbers of neutrophils, which are known targets of IFNγ[282], and an accumulation of IFNγ⁺ lymphocytes in granulomas (**Fig. 3.4b-e**). Hp infection of IFNγ-null mice showed that Sca-1 (**Fig. 3.5a**, **b**) and IFN target gene induction (**Fig. 3.5c**) were dependent on IFNγ, although down-regulation of the Lgr5-GFP reporter was unchanged (**Fig. 3.5d**). To assess the cell-autonomous effects of IFNγ on intestinal epithelia, we deleted the IFNγ receptor in intestinal epithelium and found a similar effect as with germline deletion of IFNγ (**Fig. 3.5e**). Treating intestinal organoids with IFNγ led to transcriptional

changes corresponding to those found in GCs (**Fig. 3.5f**). Together, these data demonstrate that immune cell-derived IFNγ is a critical component of the GC response.

3.3.3 The crypt response to *H. polygyrus* is a generalized response to tissue injury.

Lymphocyte activation and IFNγ production are elicited in other contexts of epithelial injury[283–285]. Therefore, we challenged uninfected mice with anti-TCRβ to assess the host response to immune cell activation. After 24 hours, *Ifng* transcript was elevated (**Fig. 3.6a**), and the intestinal epithelium broadly resembled the Hp GC response, as evidenced by reduction of Lgr5-GFP, induction of Sca-1, increased proliferation and crypt size (**Fig. 3.6b-g**), and expression of a subset of Hp-activated transcriptional targets (**Fig. 3.6h**).

The convergence of epithelial responses to immune cell activation following Hp infection and anti-TCRβ challenge might reflect a generalized reaction to tissue perturbation. To test this, we examined additional injury models. First, we lethally irradiated mice and analyzed them after three days, at which time *Lgr5* expression is lost during regeneration[222,224]. We observed Sca-1 induction (**Fig. 3.7a-d),** continued proliferation (**Fig. 3.7e-f),** an IFN response in crypt cells (**Fig. 3.7g**), as well as increased crypt depth (**Fig. 3.7h**), as previously reported[222].

Because irradiation is relatively non-specific, we sought to restrict cell death to the stem cell compartment by specifically ablating *Lgr5*-expressing cells[149]. Twenty-four hours after treatment of *Lgr5DTRGFP/+* mice with diphtheria toxin (DT), Lgr5-GFP cells were absent, and Sca-1 was highly induced (**Fig. 3.8a-d**). During recovery, Lgr5-GFP+ ISCs re-emerged and Sca-1 expression decreased to baseline levels (**Fig. 3.8e**). Notably, *Lgr5*+ cell ablation did not induce crypt hyperplasia (**Fig. 3.8f)** or GC-like IFN targets (data not shown), revealing distinctions between the Sca-1 response in *Lgr5* ablation and other epithelial perturbations. However, IFN

activation has been noted after *Lgr5*^{+} cell ablation in tumors[153]. Thus, diverse insults that disturb *Lgr5*^{+} cells induce GC-like responses during regeneration.

3.3.4 Sca-1^{+} cells arise from pre-existing *Lgr*5^{+} cells

Lgr5^{+} cells are required for regeneration after irradiation-induced injury[224]. To test their necessity for the Hp-induced GC phenotype, we ablated *Lgr5*^{+} cells immediately before infection. In this setting, although we confirmed that GC cells were part of the *Lgr5*^{+} ISC lineage hierarchy (**Fig. 3.9a**, **b**), crypt cell frequency, Sca-1 induction, and EdU incorporation were unaffected (**Fig. 3.9c-h**). These data indicate that while the Hp-induced GC phenotype is mediated by ISC progeny, it can occur independently of *Lgr5*^{+} ISCs.

3.3.5 Helminth-associated crypts acquire a fetal-like program.

Sca-1^{+} GC cells were hyper-proliferative and gave rise to granuloma-associated villus epithelium (**Fig. 3.10a, b**). To assess the generative capacity of GCs, we sorted Sca-1^{+} and Sca-1^{−} crypt cells from Hp-infected mice and cultured them under standard organoid conditions. Whereas Sca-1^{−} cells formed typical organoids (**Fig. 3.11a**), Sca-1^{+} cells formed large, smooth spheroids devoid of crypt budding (**Fig. 3.11b**) and were stably passaged for more than six months (data not shown). Sca-1^{+} spheroids lost expression of markers of differentiated epithelium (**Fig. 3.11c**), suggesting that they reflected growth of an undifferentiated cell type. Spheroids have been observed in high Wnt conditions[89]; however, in our studies, we did not add exogenous Wnt, and we found no difference in *Axin2* expression between Sca-1^{+} and Sca-1^{−} cultures (**Fig. 3.11d**), suggesting that Wnt signaling is not hyperactive in Sca-1^{+} spheroids. Recent work[275,286] has demonstrated that spheroids are formed from fetal epithelium. We tested expression of fetal epithelial markers and found that nearly all fetal genes assayed were highly

expressed in Sca-1$^+$ cultures (**Fig. 3.11e, f**). Like fetal cultures[286], Sca-1$^+$ spheroids were not sensitive to R-Spondin1 withdrawal (data not shown). Thus, Sca-1$^+$ cells adopted a state *in vitro* that was distinct from Sca-1$^-$ cells and that highly resembled fetal intestinal epithelium.

We sought to determine whether the fetal program was activated *in vivo* and found that the fetal markers *Gja1* and *Spp1* were up-regulated in GCs during Hp infection (**Fig. 3.12a**). Furthermore, Sca-1 was expressed in mouse fetal intestinal epithelium at embryonic day 15.5 (**Fig. 3.12b**). This remarkable similarity led us to re-analyze our RNAseq of GC epithelium. We found strong enrichment of the fetal signature in GC epithelium, while the adult signature was enriched in non-GCs (**Fig. 3.12c, Table 3.3,** and **Table 3.4**). Furthermore, the signatures[72] of stem cells, enterocytes, and Paneth cells, although not goblet cells, were lost in GCs (**Fig. 3.12d, Table 3.3,** and **Table 3.4**). Taken together, these data indicate that GCs adopt an undifferentiated state resembling the fetal epithelium during infection.

3.3.6 A novel subset of fetal cells arise within GCs

Enrichment of the goblet cell signature in GC epithelium suggested heterogeneity within the pool of Sca-1$^+$ cells. To investigate whether a subgroup of cells underpinned the fetal signature, we performed single-cell RNA sequencing analysis of Sca-1$^+$ and Sca-1$^-$ crypt cells. Unsupervised clustering of the merged datasets revealed that most cell clusters were composed of both Sca-1$^+$ and Sca-1$^-$ cells (**Fig. 3.13a**, **b**) and, although we excluded mature epithelium, the transcriptional signature of specific lineages could be recognized in some clusters (**Fig. 3.14**). We focused on Cluster 12, which consisted almost entirely of Sca-1$^+$ cells (98.2%). By overlying known intestinal cell type signatures[72,275], we found that Cluster 12 was depleted for mature cell markers (**Fig. 3.14**), and was strongly enriched for the fetal program (**Fig. 3.13b** and **Table 3.6**),

suggesting that this cluster represented a unique cell identity elicited by Hp infection within the larger Sca-1$^+$ pool.

3.4 Discussion

It has been postulated that intestinal crypts respond to damage by activation of reserve stem cells[222,287] or reacquisition of stem-ness by differentiated progenitors[127,150,151]. Here, our use of an evolutionarily adapted parasite led to identification of a novel infection-mediated alteration of the crypt in response to injury. By monitoring the markers Lgr5-GFP and Sca-1, respectively, we found that an overlapping injury response program was engaged by other tissue-damaging agents, indicating a generalized strategy by which the intestine copes with stress. Our data identify a novel cell type arising in the damaged crypts and suggest that crypt repair repurposes aspects of fetal development in order to restore barrier integrity. Indeed, a re-activation of fetal markers has been observed in models of injury in other tissues[288–290], including a recent report of the damaged colon which corroborates some of our findings[291]. Taken together, these data reveal that helminth-induced changes in crypt epithelia repurpose some of the functional capabilities of the developing fetal gut and point to a novel mechanism of repair in the intestinal crypt involving infection-induced developmental plasticity.
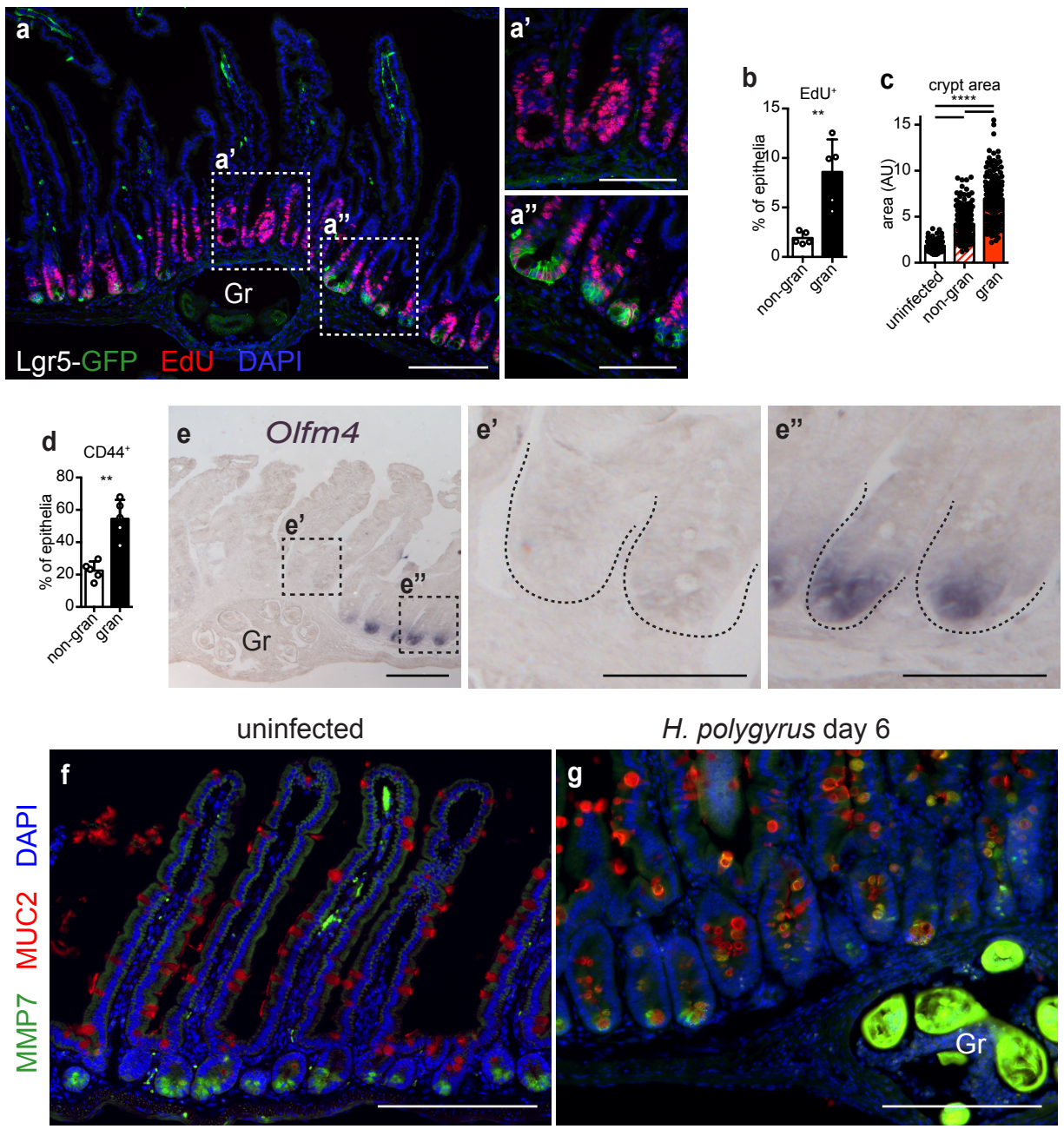
Figure 3.1 | Helminth infection induces an *Lgr5−* program in affected crypt epithelium.

Analysis of crypts overlying (gran) or adjacent to (non-gran) *H. polygyrus* granulomas (Gr) from

day 6 of infection. **a**, Representative image of Lgr5–GFP and EdU staining in thin section. **b**,

Flow cytometry of EdU in biopsies of total epithelium. **c**, Crypt area from uninfected or infected (non-gran, gran) mice. **d**, Flow cytometry of CD44$^+$ epithelium from non-granuloma or granuloma biopsies. **e**, Representative image of *in situ* hybridization for *Olfm4* in thin section. **f**, **g**, MMP7 and MUC2 staining in normal duodenum or duodenum from mice infected with *H. polygyrus*. Gr, granuloma. $n = 5$ mice (**a**, **b**, **d, e, f, g**), 6 mice (**c**, uninfected), or 15 mice (**c**, infected). Statistics represent all biological replicates, and all experiments were replicated at least twice. Graphs are centered on mean with bars showing s.d. (**b**, **c, d**). **P < 0.01, ****P < 0.0001 by unpaired, two-tailed Mann–Whitney test. Scale bars: 200 μm (**a**, **e**, **f**, **g**), 100 μm (**a'**, **a"**), 50 μm (**e'**, **e"**).
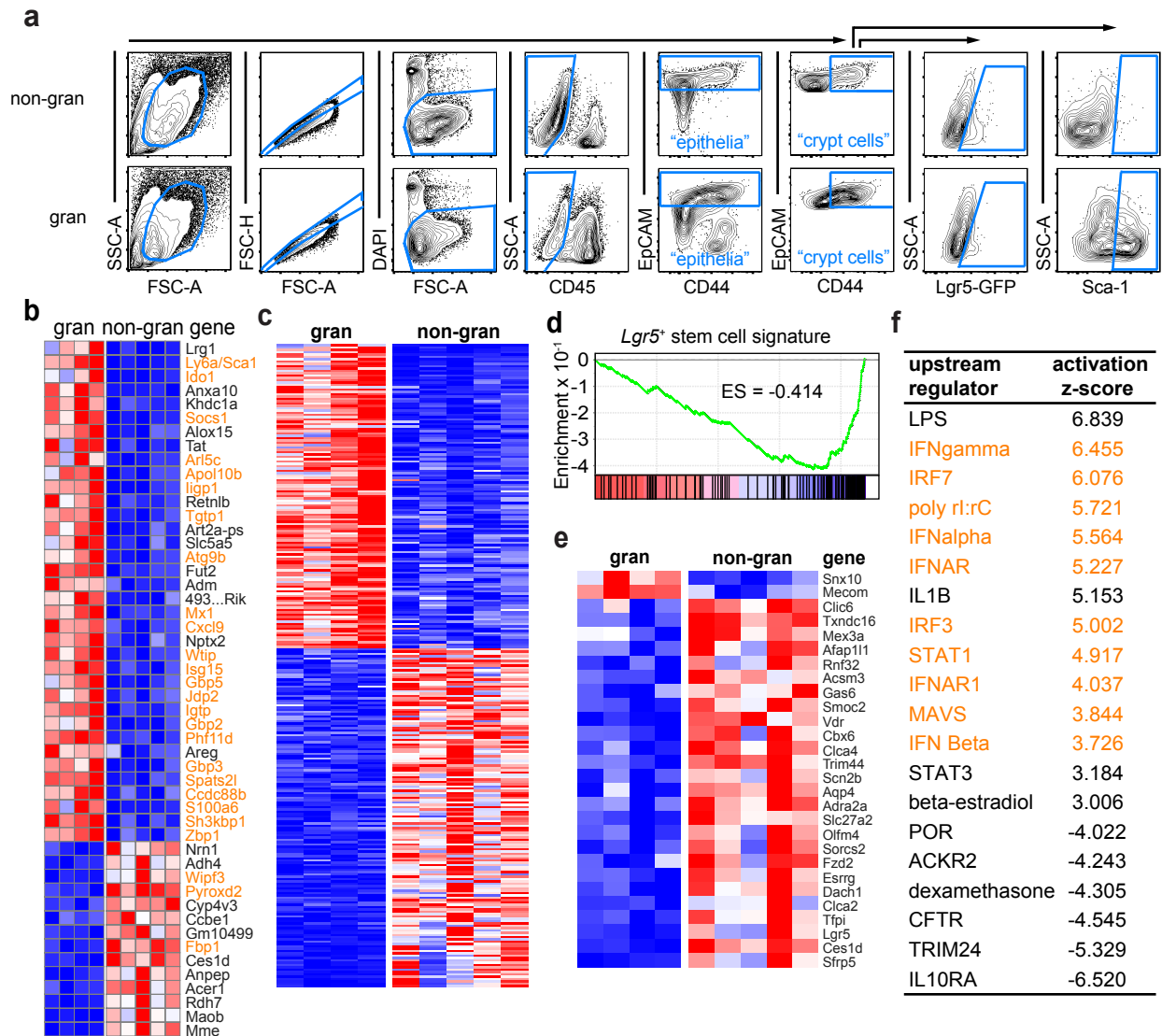
Figure 3.2 | RNA-seq analysis of granuloma-associated crypt epithelium.

a, Representative gating example of epithelia, crypt cells, Lgr5–GFP and Sca-1 in biopsied tissue six days after *H. polygyrus* infection. Unfractionated tissue preps (as in **Fig. 3.3d**) were gated similarly. **b–f**, Crypt epithelium was sorted from granuloma and non-granuloma biopsies and subjected to RNA-seq analysis as indicated in Methods. **b**, RNA-seq of sorted crypt epithelium from non-granuloma or granuloma biopsies. Data were filtered for ≥100 reads average in either

group, FDR $\leq 10^{-4}$, and the 50 genes with the greatest fold-change are presented; high (red) and low (blue) relative expression. Gene names in orange are predicted IFN targets.

c, The data were filtered for ≥ 100 reads average in either group, FDR ≤ 0.05, and fold-change comparison of ≥ 2. The 277 genes that passed were compiled into a heat map demonstrating high (red) and low (blue) relative expression. **d**, GSEA for $Lgr5^+$ signature genes[68]. FDR <0.01. ES, enrichment score. **e**, $Lgr5^+$ intestinal stem cell signature genes[68] were cross-referenced to the RNA-seq dataset. Data were filtered as in (**c**) except no fold-change requirement was applied. **e**, The unfiltered RNA-seq dataset was analyzed for upstream regulators using Ingenuity Pathways Analysis. The activation Z score indicates the extent of enrichment of targets within the RNA-seq dataset downstream of the indicated regulator, with a positive score indicating enrichment. IFN-related pathways are highlighted in orange. $n = 4$ independently sorted samples (**b**, **c**, **d**, granuloma, 20 mice total), or 5 independently sorted samples (**b**, **c**, **d**, non-granuloma, 25 mice total).
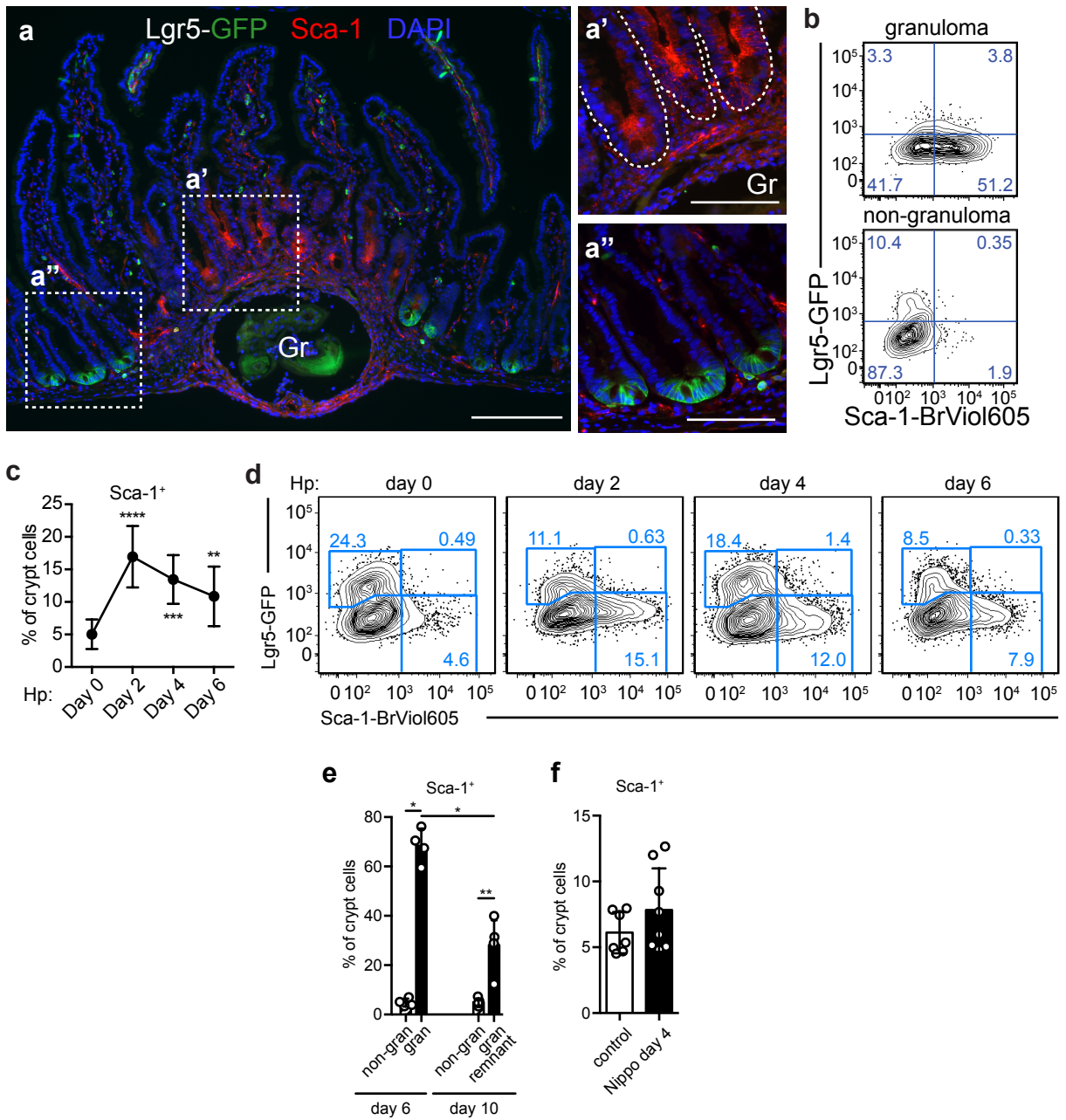
Figure 3.3 | Sca-1 is expressed in granuloma crypt epithelium.

Day 6 of *H. polygyrus* infection, except as noted. **a**, Representative image of Lgr5–GFP and Sca-1 staining in crypts overlying (**a'**) and adjacent to (**a"**) granulomas. **b**, Representative flow

cytometry of Lgr5–GFP and Sca-1 in crypt biopsies. **c**, Flow cytometry of Sca-1 in crypts from

unfractionated epithelium. **d**, Representative flow cytometry of Lgr5–GFP and Sca-1 in crypt

cells from unfractionated duodenum preps of Lgr5–GFP mice were analyzed after *H. polygyrus*

infection. **e**, Flow cytometry of Sca-1 in crypt cells from biopsies from mice 6 or 10 days after

infection with *H. polygyrus*. **f**, Flow cytometry of Sca-1 in crypt cells from unfractionated

duodenum preps of mice 4 days after infection with *N. brasiliensis* (Nippo). $n = 4$ (**b, d**, days 2,

4, 6, **e**, day 6), 5 (**a, d**, day 0, **e**, day 10), 7 (**f**, controls), 8 (**c**, day 1, 2, 4, **f**, Nippo), or 9 mice (**c**,

day 0). Statistics represent all biological replicates, and all experiments were replicated at least

twice. Graphs are centered on mean with bars showing s.d. (**c, e–f**). *$P < 0.05$, **$P < 0.01$,

***$P < 0.001$, ****$P < 0.0001$ by unpaired, two-tailed Mann–Whitney test. Scale bars: 200 μm

(**a**), 100 μm (**a', a"**).
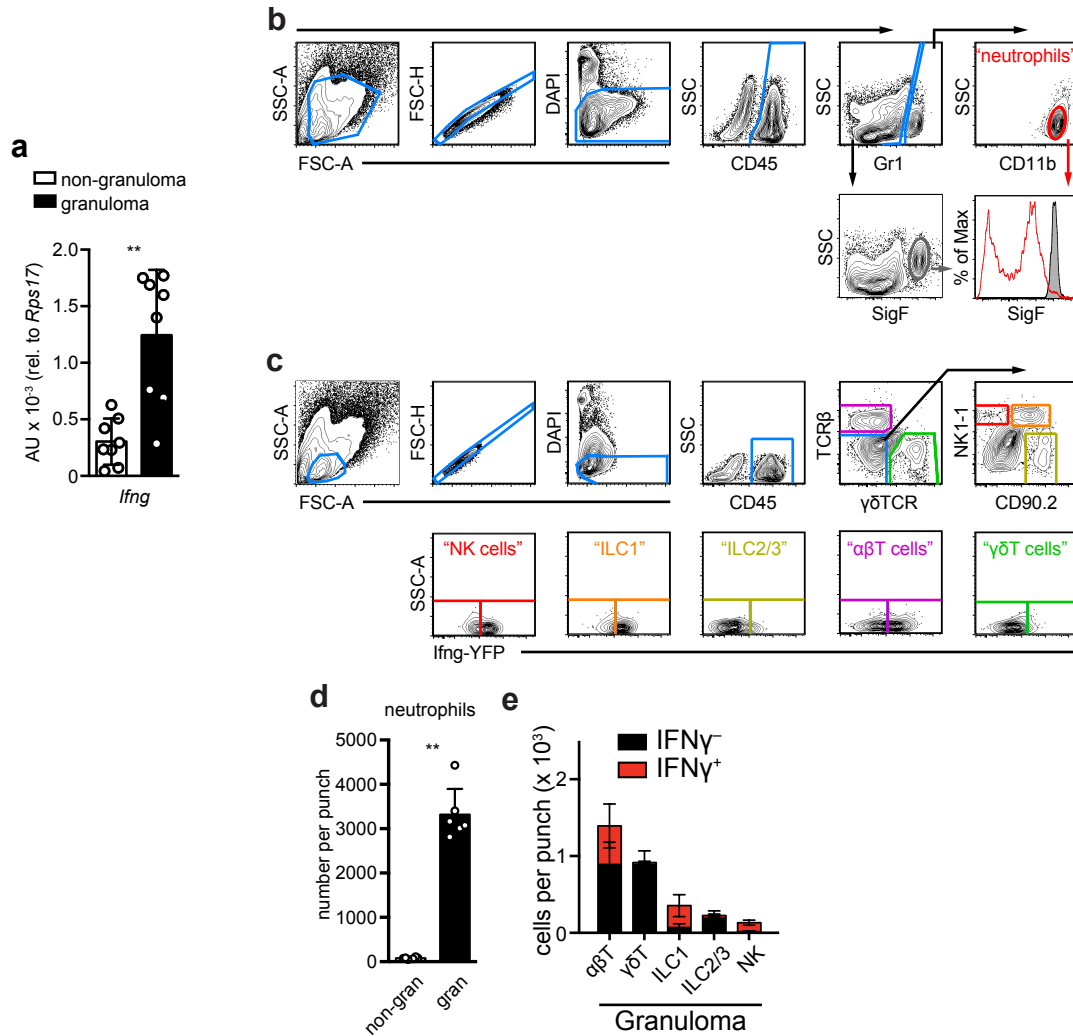
Figure 3.4 | IFNg is produced by H. polygyrus-responsive immune cells present in granulomas.

Day 6 of *H. polygyrus* infection, except as noted. **a**, Non-granuloma or granuloma biopsies from wild-type mice were analyzed by quantitative PCR for *Ifng* transcript. **b**, **c**, Representative gating example of neutrophils (**b**) and natural killer (NK) cells, ILC1, ILC2/3, αβ T cells, and γδ T cells (**c**). **d**, Neutrophils were enumerated by flow cytometry from non-granuloma (non-gran) or granuloma (gran) biopsies. **e**, *Ifng* reporter mice were untreated (uninfected) or infected (granuloma, non-granuloma) with *H. polygyrus* and analyzed by flow cytometry 5–6 days later

for hematopoietic (CD45^{+}) populations: NK cells, ILC1, ILC2/3, $\alpha\beta$ T cells and $\gamma\delta$ T cells. No reporter signal was seen in non-lymphoid populations. $n = 5$ mice (**e**, uninfected), 6 mice (**d**, **e,** infected) or 8 mice (**a**). Statistics represent all biological replicates, and all experiments were replicated at least twice. Graphs are centered on mean with bars showing s.d. (**a**, **d**–**e**). *$P < 0.05$, **$P < 0.01$, ***$P < 0.001$ by unpaired, two-tailed Mann–Whitney test.
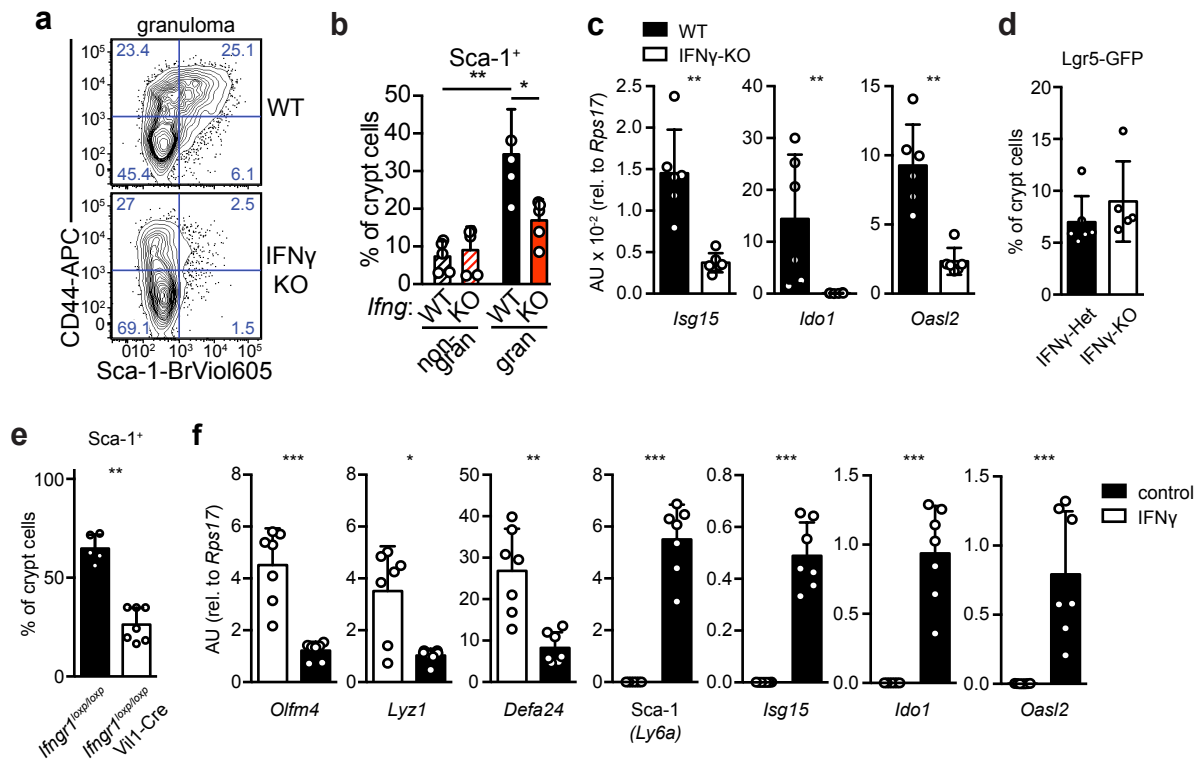
Figure 3.5 | IFNγ mediates the helminth-induced crypt phenotype.

a, Representative flow cytometry of CD44 and Sca-1 in epithelia from biopsies of IFNγ-knockout (KO) mice. **b**, Cells analyzed as in (**a**). **c**, Crypt cells were sorted from granuloma biopsies of IFNγ(KO) mice and analyzed by quantitative PCR for the indicated transcripts. **d**, Lgr5–GFP mice were bred with IFNγ-knockout (KO) mice and offspring were analyzed by flow cytometry for Lgr5–GFP expression in crypt epithelia from granuloma biopsies. **e**, *Ifngr1*$^{loxp/loxp}$ mice were bred with Vil1-Cre mice and analyzed by flow cytometry for Sca-1 expression in crypt epithelia from granuloma biopsies. **f**, Wild type organoids were treated with 5 ng ml^{-1} IFNγ for 24 h and analyzed by quantitative PCR for the indicated transcripts. *n* = 5 mice (**a**, **b**, **d**, KO, **e**, *Ifngr1*$^{loxp/loxp}$), 6 mice (**c**, **d**, heterozygous), 7 mice (**e**, *Ifngr1*$^{loxp/loxp}$;Vil1-Cre), or 7 cultures (**f**). Statistics represent all biological replicates, and all experiments were replicated at least twice.

Graphs are centered on mean with bars showing s.d. (**b**, **c**–**f**). $*P < 0.05$, $**P < 0.01$, $***P < 0.001$, $****P < 0.0001$ by unpaired, two-tailed Mann–Whitney test.
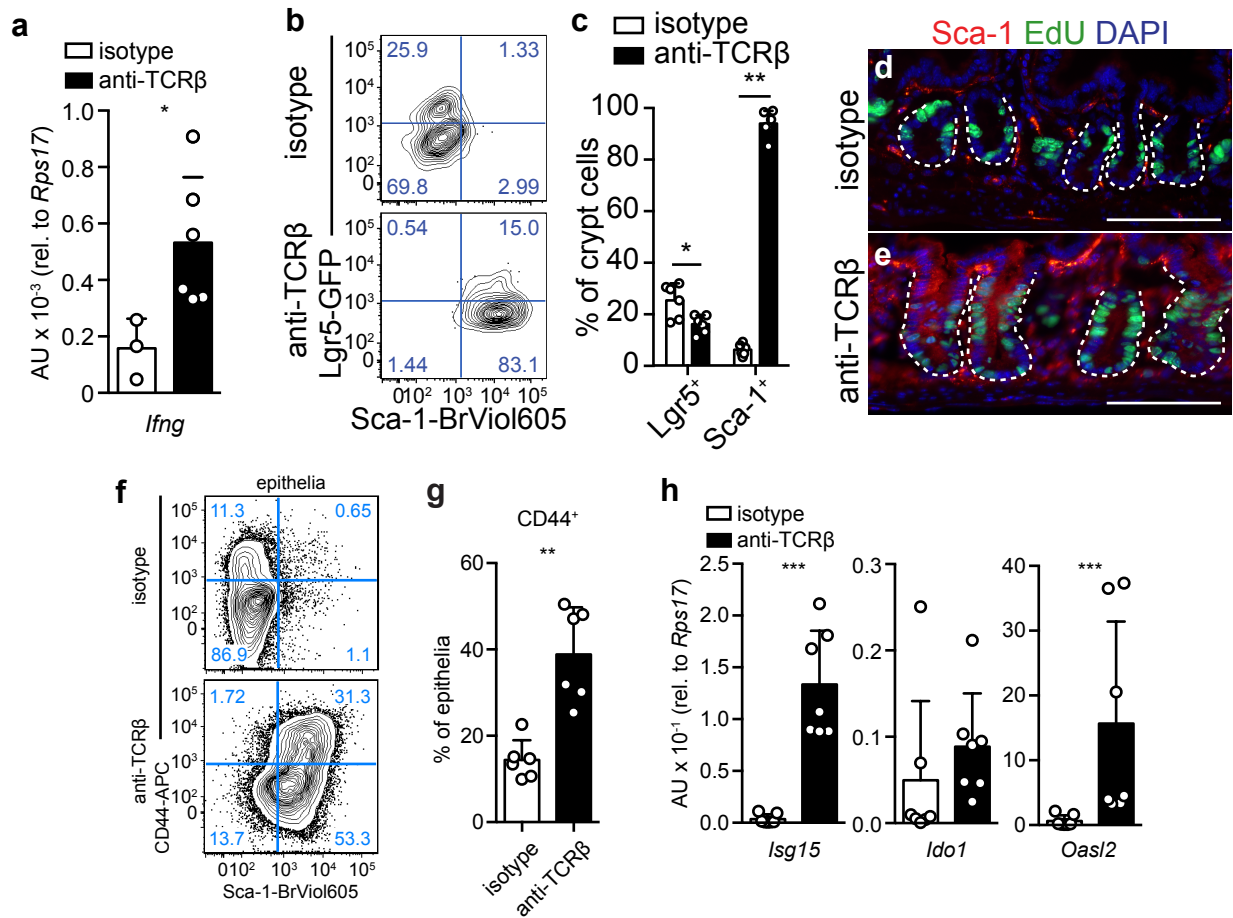
Figure 3.6 | Immune cell activation induces granuloma-like epithelial responses.

Mice were treated with 20 μg isotype antibody or anti-TCRβ antibody (clone H57) and analyzed 24 h later. **a**, Unfractionated tissue analyzed by quantitative PCR for *Ifng* transcript. **b–e**, Mice were treated with 20 μg anti-TCRβ and analyzed 24 h later by flow cytometry for Lgr5–GFP and Sca-1 in crypt cells (**b**, **c**) or for Sca-1 and EdU in thin section (**d**, **e**). **f**, Representative flow cytometry of CD44 and Sca-1 in total epithelium. **g**, Epithelium was assessed for crypt size by flow cytometry using frequency of CD44. **h**, Crypt cells were sorted and analyzed by quantitative PCR for the indicated transcripts. *n* = 3 (**a**, isotype), 4 (**d**, **e**,), 6 (**a**, anti-TCRβ, **b**, **c, f, g**), or 7 mice (**h**). Statistics represent all biological replicates, and all experiments were

replicated at least twice. Graphs are centered on mean with bars showing s.d. (**a**, **c**, **g**, **h**,). *$P < 0.05$, **$P < 0.01$, ***$P < 0.001$, ****$P < 0.0001$ by unpaired, two-tailed Mann–Whitney test. Scale bars: 100 μm (**d**, **e**).
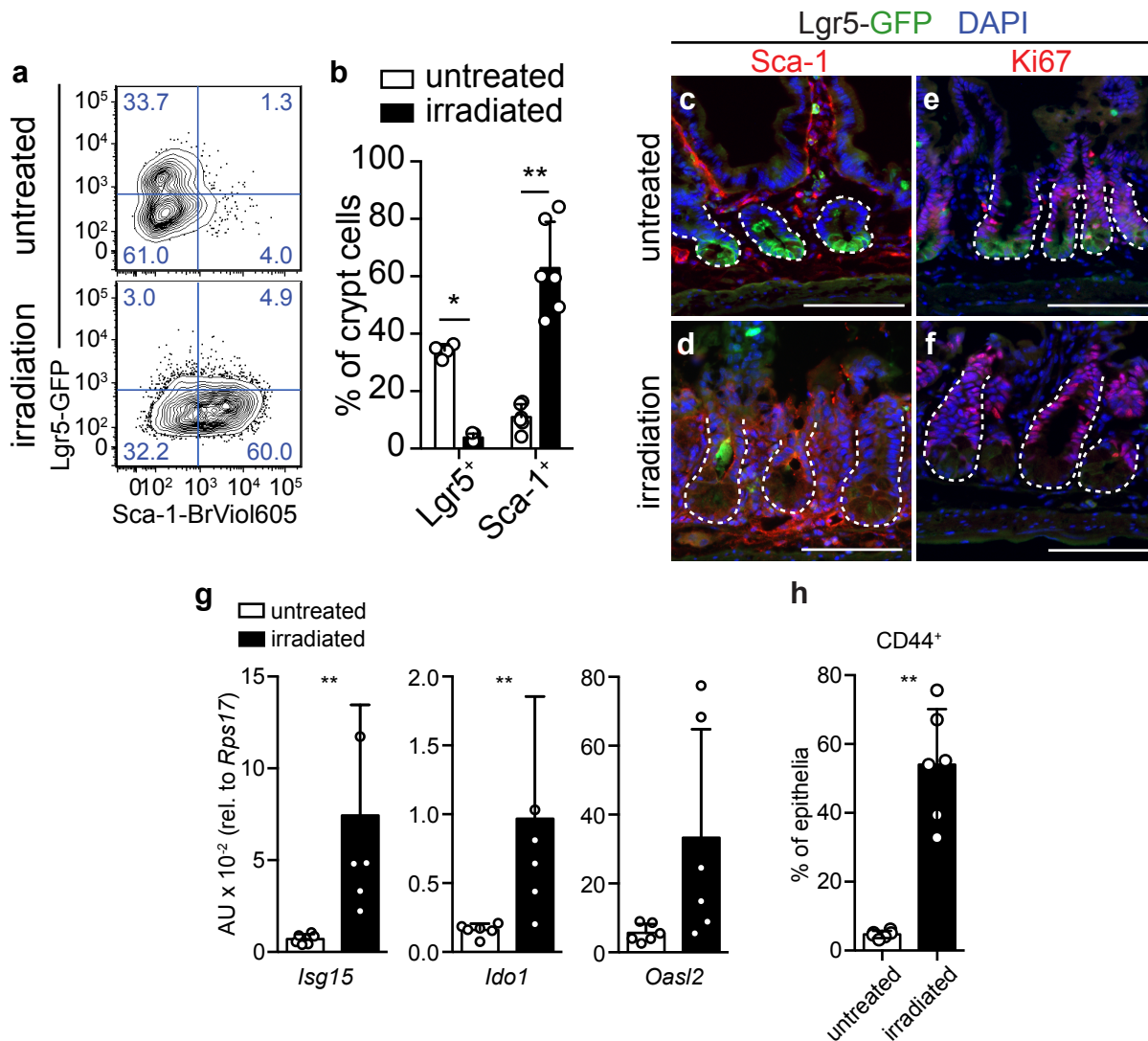
Figure 3.7 | Irradiation induces granuloma-like epithelial responses

Mice were untreated or subjected to 10 Gy irradiation and analyzed three days later.

a–f, Mice were treated with 10 Gy irradiation and analyzed at three days by flow cytometry and in thin section for Lgr5–GFP and Sca-1 in crypt cells (**a–d**) or in thin section for Lgr5–GFP and Ki67 (**e**, **f**). **g**, Crypt cells were sorted and analyzed by quantitative PCR for the indicated transcripts. **h**, Flow cytometry of the frequency of CD44$^+$ crypt cells among total epithelium.

$n = 3$ (**c-f**), 4 (**a**, **b**, Lgr5, untreated), 5 (**a**, **b**, Lgr5, irradiated), or 6 mice (**b**, Sca-1, irradiated, **g**,

h). Statistics represent all biological replicates, and all experiments were replicated at least twice. Graphs are centered on mean with bars showing s.d. (**b**, **g**, **h**). $*P < 0.05$, $**P < 0.01$, $***P < 0.001$ $****P < 0.0001$ by unpaired, two-tailed Mann–Whitney test. Scale bars: 100 μm (**c–f**).
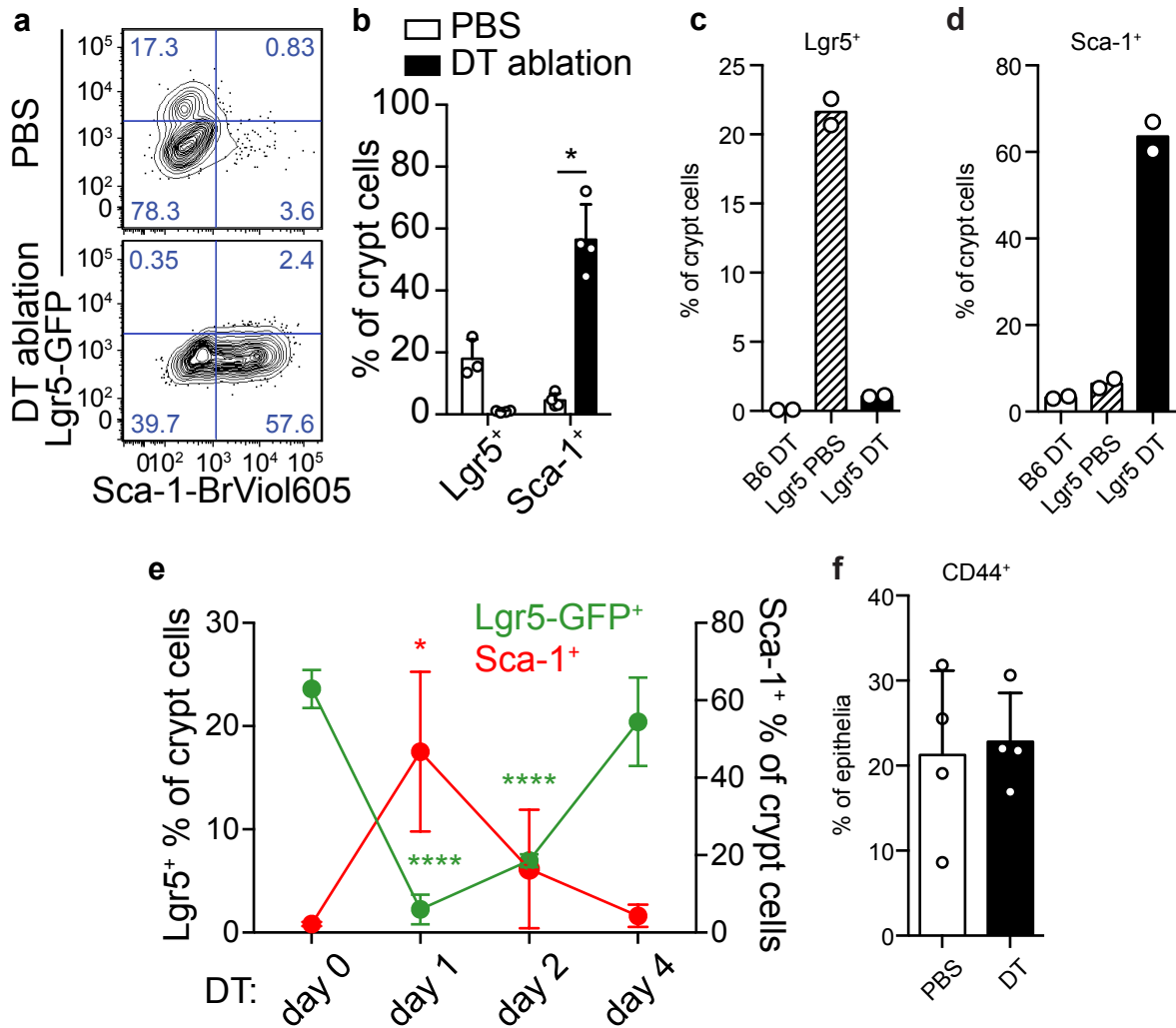
Figure 3.8 | *Lgr5*⁺ cell ablation induces granuloma-like epithelial responses

Lgr5^{DTRGFP/+} mice were treated with diphtheria toxin (DT) for at 24 h, except as noted. **a–e**, *Lgr5^{DTRGFP/+}* mice or wild-type (B6) mice were treated with diphtheria toxin (DT) and analyzed by flow cytometry for Lgr5–GFP and Sca-1 in crypt cells at 24 h (**a-d**) or indicated time points (**e**). **f**, *Lgr5^{DTRGFP/+}* mice were treated with diphtheria toxin (DT) and analyzed a day later by flow cytometry for frequency of crypt cells among total epithelium. $n = 2$ (**c**, **d**,) 3 (**a**, **b**, Lgr5, untreated; **e**, day 0), or 4 mice (**a**, **b**, all others; **e**, day 1, 2, 4; **f**). Experiments were replicated at least twice, except in **Fig. 3.8c, d**, which was performed once. Graphs are centered on mean with

bars showing s.d. (**b**, **e, f**). *$P < 0.05$, ****$P < 0.0001$ by unpaired, two-tailed Mann–Whitney test (**b**) or unpaired, two-tailed *t*-tests (**e**).
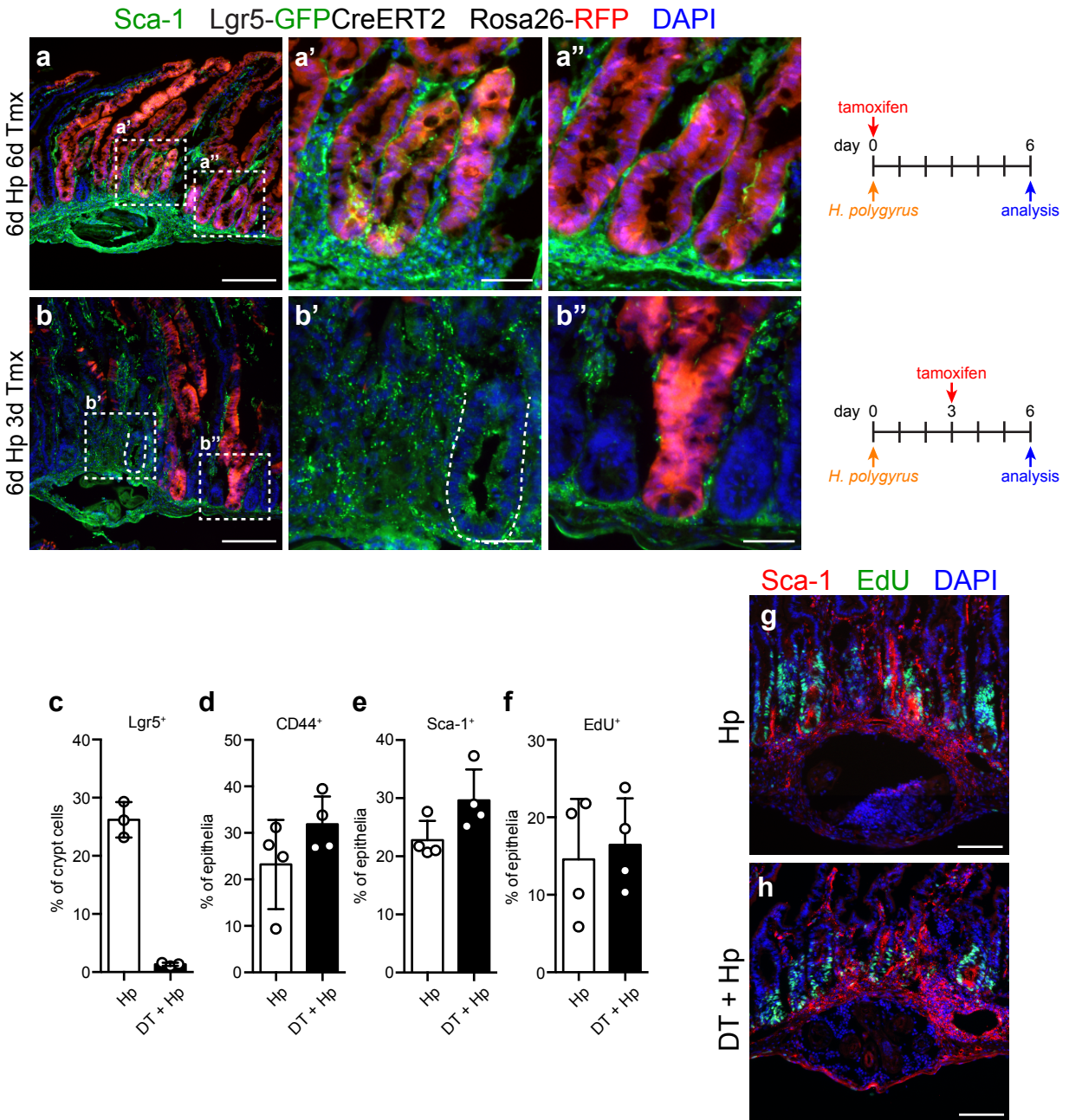
Figure 3.9 | Granuloma crypt epithelium arises from pre-existing *Lgr5*^{+} cells but does not require *Lgr5*^{+} cells.

a, **b**, Representative images of lineage tracing of *Lgr5*^{+} precursors and Sca-1 staining in crypts overlying (gran) and adjacent to (non-gran) *H. polygyrus* (Hp) granulomas. *Lgr5*[GFP-creERT2/+] *Rosa26*[RFP/+] mice were administered 2.5 mg tamoxifen either immediately before (**a**) or three days after (**b**) infection with *H. polygyrus*. Mice were analyzed at day 6. **c**–**h**, *Lgr5*[DTRGFP/+] mice were treated with diphtheria toxin immediately before infection with *H. polygyrus* and analyzed by flow cytometry at day 1 for Lgr5–GFP (**c**), or at day 6 for CD44 (**d**), Sca-1 (**e**) and EdU (**f**) in epithelial cells from granuloma biopsies. **g**, **h**, Representative images of Sca-1 and EdU detection. *n* = 2 (**b**), 3 (**a**, **c**, **g**, **h**), or 4 mice (**d**–**f**). Experiments were replicated at least twice. Graphs are centered on mean with bars showing s.d. (**c**–**f**). Scale bars: 200 μm (**a**, **b**), 50 μm (**a'**, **a"**, **b'**, **b"**), 100 μm. (**g**, **h**).
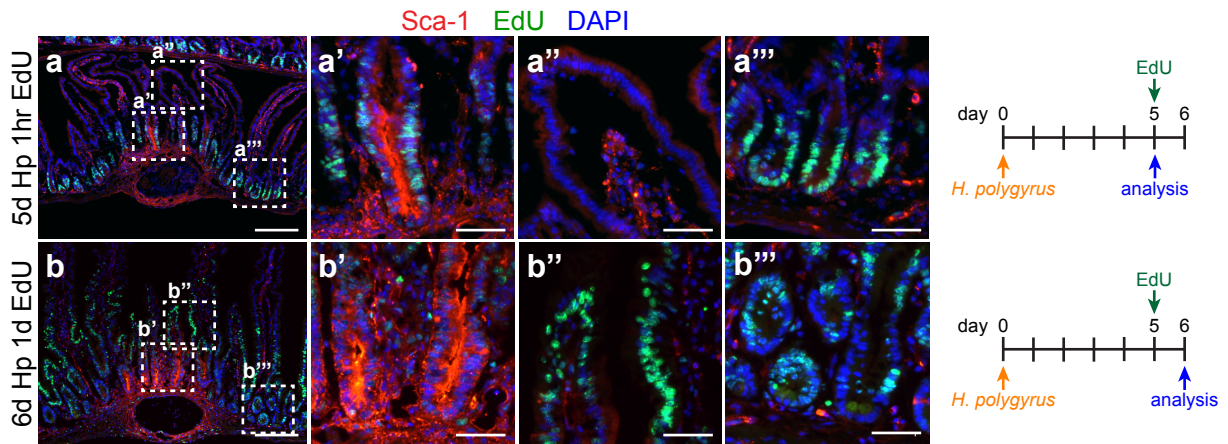
Figure 3.10 | Granuloma crypt epithelium contributes to epithelial turnover.

a, **b**, Representative images of Sca-1 and EdU staining. Wild-type mice were injected with EdU at day 5 of infection and analyzed after 1 h (**a**) or 24 h (**b**) to localize labeled cells within villi (**a"**, **b"**), and within crypts overlying (**a'**, **b'**) or adjacent to (**a'''**, **b'''**) *H. polygyrus* granulomas. $n = 4$ (**a**) or 6 mice (**b**). Experiments were replicated at least twice. Scale bars: 200 μm (**a**, **b**), 50 μm (**a'-a'''**, **b'-b'''**)
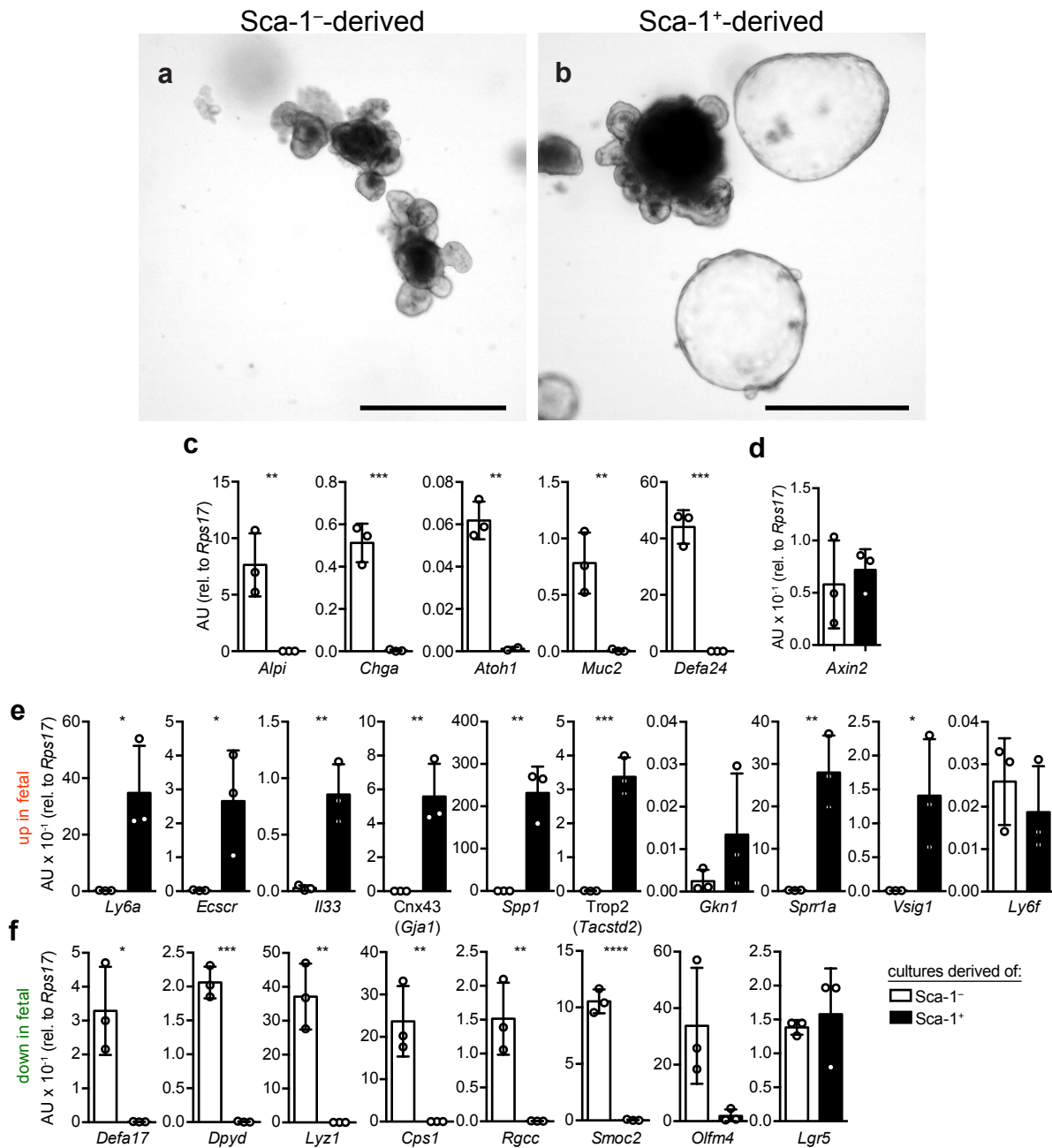
Figure 3.11 | Helminth-associated crypts acquire a fetal-like program *in vitro*.

a–e, Sorted Sca-1⁻ (**a**) or Sca-1⁺ (**b**) crypt cells from *H. polygyrus*-infected mice were cultured in organoid conditions, imaged after one passage (**a**, **b**), and analyzed by quantitative PCR for

markers of differentiated cells (**c**), *Axin2* transcript (**d**), or fetal-derived cultures[275] (**e**, **f**). $n = 3$ cultures from 3 mice (**c-f**), or 15 cultures from 15 mice (**a**, **b**). Statistics represent all biological replicates, and all experiments were replicated at least twice. Graphs are centered on mean with bars showing s.d. (**c–f**). *$P < 0.05$, **$P < 0.01$, ***$P < 0.001$, ****$P < 0.0001$ by unpaired two-tailed *t*-tests. Scale bars: 500 μm (**a**, **b**).
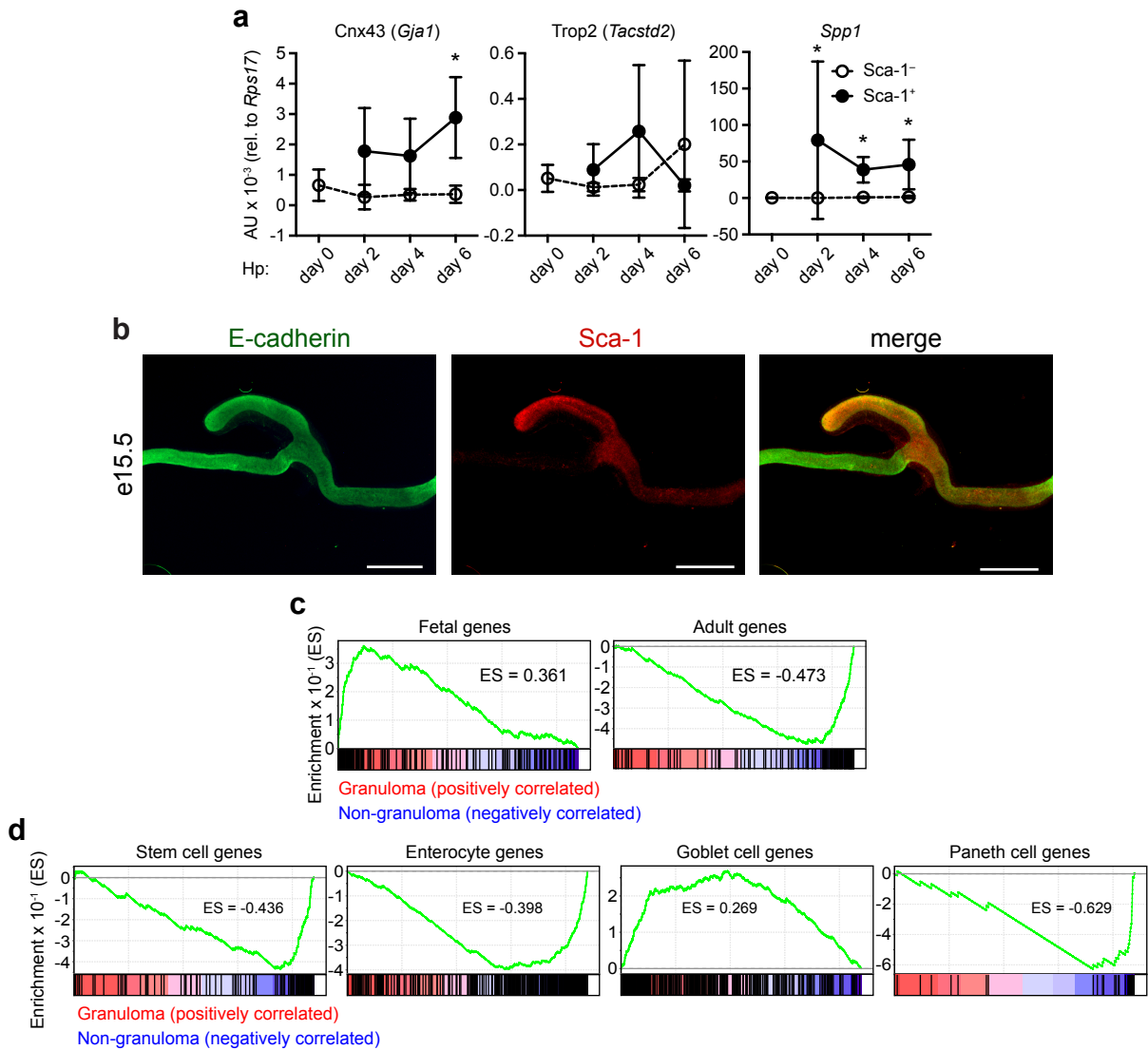
**Figure 3.12 | Granuloma crypts activate a fetal-like program *in vivo*.**

a, Sca-1^{+} or Sca-1^{-} crypt cells were sorted from mice infected with *H. polygyrus* for the indicated times and analyzed by quantitative PCR for fetal transcripts. **b**, Whole-mount e15.5 fetal intestine was fixed and stained for Sca-1 and E-cadherin. **c-d,** Bulk RNA-seq data (as in **Fig. 3.2c**) were analyzed by GSEA for fetal signature genes[275] (**c**) or intestinal epithelial signature genes[72] (**d**). Enrichment score (ES) is indicated and all analyses have FDR $<10^{-3}$. $n = 3$ fetuses

(**b**), 4 mice (**a**, day 2, 4, 6), 4 independently sorted samples (**c-d**, granuloma, 20 mice total), 5 mice (**a**, day 0), or 5 independently sorted samples (**c-d**, non-granuloma, 25 mice total). Statistics represent all biological replicates, and all experiments were replicated at least twice. Graphs are centered on mean with bars showing s.d. (**a**). *$P < 0.05$ by unpaired, two-tailed Mann–Whitney test. Scale bar: 1 mm (**b**).
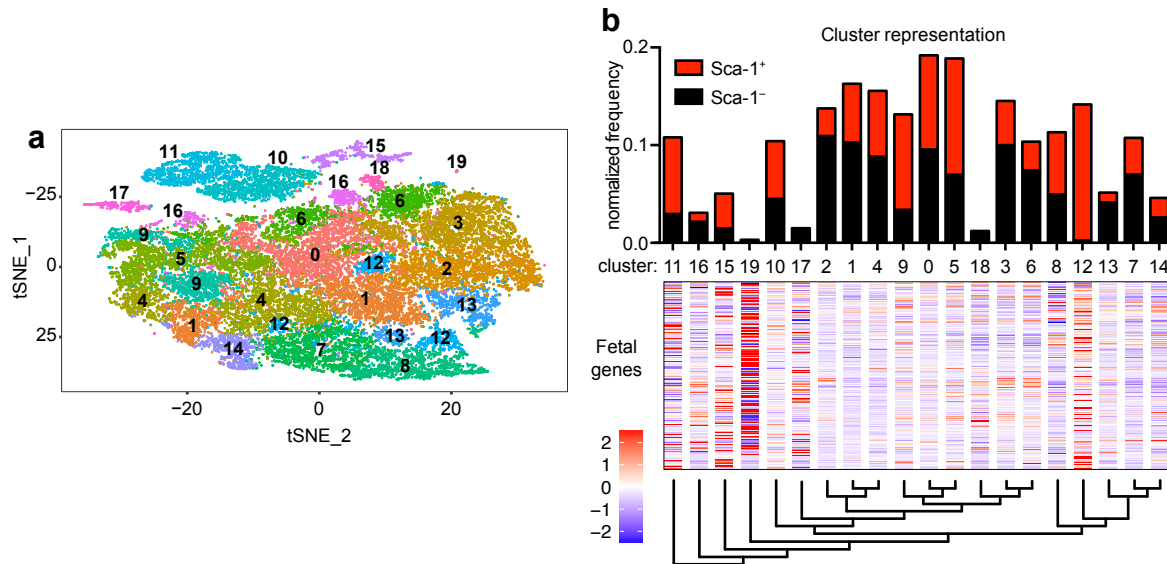
Figure 3.13 | A subset of helminth-associated crypt cells activate a fetal-like program.

a, **b**, Single-cell RNA-seq from $n = 19,754$ Sca-1⁻ and $n = 6,669$ Sca-1⁺ individually sorted crypt cells from one *H. polygyrus*-infected mouse. **a**, t-distributed stochastic neighbor embedding (*t*-SNE) distribution, color coded to represent clusters identified independently by unsupervised hierarchical clustering. The relation of cluster identity to transcriptional signatures of mature lineages is shown in **Fig. 3.14**. **b**, Sca-1⁻ and Sca-1⁺ cell frequency within each cluster, normalized to the total number of cells sequenced from each population (top). Normalized expression values for the fetal gene signature[275] were mapped to the clusters (middle) and arranged per the unsupervised dendrogram of cluster relatedness (bottom). The experiment was performed once.
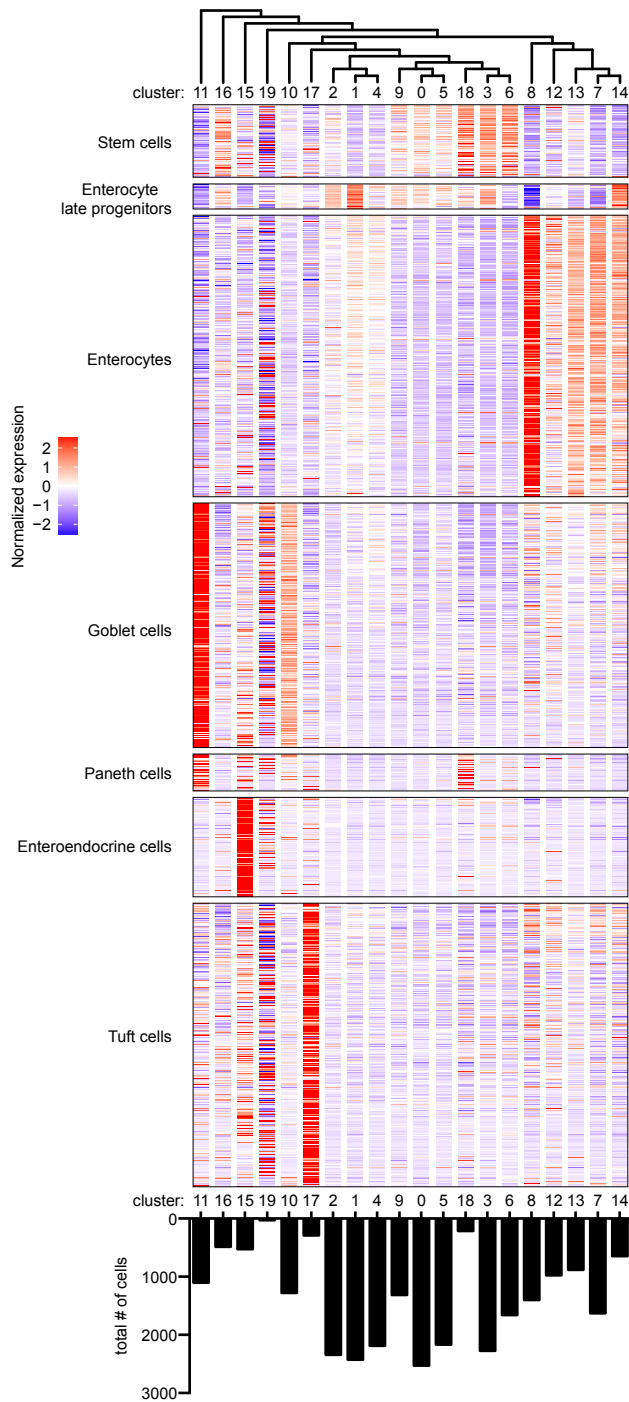
Figure 3.14 | Markers of intestinal cell types in single-cell RNA-seq

Clusters identified by unsupervised hierarchical clustering were arranged per the unsupervised

dendrogram of cluster relatedness (top) and normalized expression values for intestinal cell type

gene signatures[72] were displayed as a heat map in each cluster (middle). The total number of

cells in each cluster is shown (bottom). The experiment was performed once.

Gene	Fold Change	Raw P value	False Discovery Rate	mean Granuloma	mean Non-Granuloma
Gm26656	16.87	4.85E-05	2.94E-03	201.40	11.94
Lrg1	12.65	3.77E-08	6.34E-06	461.43	36.47
Ly6a	11.44	1.25E-29	1.08E-25	4135.88	361.44
Ido1	9.40	5.91E-07	6.93E-05	653.69	69.54
Anxa10	8.64	7.42E-23	2.40E-19	321.01	37.16
Khdc1a	7.04	4.89E-15	3.52E-12	105.43	14.98
Ubd	7.03	2.46E-06	2.40E-04	120.48	17.14
Socs1	6.54	2.56E-21	6.03E-18	291.87	44.61
Alox15	6.18	3.72E-15	2.84E-12	289.29	46.78
Tat	6.17	4.09E-08	6.80E-06	134.38	21.76
Arl5c	6.14	6.16E-08	9.73E-06	853.12	139.05
Apol10b	5.99	2.33E-11	8.75E-09	135.54	22.63
Iigp1	5.96	4.57E-24	1.97E-20	1501.04	251.88
Retnlb	5.71	1.35E-10	4.25E-08	3596.83	629.64
Tgtp1	5.25	1.52E-23	5.64E-20	536.69	102.14
Art2a-ps	4.93	5.62E-13	2.69E-10	143.43	29.10
Slc5a5	4.78	5.62E-08	8.99E-06	115.21	24.10
Atg9b	4.77	1.72E-11	6.54E-09	529.33	110.92
Hspa1a	4.70	3.25E-04	1.33E-02	3049.50	648.74
Fut2	4.68	1.08E-37	1.39E-33	692.27	148.05
Adm	4.59	4.71E-12	1.94E-09	236.05	51.45
4930461G14	4.37	5.63E-09	1.21E-06	135.00	30.89
Mx1	4.25	4.16E-15	3.08E-12	244.75	57.63
Cxcl9	4.13	8.40E-22	2.18E-18	377.73	91.38
Nptx2	4.10	2.24E-13	1.26E-10	123.64	30.18
Wtip	4.00	2.32E-15	1.88E-12	779.89	194.80
Isg15	3.99	2.86E-20	5.29E-17	530.49	132.91
Gbp5	3.89	3.45E-08	5.92E-06	108.42	27.89
Trib3	3.80	3.39E-06	3.08E-04	328.90	86.54
Jdp2	3.78	2.20E-09	5.05E-07	144.86	38.29
Igtp	3.76	1.27E-28	8.22E-25	3945.28	1049.97
Gbp2	3.73	1.02E-08	1.99E-06	411.29	110.39
Phf11d	3.71	2.78E-16	2.67E-13	255.57	68.84
Areg	3.69	1.10E-07	1.59E-05	439.22	119.14
Gbp3	3.65	3.07E-13	1.62E-10	235.83	64.61
Hspa1b	3.64	7.06E-04	2.49E-02	7101.46	1949.58
Spats2l	3.64	3.10E-38	8.05E-34	1418.41	390.05
Ccdc88b	3.49	1.02E-09	2.60E-07	213.33	61.17
S100a6	3.35	9.09E-08	1.38E-05	2411.01	719.89
Pear1	3.34	3.55E-04	1.43E-02	149.41	44.69

Table 3.1 | Granuloma vs. non-granuloma bulk RNAseq up-regulated genes.

This table shows RNAseq data comparing Granuloma (Gr) to Non-Granuloma (NonGr) crypt epithelium, filtered for expression greater than 100 reads, False Discovery Rate (FDR) < 0.05, Fold Change (FC) > 2, top 40 hits ranked by fold change. FC is unlogged fold change, raw p is adjusted p-value calculated by Holm–Bonferroni method, and FDR is the multiple comparisons adjusted p-value. n=4 (granuloma), and 5 (non-granuloma) samples, from 20 and 25 mice, respectively.

Gene	Fold Change	Raw P value	False Discovery Rate	mean Granuloma	mean Non-Granuloma
Ugt2a3	-3.69	9.91E-05	5.19E-03	188.36	695.94
Gm15315	-3.72	7.43E-04	2.60E-02	35.33	131.26
Pyroxd2	-3.83	4.60E-17	5.18E-14	64.16	245.42
Cyp4v3	-3.85	1.85E-16	1.85E-13	200.06	771.15
Ccbe1	-3.88	6.47E-09	1.34E-06	26.55	102.91
Gm10499	-3.93	3.60E-12	1.53E-09	52.14	204.85
Fbp1	-4.00	2.15E-18	3.27E-15	118.97	476.21
Ces1d	-4.13	2.33E-13	1.26E-10	37.98	156.71
Anpep	-4.15	3.70E-10	1.06E-07	1766.90	7328.14
Acer1	-4.19	1.32E-12	5.99E-10	52.07	217.92
Adh1	-4.24	9.46E-07	1.07E-04	1383.01	5869.17
Enpep	-4.55	5.20E-05	3.12E-03	584.04	2655.53
Cyp2c55	-4.55	2.28E-04	1.00E-02	27.52	125.23
Slc14a1	-4.60	5.55E-04	2.06E-02	79.94	367.50
Cyp2c66	-4.63	5.35E-06	4.62E-04	33.53	155.13
Arg2	-4.65	2.63E-06	2.52E-04	857.43	3991.13
Rdh7	-4.90	9.55E-10	2.45E-07	97.13	475.71
Maob	-4.91	1.03E-08	1.99E-06	106.25	521.59
Cyp3a25	-5.04	5.89E-05	3.44E-03	60.03	302.65
Ces1f	-5.14	2.01E-04	9.08E-03	390.17	2007.22
Lct	-5.38	7.14E-05	3.98E-03	93.67	503.52
2010106E10I	-5.64	1.32E-05	9.86E-04	57.97	326.99
Mptx2	-5.70	2.21E-05	1.52E-03	598.16	3408.22
Defa17	-5.80	6.64E-05	3.77E-03	274.48	1592.54
Mme	-5.91	2.68E-15	2.10E-12	189.85	1122.17
Defa24	-6.21	1.08E-04	5.57E-03	4845.71	30099.20
Hmgcs2	-6.22	1.24E-03	3.83E-02	54.57	339.18
Cyp2b10	-6.37	1.72E-03	4.92E-02	29.21	186.05
Defa22	-6.77	8.08E-04	2.78E-02	22.03	149.14
Defa5	-7.32	1.02E-03	3.32E-02	20.13	147.31
Defa3	-7.43	6.91E-05	3.88E-03	24.50	181.94
Gm15292	-8.28	7.71E-05	4.22E-03	26.62	220.31
Cyp3a11	-8.67	9.13E-04	3.05E-02	31.50	272.98
Defa-rs1	-8.74	1.19E-04	5.99E-03	58.06	507.32
Gm15284	-9.20	6.60E-05	3.76E-03	1789.00	16461.94
Sfrp5	-9.29	2.25E-06	2.26E-04	17.93	166.52
Gm14851	-9.81	8.41E-05	4.48E-03	921.90	9045.39
Defa21	-9.90	1.94E-05	1.37E-03	13.17	130.33
AY761184	-10.32	1.29E-04	6.37E-03	623.51	6434.77
Defa26	-12.08	2.14E-05	1.50E-03	38.99	470.89

Table 3.2 | Granuloma vs. non-granuloma bulk RNAseq down-regulated genes.

This table shows RNAseq data comparing Granuloma (Gr) to Non-Granuloma (NonGr) crypt epithelium, filtered for expression greater than 100 reads, False Discovery Rate (FDR) < 0.05, Fold Change (FC) > 2, bottom 40 hits ranked by fold change. FC is unlogged fold change, raw p is adjusted p-value calculated by Holm–Bonferroni method, and FDR is the multiple comparisons adjusted p-value. n=4 (granuloma), and 5 (non-granuloma) samples, from 20 and 25 mice, respectively.

GSEA report for Non-gran

NAME	SIZE	ES	NES	NOM p-val	FDR q-val	FWER p-val
ENTEROCYTE	449	-0.3975748	-9.722712	0	0	0
MUSTATA ADULT ORGANOID UPREGULATED	135	-0.4731836	-6.482619	0	0	0
MUNOZ LGR5 SIGNATURE	133	-0.41403824	-5.5870194	0	0	0
STEM	112	-0.43567035	-5.428972	0	0	0
PANETH	35	-0.62889457	-4.3999834	0	0	0
HALLMARK_BILE_ACID_METABOLISM	75	-0.34099352	-3.4745095	0	0	0
HALLMARK_FATTY_ACID_METABOLISM	122	-0.2547201	-3.3118515	0	0	0
TUFT	378	-0.13534263	-3.0067306	0	0	0
HALLMARK_XENOBIOTIC_METABOLISM	133	-0.19701444	-2.6841125	0	1.03E-04	0.001
ENTEROENDOCRINE	77	-0.24516346	-2.5202742	0	5.46E-04	0.006
HALLMARK_UV_RESPONSE_DN	97	-0.2023586	-2.34522	0	0.00117408	0.014
HALLMARK_KRAS_SIGNALING_DN	48	-0.25262338	-2.0455697	0.00207039	0.00705115	0.088
HALLMARK_PEROXISOME	81	-0.19041722	-1.9806521	0.00193424	0.00990066	0.135
HALLMARK_EPITHELIAL_MESENCHYMAL_TRANSITION	93	-0.17115663	-1.9402541	0.00394477	0.01221634	0.179
HALLMARK_ANGIOGENESIS	18	-0.31860587	-1.6183819	0.03543307	0.06953927	0.696
HALLMARK_HEDGEHOG_SIGNALING	21	-0.28649503	-1.5351278	0.05523809	0.09759563	0.841
HALLMARK_ADIPOGENESIS	158	-0.10114206	-1.451464	0.0956341	0.13135536	0.926
HALLMARK_COAGULATION	59	-0.14108855	-1.2946448	0.14741036	0.2353241	0.994
HALLMARK_HEME_METABOLISM	130	-0.094906464	-1.2347506	0.21428572	0.28071222	1
HALLMARK_OXIDATIVE_PHOSPHORYLATION	181	-0.07661622	-1.2227124	0.23173277	0.2779279	1
HALLMARK_KRAS_SIGNALING_UP	103	-0.10347431	-1.217112	0.22862823	0.2696519	1
HALLMARK_TGF_BETA_SIGNALING	45	-0.14048037	-1.1487123	0.24273859	0.3270778	1
HALLMARK_SPERMATOGENESIS	56	-0.12917912	-1.1240076	0.28375733	0.33980602	1
HALLMARK_PANCREAS_BETA_CELLS	23	-0.188114	-1.0837743	0.36575052	0.37063798	1
HALLMARK_WNT_BETA_CATENIN_SIGNALING	26	-0.15671682	-0.97475016	0.49079755	0.4882261	1
HALLMARK_NOTCH_SIGNALING	24	-0.14645782	-0.8674448	0.6229839	0.61591756	1

Table 3.3 | Gene Set Enrichment Analysis datasets enriched in non-granuloma samples.

This table shows Gene Set Enrichment Analysis (GSEA) of bulk Granuloma vs. Non-granuloma RNAseq. GSEA reports an enrichment score (ES), a weighted Kolmogorov-Smirnov statistic, and false discovery rate (FDR), an estimated probability of a false positive finding adjusted for multiple comparisons. This table shows genes sets enriched in granuloma samples n=4 (granuloma), and 5 (non-granuloma) samples, from 20 and 25 mice, respectively.

NAME	SIZE	ES	NES	NOM p-val	FDR q-val	FWER p-val
GOBLET	371	0.2689914	5.9870324	0	0	0
MUSTATA FETAL SPHEROID UPREGULATED	182	0.3612334	5.620582	0	0	0
HALLMARK_INTERFERON_GAMMA_RESPONSE	131	0.3884399	5.1207104	0	0	0
HALLMARK_INTERFERON_ALPHA_RESPONSE	70	0.4991909	4.992879	0	0	0
HALLMARK_MYC_TARGETS_V1	175	0.2834004	4.258201	0	0	0
HALLMARK_MTORC1_SIGNALING	173	0.252073	3.8104837	0	0	0
HALLMARK_TNFA_SIGNALING_VIA_NFKB	134	0.24866508	3.316435	0	0	0
HALLMARK_UNFOLDED_PROTEIN_RESPONSE	97	0.27533394	3.157739	0	0	0
HALLMARK_CHOLESTEROL_HOMEOSTASIS	64	0.32580304	3.0462077	0	0	0
HALLMARK_IL6_JAK_STAT3_SIGNALING	49	0.33871213	2.786276	0	1.17E-04	0.001
HALLMARK_MYC_TARGETS_V2	47	0.32339954	2.668534	0	2.35E-04	0.002
HALLMARK_E2F_TARGETS	171	0.16915753	2.5350513	0	4.96E-04	0.005
HALLMARK_G2M_CHECKPOINT	172	0.16443709	2.4995203	0	7.26E-04	0.008
ENTEROCYTE PROGENITOR (LATE)	40	0.32933435	2.4927695	0	6.74E-04	0.008
HALLMARK_ALLOGRAFT_REJECTION	81	0.2345306	2.4086742	0	0.00104133	0.013
HALLMARK_INFLAMMATORY_RESPONSE	92	0.21160424	2.4017332	0	9.76E-04	0.013
HALLMARK_DNA_REPAIR	125	0.18560238	2.36618	0	0.00112908	0.016
HALLMARK_UV_RESPONSE_UP	111	0.18730599	2.3182323	0.00210526	0.00141419	0.022
HALLMARK_MITOTIC_SPINDLE	173	0.14631176	2.2096949	0.00207039	0.00268154	0.044
HALLMARK_P53_PATHWAY	152	0.14611426	2.08661	0	0.00595255	0.1
HALLMARK_APICAL_JUNCTION	113	0.14392766	1.7510992	0.03754941	0.0331373	0.452
HALLMARK_PI3K_AKT_MTOR_SIGNALING	85	0.15422395	1.6666174	0.02912621	0.04793878	0.61
HALLMARK_IL2_STAT5_SIGNALING	121	0.12507312	1.6336944	0.02994012	0.05365814	0.664
HALLMARK_GLYCOLYSIS	147	0.114766136	1.6233592	0.04848485	0.05428844	0.678
HALLMARK_MYOGENESIS	93	0.13863435	1.543368	0.0604915	0.07804006	0.807
HALLMARK_REACTIVE_OXIGEN_SPECIES_PATHWAY	39	0.19612579	1.4075372	0.11290322	0.1364751	0.947
HALLMARK_HYPOXIA	133	0.10240748	1.3835852	0.13953489	0.14486271	0.964
HALLMARK_PROTEIN_SECRETION	84	0.124809705	1.3301038	0.13480885	0.17293864	0.986
HALLMARK_COMPLEMENT	110	0.103544846	1.2578467	0.17519686	0.21797924	0.995
HALLMARK_APICAL_SURFACE	22	0.2257199	1.2480519	0.1961165	0.21803878	0.995
HALLMARK_ANDROGEN_RESPONSE	79	0.11500325	1.1925955	0.23443983	0.25748885	0.999
HALLMARK_ESTROGEN_RESPONSE_LATE	132	0.081080206	1.0769233	0.3256262	0.3679453	1
HALLMARK_APOPTOSIS	118	0.081572756	1.029233	0.40042827	0.4124211	1
HALLMARK_ESTROGEN_RESPONSE_EARLY	130	0.072676	0.9883815	0.45147678	0.4524696	1

Table 3.4 | Gene Set Enrichment Analysis datasets enriched in granuloma samples.

This table shows Gene Set Enrichment Analysis (GSEA) of bulk Granuloma vs. Non-granuloma RNAseq. GSEA reports an enrichment score (ES), a weighted Kolmogorov-Smirnov statistic, and false discovery rate (FDR), an estimated probability of a false positive finding adjusted for multiple comparisons. This table shows genes sets enriched in non-granuloma samples n=4 (granuloma), and 5 (non-granuloma) samples, from 20 and 25 mice, respectively.

gene	fold change (gran/non-gran)	mean granuloma read count	mean non-granuloma read count
Ifna-ps1	NA	0.00	0.00
Ifna1	NA	0.00	0.00
Ifna2	NA	0.00	0.00
Ifna4	NA	0.00	0.00
Ifna5	NA	0.00	0.00
Ifna6	NA	0.00	0.00
Ifna7	NA	0.00	0.00
Ifna9	NA	0.00	0.00
Ifna11	NA	0.00	0.00
Ifna12	NA	0.00	0.00
Ifna13	NA	0.00	0.00
Ifna13	NA	0.00	0.00
Ifna14	NA	0.00	0.00
Ifna15	NA	0.00	0.00
Ifna16	NA	0.00	0.00
Ifnab	NA	0.36	0.00
Ifnb1	NA	0.00	0.00
Ifne	NA	0.00	0.00
Ifng	NA	0.00	0.00
Ifnk	1.18	7.95	6.72
Ifnl2	NA	0.00	0.00
Ifnl3	NA	1.10	0.00
Ifnz	NA	0.56	0.00
Ifnar1	1.11	1412.08	1267.17
Ifnar2	1.22	253.56	207.64
Ifngr1	-1.06	4043.45	4290.54
Ifngr2	-1.12	3368.70	3784.38
Ifnlr1	1.22	513.01	421.71
Il10rb	-1.02	1357.28	1381.12

Table 3.5 | IFN transcripts detected in granuloma epithelium.

This table shows fold change and read counts of IFN and IFN receptor genes from RNAseq performed as in **Fig. 3.2c** with no filter applied. "NA" results from division by zero.

cluster	Total genes in the data set	Number of genes within the cluster with expression greater than the global mean of that gene	Total number of genes from the fetal program signature that are detectable in the entire	Number of fetal program genes within the cluster with expression greater than the global mean of	Hypergeometric test P value
0	14420	6829	257	81	1.0000
1	14420	6267	257	42	1.0000
2	14420	7635	257	65	1.0000
3	14420	7422	257	94	1.0000
4	14420	5499	257	44	1.0000
5	14420	6646	257	80	1.0000
6	14420	6068	257	86	0.9982
7	14420	4016	257	32	1.0000
8	14420	4977	257	58	1.0000
9	14420	6978	257	93	1.0000
10	14420	8776	257	129	0.9998
11	14420	4082	257	96	0.0010
12	14420	7917	257	164	0.0022
13	14420	6839	257	77	1.0000
14	14420	6097	257	50	1.0000
15	14420	6901	257	105	0.9903
16	14420	3674	257	42	0.9999
17	14420	5300	257	77	0.9912
18	14420	5989	257	66	1.0000
19	14420	4885	257	132	0.0000

Table 3.6 | Fetal Signature Single Cell Hypergeometric Distribution Test.

This table shows the hypergeometric distribution test of enrichment for fetal signature genes within each cluster identified by single cell RNAseq analysis of n=19,754 Sca-1⁻ and n=6,669 Sca-1⁺ individually sorted crypt cells from one mouse infected with *H. polygyrus* for six days.

Gene	Primer 1	Primer 2
Alpi	GCT CAA AGA GGC CCA TGA	ATG ATC AGA ACC TGG TGC AA
Atoh1	TCC CTG AAA ACT GAG ACA ACC	GCT AAC AAC GAT CAC CAC AGA
Axin2	AGT GTC TCT ACC TCA TTT TCC G	CTT TCC AGC TCC AGT TTC AGT
Chga	CGC TCC TTG GCA CCT TG	TGT CAG CCC TGA GTG TCT
Cnx43 (Gja1)	CCT TTG ACT TCA GCC TCC AA	GAC CTT GTC CAG CAG CTT C
Cps1	CTG TTG CTG GTG AAG TGG T	CCC ACC GTT CCC AAT GAT AG
Defa17	GAG GAC AAG ACG AAC ATG AGT	GCA TAT TGC GAA CAA TTT ATT GCG
Defa24	AGG ACC AGG CTG TGT CTG TC	TCT TCC TTT GCA GCC TCT TG
Dpyd	CCT GCG AGT ATA AGC TGT GC	GGA GTC GAA ACT GAG GGA TT
Ecscr	AGT CAG AGG CTA CAG CTC TC	TGT CAC AGG CTG ATT GGA TAC
Gkn1	CCG CCA TGA AGC TCA CA	TCC ACT TCC GTC TAC ATT GC
Ido1	GAT GAA GAT GTG GGC TTT GC	CAG GCA GAT TTC TAG CCA CAA G
Ifng	TCC TCA TGG CTG TTT CTG G	TCT TCC ACA TCT ATG CCA CTT G
Il33	GTA TTC CAA CTC CAA GAT TTC CC	CAT GCA GTA GAC ATG GCA GA
Isg15	CAC AGT GAT CAA GCA TTT GCG	CCC CCA TCA TCT TTT ATA ACC AAC
Lgr5	CTC CAA CCT CAG CGT CTT C	GTC AAA GCA TTT CCA GCA AGA
Lrg1	TGA GGA CAG ACA TAG AGG AGC AG	AAG AGG GCC AGG AGA AAC AG
Ly6f	AGA GGA AGT AAG GAC TGG TGT	GCT CTT TCT GCA CAC AAT AGG A
Lyz1	CCC AAG ATC TAA GAA TGC CTG T	CCC ATG CTC GAA TGC CTT
Muc2	ACC ACA ATC TCT ACT CCC ATC T	TCC AGT CAG ACC AAA AGC AG
Oasl2	TCT GTT GCA CGA CTG TAG GC	CAA TCC ACT GTT CCC GTT TG
Olfm4	ACA CAG CTC ACA TCC TTT CTC	GAT GCT GTC CTT CTC CAT GAC
Rgcc	CAC TTC CAC TAT GAG GAG CAC	CCT GTA CAC TGA GTC TGC AC
Rps17	GCC CTA GAT CAG GAG ATC ATT G	ATG CCA ACT GTA GGC TGA GTG
Sca1 (Ly6a)	GAT GGA CAC TTC TCA CAC TAC A	GCA GGT AAT GTA TGG GCA AGA
Smoc2	ACC TTC CTG TCC CGA TGT	CTT CCT CTC AGC CAC ACA C
Spp1	AGA ATG CTG TGT CCT CTG AAG	TCG TCA TCA TCG TCG TCC A
Sprr1a	AGC AGA AGA CAA AGC AGA AGT	GGA CTC ATA AGC AGG ATA GAC AG
Trop2 (Tacstd2)	TCA ACC ACT CTG ACC TAG ACT	TGC CGA AGC TCT ATC TGA ATG
Vsig1	AAG TTA AAT CCA AGC AGC AGA AG	GGA TGG AAG ATG GCA GAG TT

Table 3.7 | qPCR Primers.

This table lists the sequences of primers used for qPCR analysis throughout the study.

Chapter 4: Discussion

In this chapter, I first expand and discuss our findings, adding context and additional explanation for the work done in Chapter 3. I also discuss caveats and shortcomings of experiments. I then expound on the implications of the study, identify unanswered questions, and suggest avenues for future projects emanating from this work.

4.1 Summary

4.1.1 Granuloma crypts adopt a hyper-proliferative state lacking *Lgr5*⁺ cells

In summary, we found that granulomatous reactions to Hp larvae have a dramatic effect on the intestinal crypt and the progenitors that populate it. Soon after larval penetration, the overlying crypts at the sites of larval penetration lose the canonical stem cell pool of *Lgr5*⁺ CBCs (**Fig. 3.1a**). Importantly, this phenotype was restricted to crypts that were immediately overlying sites of Hp penetration, which we term granuloma crypts, or GCs. Nearby non-granuloma crypts retained expression of the Lgr5-GFP reporter (**Fig. 3.1a**), and appeared to be unaffected, suggesting that loss of *Lgr5* expression was due to a local effect of Hp, not a global response to infection. We leveraged this observation to study the local effects and signals controlling the GC phenotype by using internal non-GC controls rather than uninfected controls. While our analysis of crypt area of uninfected versus infected non-involved crypts suggests that there are also global effects of early Hp infection (**Fig. 3.1c**), we chose to focus on the local stem cell specific effects of Hp.

We initially noted an absence of the Lgr5-GFP reporter and then found that not just this one marker gene was lost, but also the surrogate ISC marker *Olfm4* (**Fig. 3.1e**), as well as an entire suite of intestinal stem cell signature genes (**Fig. 3.2d, e, Table 3.3**). This suggested that GCs truly lack *Lgr5*⁺ ISCs. We also noted that the niche was disrupted, as markers of Paneth cells, which are important components of the *Lgr5*⁺ cell niche[89], were mis-localized within GCs (**Fig. 3.1f, g**). In support of this, our RNAseq analysis comparing GCs to non-GCs demonstrated a repression of many Paneth cell related genes, such as defensins within the GC signature (**Table**

3.2). The observation that the niche was abnormal could perhaps explain why the *Lgr5*⁺ cells were absent, which is expanded upon below in **Section 4.4.1**.

Paradoxically, though, the *Lgr5*⁻ GCs continued to proliferate, and in fact were hyper-proliferative and expanded relative to *Lgr5*⁺ GCs (**Fig. 3.1a-d**). This was a curious observation, because *Lgr5*⁺ stem cells are an important long-term source of new cells during epithelial turnover. We initially observed that GCs lacked *Lgr5*⁺ six days after infection, and analysis of earlier time points indicated the *Lgr5*⁺ cells had disappeared within two days of infection (**Fig. 3.3d**), suggesting that GCs maintained proliferation over a period of time that the epithelium completely turns over. We also found that GCs rapidly contributed to epithelial turnover (**Fig. 3.10a, b**). Furthermore, we observed that the GC response was maintained up to at least 10 days after infection (**Fig. 3.3e**). While this scenario does not preclude the maintenance of epithelial turnover purely by TA cells in the absence of *Lgr5*⁺ stem cells, it suggests that the GCs are maintained through other mechanisms.

It is important to note that these data do not necessarily indicate that the *Lgr5*⁺ cells are killed or absent in GCs. The cells initially marked by *Lgr5* expression may still be present within these crypts but with a silenced transcriptional program, and they may have adopted a new infection or injury specific state. Indeed, a lineage tracing analysis we conducted suggests that *Lgr5*⁺ cells existing immediately before infection are capable of giving rise to granuloma-associated crypts (**Fig. 3.9a, b**). We found that genetically labeling *Lgr5*⁺ cells immediately before infection demonstrated continued stem cell like lineage tracing ribbons within GCs after *Lgr5* expression is lost. However, a number of technical caveats inherent to these experiments make conclusive interpretation of these results difficult. First, the *Lgr5*^{GFP-CreERT2/+} allele used to label *Lgr5*⁺ cells is not ubiquitously expressed in all *Lgr5*⁺ cells, as it is silenced in about 50% of

small intestinal crypts. This makes a negative result difficult to interpret, as a lack of labeling could be due to the loss of the labeled cell, or merely due to a silencing of the reporter allele. Second, and critically, we are not able to precisely control the timing of induction of labeling relative to the loss of *Lgr5* expression. Ideally, we would label all and only *Lgr5*$^+$ cells immediately before the upstream signals controlling *Lgr5* repression occurred, and not before the cells divided. However, as we cannot precisely control the timing of Hp penetration, GC response induction, and tamoxifen dosing, we cannot rule out the possibility that labeled *Lgr5*$^+$ cells divide to produce a daughter cell that ultimately maintains the crypt, while the initially labeled (and now *Lgr5* negative) cell is lost. We interpret our lineage tracing results to suggest that pre-existing *Lgr5*$^+$ cells are still present within the crypt in an *Lgr5* negative state, but formal testing of this remains to be done.

All in all, we found that crypts damaged during Hp larval penetration, or the immune response to the worm, adopt a novel hyper-proliferative state lacking *Lgr5*+ ISCs. These crypts maintained proliferative capacity, while shifting away from the normal stem cell program, raising the question of what was responsible for repressing the ISCs, and how the crypts were maintained without the canonical stem cell pool.

4.1.2 Sca-1 and an interferon response are engaged by GCs

Our RNAseq dataset indicated that an interferon (IFN) response was mounted within GCs (**Fig. 3.2b**, **f**, **Table 3.4**). Many IFN target genes were highly up-regulated within GC samples, notably *Ly6a*/Sca-1. Sca-1 is an extra-cellular epitope that has been extensively used in flow cytometry, and is a IFN target gene that also is induced in intestinal epithelial cells during colitis[281]. Sca-1 is also notable for its expression on multiple types of tissue stem cells, yet is not

present in humans[292]. We found that Sca-1 was specifically expressed in *Lgr5* negative GCs (**Fig. 3.3a-b**), was induced soon after infection (**Fig. 3.3c**), and its expression was always mutually exclusive with Lgr5-GFP expression (**Fig. 3.3d**). We found that IFNγ was responsible for driving the IFN response and Sca-1 expression within GCs (**Fig. 3.5a-c, e**), and that populations of immune cells (mainly αβT-cells, ILC1s, and NK cells) within granulomas were the source of IFNγ (**Fig. 3.4a-e**). Unfortunately, IFNγ did not solely control the repression of *Lgr5*, as infection of IFNγ knockout mice had no effect on the repression of Lgr5 in GCs (**Fig. 3.5d**). However, IFNγ treatment of organoids recapitulated many of the transcriptional changes we detected in GCs, including repression of the ISC gene *Olfm4,* and the Paneth genes *Lyz1* and *Defa24 (***Fig. 3.5f**). This suggests that IFNγ contributes to the loss of *Lgr5*$^+$ ISCs in GCs, but other factors are also involved.

It is important to note that while IFNγ did control Sca-1 induction and many of the transcriptional features of the GC response, we were not able to demonstrate that IFNγ controlled other aspects of the GC phenotype. IFNγ-deficient mice still induced a hyper-proliferative response in GCs, demonstrating that IFNγ did not stimulate epithelial proliferation after Hp. We also did not detect any deleterious effect on the health of the mice or the ability of the worm to complete their life cycle in the context of IFNγ deficiency. The immune response to Hp infections is complex and dynamic, and as such many of these processes may be have other or multiple upstream regulators. Additionally the physiologic role of IFNγ in Hp infections is of interest, as we did not find a phenotype in IFNγ deficient mice other than changes in expression of IFN target genes. This may be due to the methods we used to assay these phenotypes, or the time points chosen. It is also possible IFNγ signaling may be an early response to damage in the

intestine which activates immune cells and heightens sensing in the epithelium, but plays no specific role in helminth immunity or epithelial repair.

Altogether, we found that an IFNγ response was activated within GCs, driving expression of Sca-1. Sca-1 was specifically expressed by *Lgr5*-negative crypt cells, and was always mutually exclusive of Lgr5-GFP, suggesting they may be co-regulated. While IFNγ alone did not control the repression of *Lgr5*, Sca-1 was a highly useful marker for tracking the GC response.

4.1.3 The GC injury response is a conserved across multiple epithelial perturbations

An outstanding question was whether the GC response was a unique process elicited by Hp, or whether other perturbations of the intestinal epithelium resulted in similar responses. We examined a few different models to answer this question.

First, we infected mice with *Nippostrongylus brasiliensis* (Nb), another parasitic helminth[293]. Nb is not a natural helminth of mice, but rather is adapted to rats. Mice infected with Nb rapidly mount an immune response dependent on Type 2 processes and expel the parasites. Nb has a markedly different life cycle than Hp. Infective larvae penetrate through the skin, and migrate to the lung through the vasculature. Within the lung, they cause hemorrhage and damage, and are coughed and swallowed by their hosts. As a result, the worms move into the intestinal tract, where they are expelled by Type 2 cytokine-driven processes. Like Hp, Nb infections result in alterations of the intestinal epithelium, notably expansion of goblet cells, but importantly do not transit through the epithelial barrier or cause granulomas. We found that Nb infections do not result in significant Sca-1 induction at day 4 of infection (**Fig. 3.3f**) suggesting that Sca-1 expression is not dependent on Type 2 cytokines, and may require physical disruption of the epithelial barrier.

We next moved on to inflammation driven by T-cell activation. Treating mice with an antibody that cross-links and activates the T-cell receptor results in T-cell activation, cytokine release, and broad inflammation. Treating mice with anti-TCRβ resulted in a response that was extremely similar to the GC response, as evidenced by activation of IFN signaling, Sca-1 induction, reduction of *Lgr5* expression, and crypt proliferation and expansion (**Fig. 3.6a-h**). This suggests that the GC-like response can be elicited purely by the immune system, which has mechanistic implications for our understanding of upstream regulators of the GC phenotype that were IFNγ-independent (see above in **Section 3.1.2**). However, we were unable to sustain this treatment for longer than one day, presumably because the T-cells were lost after anti-TCRβ treatment, and could not be re-stimulated. While this caveat potentially lessens the application of anti-TCRβ as a surrogate of Hp driven GC phenotypes, it will be of interest to identify the cytokines released by anti-TCRβ that drive crypt expansion, as this phenotype was IFNγ-independent in GCs.

Irradiation is a broadly used model of intestinal injury. As elaborated in **Section 1.10.1**, high dosage irradiation results in damage to the epithelium, and loss of ISCs[222,224]. During the early reaction to irradiation, proliferative and regenerative crypts lack *Lgr5*^{+} ISCs, echoing our observations in GCs. We found that after irradiation, regenerative crypts indeed lacked *Lgr5*^{+} ISCs, while also activating a GC-like program including crypt expansion, Sca-1 expression, and an IFN response (**Fig. 3.7a-h**). This suggests that irradiation may drive a regenerative response that parallels what we uncovered in GCs, but some important differences should be noted. *Lgr5*^{+} cells are required for recovery after irradiation, even though they are not present in early regenerative crypts[224]. This suggests that the *Lgr5*^{+} ISCs may not be killed by irradiation, but merely shift into an *Lgr5* negative state that is required for regeneration. Another possibility is

that an *Lgr5*-negative cell is required for regeneration in this context, but is killed by irradiation. We found that ablation of *Lgr5*$^+$ cells has no effect on GCs (**Fig. 3.9c-h**), unveiling some differences between irradiation and the GC response. Nevertheless, it is apparent that the GC phenotype is highly conserved between these models.

Last, we examined ablation of *Lgr5*$^+$ cells. *Lgr5*$^+$ cells can be killed by administration of diphtheria toxin (DT) to *Lgr5*$^{DTRGFP/+}$ mice, but are rapidly regenerated after killing. The precise mechanism regenerating the pool of *Lgr5*$^+$ cells after ablation remains mysterious, perhaps through activation of reserve stem cells, or de-differentiation of committed progenitor cells (See **Section 1.7** for further discussion). Strikingly, no phenotype is readily apparent after *Lgr5*$^+$ cell ablation. The crypt architecture and proliferation remain normal, and no influx of inflammatory cells is apparent. We found that *Lgr5*$^+$ cell ablation rapidly resulted in a GC like response, but with some important differences compared with anti-TCRβ and irradiation. 24 hours after DT administration, *Lgr5*$^+$ cells were lost, and we detected induction of Sca-1 in the crypt (**Fig. 3.8a-d**). This was not due to a non-specific effect of DT, as DT treatment of wild-type mice did not induce Sca-1 (**Fig. 3.8c, d**). However, in agreement with published work, we did not observe expansion of the crypt, hyper-proliferation, or an IFN response after DT ablation, as we saw in irradiation and anti-TCRβ treatment (**Fig. 3.8f**). That being said, Sca-1 is thought of as an "IFN response gene" and may be reading out an IFN signal, perhaps other than the Type I and II IFNs. As such, we may not have assayed the right target genes to see induction of an IFN response. In fact, an inflammatory IFN signature has been detected in an RNAseq study of *Lgr5*-DT ablation within intestinal tumors[153], suggesting that an IFN response may be a feature of *Lgr5*$^+$ cell killing. Nonetheless, the lack of crypt expansion points to the fact that, while *Lgr5*$^+$ cell ablation results in a GC-like response in some aspects (Sca-1 induction, *Lgr5*$^+$ cell-independent

proliferation, and potentially IFN activation), it is a distinct response from Hp granulomas, irradiation, and anti-TCRβ.

Interestingly, we observed that as $Lgr5^+$ cells re-emerged after ablation, Sca-1 was turned off in a tightly anti-correlated pattern (**Fig. 3.8e**). This suggests that $Lgr5$ and Sca-1 may be co-regulated, perhaps such that the $Lgr5^+$ and Sca-1$^+$ cells states are mutually exclusive. Indeed, we did not observe $Lgr5^+$/Sca-1$^+$ double positive cells in Hp infections, irradiation, or $Lgr5$-DT ablation (**Fig. 3.3b**, **d**, **Fig. 3.7a**, and **Fig. 3.8a**). We did observe $Lgr5^+$/Sca-1$^+$ double positive cells 24 hours after anti-TCRβ treatment however (**Fig. 3.6b**). However, since we could not maintain anti-TCRβ treatment beyond one day, it could be possible that $Lgr5$ expression would be suppressed if the anti-TCRβ stimulus were sustained beyond one day. The precise control of the $Lgr5^+$ and Sca-1$^+$ cell states is of interest in the future.

All in all, we found that multiple modes of intestinal injury engage a GC like response. Irradiation and inflammation driven by T-cell activation all induced a crypt program that was highly reminiscent of that found in Hp GCs. The crypts in these systems all were hyper-proliferative without $Lgr5^+$ cells, expressed Sca-1, and activated an IFN response. $Lgr5^+$ cell ablation behaved somewhat similarly, but did not feature a hyper-proliferation. Nb infections, which did not cause extensive epithelial damage, presumably did not cause a GC like state as we measured (**Fig. 3.3f**). These results suggest that the GC response is a conserved response in the intestinal crypt to damage. It will be of interest to see if other models of intestinal damage behave similarly. Indeed, a study of the regenerative colon suggests that this is the case after DSS colitis[291], further discussed below in **Section 4.3.2**.

107

4.1.4 GCs adopt a fetal-like state

An outstanding question was whether the *Lgr5*-negative, hyper-proliferative granuloma-crypts in Hp infections harbored a functional long-lived progenitor cell. We surmised that the GCs must contain such a cell, as these crypts were maintained over a relatively long period of time in which the epithelium replaced itself (**Fig. 3.10a**, **b**). These putative cells could be the altered *Lgr5*-expressing CBCs; or an activated alternative stem cell; or a de-differentiated TA cell; or some novel other cell.

An ideal assay for this question would be to perform lineage-tracing analysis of cells within GCs, using a gene that was uniquely expressed within GCs and not non-GCs to drive expression of an inducible CreER recombinase. Unfortunately, while our RNAseq dataset revealed many potential candidate genes that were up-regulated in GCs relative to non-GCs (for instance Sca-1), no reporter mice were available that drove a Cre-ER recombinase under the control of one of these genes.

We therefore moved to query whether GCs contained cells that could form long-term colonies *in vitro*. As discussed in **Section 1.3.2**, colony formation can be used to assay stem cell growth potential in culture, with important caveats that the ability to grow *in vitro* may not reflect true *in vivo* potential. We sorted Sca-1 positive and negative cells from mice infected with Hp for 6 days, corresponding to GC and non-GC cells respectively, and cultured them in the organoid system developed by the Clevers lab[16]. We found that Sca-1 negative cells formed organoids, characterized by dense and thick colonies with multiple crypt-like buds emanating from the larger structure (**Fig. 3.11a**). This was expected, as the Sca-1 negative fraction represented normal crypts cells that harbored *Lgr5*$^+$ stem cells, which form organoids when cultured in this system. Sca-1 positive cells, on the other hand, formed large cystic spheroids

(**Fig. 3.11b**). These colonies were quite morphologically distinct from the organoids we observed in the Sca-1 negative cultures, as they were quite large, had a very thin wall, and did not feature crypt budding. Remarkably, these colonies were stable and could be passaged over an extended period of time while maintaining their distinct architecture. This was especially interesting, as the spheroids derived from Sca-1^{+} cells were stable and distinct from organoids while being cultured in the exact same conditions as the organoids from the Sca-1-negative population. The only difference between the two cultures was the populations that were initially sorted from the same mouse. While intestinal epithelium has been shown to form spheroids when hyper-stimulated with Wnt ligands, we were not adding exogenous Wnt to the cultures, and we found no difference in Wnt activation within the Sca-1^{+} cultures as assayed by *Axin2* expression (**Fig. 3.11d**), a hallmark conserved Wnt target gene[105,294]. Therefore, the spheroids were formed through other mechanisms.

We next assessed the relative presence of known intestinal cell types. Using qPCR, we measured expression of marker genes of intestinal cell types, and found that they were all lost in Sca-1^{+} spheroid cultures. *Alpi*, a marker of enterocytes; *Chga*, a marker of enteroendocrine cells; *Atoh1*, a general marker of secretory cells; *Muc2*, a marker of goblet cells; *Lyz1*, *Defa17*, and *Defa24*, markers of Paneth cells; *Olfm4* and *Smoc2*, markers of ISCs, were all absent in Sca-1 positive derived cultures, while robustly expressed in Sca-1 negative cultures from paired experiments (**Fig. 3.11c, e**). This intriguingly suggested that the Sca-1^{+} spheroid cultures represented the growth of proliferative, undifferentiated cells, but not stem cells, as shown by the lack of *Smoc2* and *Olfm4* expression.

Given that the Sca-1^{+} spheroid cultures had a high growth capacity lacking differentiation, we hypothesized that these cultures might resemble those from the fetal intestine.

It has been demonstrated that fetal epithelium from the developing embryonic intestine forms spheroids in culture, rather than organoids[275,286]. As development progresses, the maturing intestine gradually shifts from forming spheroids to adult organoids. At embryonic day 14, intestinal cultures completely form spheroids, at birth the cultures consists of approximately 80% spheroids and 20% organoids, and at weaning only organoids are formed[275]. Fetal derived spheroids are morphologically distinct from organoids, featuring smooth surfaces devoid of crypts, and expanding to a large size. Transcriptional profiling of fetal derived spheroids elucidated the molecular signature of fetal spheroids, revealing marker genes that distinguish fetal spheroids from adult organoids.

We tested whether the spheroids derived from Hp infected Sca-1$^+$ cells transcriptionally resembled fetal spheroids. We assayed a broad panel of genes distinguishing fetal cultures from adult organoids by qPCR, and found that nearly all genes predicted to be up-regulated in fetal cultures were strongly induced in Sca-1$^+$ cultures (**Fig. 3.11d**), while genes enriched in adult organoids tracked with Sca-1$^-$ organoids (**Fig. 3.11e**). This exciting result suggested that our Sca-1$^+$ cultures were fetal-like, and that the Sca-1$^+$ cells from Hp might have acquired the functional growth capacity of the developing embryonic intestine. To explore this concept, we returned to our RNAseq dataset of granuloma vs. non-granuloma crypt epithelium. We used gene set enrichment analysis (GSEA) to query whether the signatures of fetal spheroids and adult organoids were enriched in either the granuloma or non-granuloma datasets. This analysis revealed that, indeed, the fetal signature was enriched in granuloma samples, while the adult signature was enriched in non-granuloma samples (**Fig. 3.12c, Table 3.3,** and **Table 3.4**). Furthermore qPCR analysis of sorted Sca-1$^+$ cells from Hp infections demonstrated that hallmark fetal spheroid genes were induced (**Fig. 3.12a**). It should be noted that the fetal signature we

utilized was derived from cultured materiel, and may not fully represent *in vivo* expression. As such, the hallmark fetal spheroid marker genes we assayed, while enriched in Sca-1$^+$ cells *in vivo,* were expressed at an extremely low level. Ideally, we would use a transcriptional profiling dataset of *in vivo* fetal epithelium vs. adult epithelium for these analyses, but a dataset of this nature was not available at the time of this study. Nevertheless, we found that the fetal signature derived from *in vitro* epithelium was enriched in our *in vivo* granuloma dataset, and that the Sca-1$^+$ cultures highly mimicked fetal cultures. This strongly argues that GC cells acquired both functional properties and a transcriptional program highly reminiscent of the fetal epithelium, which suggests that the tissue had been "reprogrammed", a novel and exciting finding.

To further test our hypothesis that GCs adopted a fetal-like state, we asked whether any properties of GCs could be found *a priori* in fetal epithelium. We examined the intestines of embryonic fetuses at E15.5, and found that Sca-1 was expressed within the fetal epithelium (**Fig. 3.12b**). Sca-1, which was not previously known to be expressed in the fetal intestine, is not expressed in the adult intestine under normal conditions. Thus, we were able to identify properties of the fetal intestine derived from our study of GCs.

We further characterized the fetal reversion by probing whether GCs also lost intestinal differentiation. Our early phenotyping suggested that Paneth cells were lost in GCs, while harboring abnormal goblet cells aberrantly expressing markers of Paneth cells (**Fig. 3.1f, g**). Utilizing GSEA to assay signatures of intestinal cell types derived from a single-cell RNAseq dataset[72], we found that signatures of stem cells, Paneth cells, enterocytes, enteroendocrine, and tuft cells were all de-enriched in the granuloma dataset (**Fig. 3.12d, Table 3.3**). Notably, and agreeing with our staining data, the signature of goblet cells was enriched in granuloma (**Fig. 3.4d, Table 3.4**).

4.1.5 A novel subset of fetal-like cells arise in Sca-1$^+$ GC cells.

To conclude our study, we asked whether we could further elucidate the population of cells responsible for the fetal signature we identified in GCs and forming spheroids in culture. Towards this, we conducted a single-cell RNAseq experiment of Sca-1$^+$ and Sca-1$^-$ crypt epithelium from one mouse infected with Hp for 6 days. We sorted and conducted whole mRNA sequencing of 20,000 Sca-1$^-$ and about 7,300 Sca-1$^+$ cells separately, before re-merging the two datasets together so we could directly compare the two populations. As we wished to identify novel populations that were unique within the Sca-1$^+$ pool, and identify how known populations of crypt cells behaved within GCs, we were required to merge the dataset. After merging, we conducted unsupervised clustering to group populations of cells with similar transcriptional signatures together, revealing 20 clusters of crypt cells (**Fig. 3.13a**). Most of these clusters were composed of varying but comparable frequencies of Sca-1$^+$ and Sca-1$^-$ cells, which we could track from the original sort (**Fig. 3.13b upper panel**). Many of these clusters could be readily identified to represent known populations of crypt cells. By mapping signatures identified in a single cell RNAseq study of the normal intestinal epithelium[72], we could find certain clusters represented well known cell types (**Fig. 3.14**). Cluster 15 was highly enriched for the signature of enteroendocrine cells, cluster 17 was enriched for markers of tuft cells, cluster 10 and 11 were enriched for the goblet cell signature, while cluster 11 and 18 were enriched for the Paneth signature. That cluster 11 was enriched for both goblet and Paneth cell signatures could suggest that cluster 11 represents the Paneth-Goblet intermediate cells we observed in GCs (**Fig. 3.1f, g**).

We also noted that several clusters were enriched for markers of ISCs. Clusters 3, 6, 16, and 18 appear to be enriched for the ISC signature. This may be due to the clustering algorithm failing to neatly cluster these cells into one population, which is plausible because we

deliberately chose not to force clustering into known subsets. As we did not know what cell types were present within GCs, we conducted unsupervised clustering using unbiased methods to discern individual clusters without any expectation of cell types or frequency. Alternatively, the multiple, separate clusters of ISCs may in fact represent distinct subsets within ISCs, which is interesting in and of itself. Cluster 18 is in fact also enriched for Paneth cell markers, which perhaps could represent an intermediate state during de-differentiation of Paneth cells in injury[150,295].

It was also noteworthy that we detected clusters of cells enriched for the ISC signature in the Sca-1$^+$ pool. Clusters 3, 6, 16, all enriched for the ISC signature, were composed of both Sca-1$^+$ and Sca-1$^-$ cells (**Fig. 3.13b upper panel, Fig. 3.14**). As we had demonstrated conclusively that GCs lacked *Lgr5*$^+$ ISCs (**Fig. 3.1a**, **e**, **Fig. 3.2d**, **e**) we were perplexed to find cells positive for ISC markers within the Sca-1$^+$ fraction. We expected to find ISCs only in the Sca-1$^-$ sample. However, these putative Sca-1$^+$ ISCs could perhaps be ISCs that had down-regulated their signature in GCs without completely extinguishing it, potentially the shifted *Lgr5*$^-$ state hypothesized in **Section 4.1.1** (**Fig. 3.9a**, **b**). The precise identity of these cells is of interest in the future.

We noted that one cluster was unique to the Sca-1$^+$ sample, cluster 12. Cluster 12 was composed almost exclusively of Sca-1+ cells (**Fig. 3.13b upper panel**). It was also de-enriched for markers of any adult cell, although weakly enriched for markers of enterocytes **Fig. 3.14**). However, it was enriched for the fetal signature (**Fig. 3.13b lower panel**, and **Table 3.6**).

This exciting result suggested that within Hp responsive GCs, a unique fetal-like cell appeared. While we could not formally prove that these fetal-like cells were responsible for generating spheroids *in vitro*, it seems likely that they are and will be an important area for future

113

study. We conclude that a major feature of the injury response to Hp involves the reprogramming of a population of crypt cells into a novel fetal-like state.

4.2 Short Summary

In short, we found that crypts overlying sites of Hp larval penetration lose the activity of *Lgr5*$^+$ ISCs, while adopting a hyper-proliferative state (**Fig. 4**). Meanwhile, immune cells responding to Hp infection signal to GCs through IFNγ, driving the expression of Sca-1 on regenerating *Lgr5*$^-$ crypts. Many other models of intestinal injury and disruption elicited a similar phenotype in the crypt, suggesting that this is a conserved response. In Hp infections, a subset of Sca-1$^+$ crypt cells adopted a novel fetal-like state, and Sca-1$^+$ cells generated undifferentiated fetal-like spheroids in culture. This suggests that the crypt responds to injury by silencing the canonical stem cell program while activating a hyper-proliferative state that recapitulates aspects of fetal development, and may represent the *in vivo* reprogramming of crypt cells to maintain the crypt.

4.3 Implications

We identified that the intestinal crypt responds to damage from Hp infection by silencing the adult stem cell program and activating a hyper-proliferative, fetal-like state. This suggests that the tissue is re-programmed *in vivo* to a developmentally primitive state[296,297], perhaps allowing the tissue to rapidly proliferate to repair the barrier breach after the larval worms penetrate the epithelial barrier. During embryogenesis, the primordial intestinal epithelium proliferates rapidly in an undifferentiated state, expanding alongside organ growth. By tapping into this program, the adult intestine may unleash a proliferative capacity restricted during adult homeostasis. A major aspect of intestinal maturation is the progressive restriction of proliferative

capacity to the stem cells, and so, temporarily shifting away from the adult program featuring stem cell-restricted proliferation to a fetal state may enable efficient tissue repair. This is an exciting and novel phenomenon, which furthers our understanding of how tissues repair from damage, and may elucidate how cell plasticity is accomplished.

We speculate that fetal reprogramming is important in maintaining intestinal integrity after injury. The intestinal epithelium is a critical barrier that separates microbial commensals from the host, and must be maintained to prevent widespread infection. Breaches to the epithelial barrier are repaired by the production of new epithelial cells. By adopting aspects of fetal development, a stage in which the tissue rapidly proliferates during organ growth, the tissue may unlock proliferative capacity silenced during homeostasis. As other models of intestinal injury also elicited aspects of this program, we may have uncovered a conserved response to injury in the intestine. This regenerative response echoes those seen in highly regenerative species such as zebrafish and salamanders, in which the regeneration of limbs recapitulates the embryonic development of those organs[298–300]. Mammals do not display the regenerative capacity of these other vertebrates, but that distantly related mechanisms are conserved between these species is an exciting proposition for regenerative medicine.

4.3.1 Links to injury induced plasticity

Injury-induced cell plasticity in mammals is now a well-established phenomenon[97], which has largely focused on the de-differentiation of committed cells into a stem cell like state (See **Section 1.7**). After damage or cell death, it is known that previously committed progenitor cells can acquire stem cell growth capacity. This has been documented in the intestine, in which secretory progenitors, enterocyte progenitors, and Paneth precursors can give rise to self-

renewing cell clones after damage or *Lgr5*^{+} cell ablation[86,127,150–152,295]. In other tissues, growth restricted adult cells can acquire stem cell capacity after injury, notably the skin, airway epithelium, olfactory epithelium, and certain nervous tissues[289,301–304]. In this way, de-differentiation of mature cells into stem cells seems to be a common feature of many injuries, and is compelling – stem cells are important in maintaining tissues, and that if they are lost during damage, mechanisms for their rapid regeneration are in place.

Our findings are not in conflict with this theory, and may provide some insight into how cells acquire a plastic state. By reactivating a developmental program, differentiated cells may acquire the capacity to become a stem cell. Most studies of injury-induced plasticity in the intestine have focused on homeostatic cell populations that exist before injury, and assess their clonogenic potential long after resolution. As such, these studies did not probe the cellular transitions between these two conditions, and may have missed cells transiting through a fetal state before ultimately reconstituting the stem cell pool. It will be of interest to ask whether fetal reprogramming occurs during de-differentiation events in the intestine and in other tissues.

4.3.2 Colonic regeneration demonstrates fetal reprogramming linked to Hippo signaling

We showed that aspects of the GC phenotype were conserved across several types of intestinal injury or perturbation. Irradiation, inflammation driven by T-cell activation, and stem cell ablation all featured a regenerative response that lacked *Lgr5*^{+} ISCs, and featured proliferative Sca-1^{+} cells. We did not assess whether a fetal-like state was achieved, or a subgroup of fetal cells arose in these conditions, so we cannot yet state if these injuries involve fetal reprogramming. However, recently published work that complements our study suggests that fetal reprogramming is a common feature of intestinal injury repair.

116

As our study was completed, work from Kim Jensen's group at the University of Copenhagen described a similar phenomenon in the regenerating colonic epithelium as we had found in GCs[291]. Yui *et al.* used a DSS colitis model to study colonic regeneration. They found that early regenerative crypts express Sca-1, and that Sca-1$^+$ regenerative colonic crypts repress the gene signature of *Lgr5*$^+$ ISCs. Furthermore, Sca-1+ epithelium was enriched for a gene signature of the fetal epithelium, notably for expression of *Anxa1*, which was also expressed in inflamed human colonic epithelium.

These results closely mimic what we uncovered in Hp infections. However, Yui *et al.* went on to describe that Sca-1$^+$ colonic crypts were hyper-active for YAP/TAZ signaling, which they linked to mechano-transductive signals from the stroma through integrin-collagen signaling. Yui *et al.* modeled this *in vitro* by showing that small intestinal organoids could be transformed into fetal-like spheroids by culturing in Type I collagen and Wnt. This was reversible, as plating collagen/Wnt induced spheroids back in Matrigel and organoid media reverted the spheroids to organoids. They then found that deletion of YAP and TAZ in the epithelium abrogated repair after DSS. All together, they argue that stromal matrix remodeling was responsible for reprogramming the colonic epithelium into a fetal-like state through YAP/TAZ, and was essential for repair.

This study nicely complemented ours, providing independent evidence that fetal reprogramming is an integral part of intestinal repair. Closely paralleling our work, Yui *et al.* showed that damage to the epithelium represses the activity of *Lgr5*$^+$ ISCs, induces the expression of Sca-1 on the regenerating epithelium, and activates the signature of the fetal epithelium *in vivo*. They also provide mechanistic insight into potential upstream factors of fetal reprogramming in the intestine, which was lacking in our study. However, a number of

distinctions between our study and Yui *et al.* are notable. Yui and colleagues found that sorted Sca-1$^+$ colonic cells formed organoids when plated in Matrigel, not spheroids. We were able to grow fetal-like spheroids directly from Sca-1$^+$ cells in Matrigel without manipulation. This may reflect an inherent difference in the culture between the colon and the small intestine[305], a technicality in the establishment of the cultures, or reflect relevant biological differences in repair between Hp and DSS.

Yui and colleagues also relied on a synthetic bottom-up approach to argue that extra-cellular collagen reprogrammed the colonic epithelium to a fetal-like state. While compelling, it remains unclear whether mechanically induced YAP-TAZ signaling is truly responsible for fetal reprogramming *in vivo*, or is more broadly required for epithelial repair. Deletion of YAP and TAZ completely abrogated epithelial repair, so the specific contribution of this pathways to fetal reprogramming is difficult to ascertain. Fetal reprogramming via YAP/TAZ may be absolutely essential for repair and epithelial cell survival, and so unlinking the two may be experimentally difficult. Nonetheless, the precise mechanistic link between YAP activation and induction of the fetal program will be important to discern.

Yui *et al.* also did not explore the role of immune responses to DSS induced damage and microbial translocation after loss of epithelial barrier integrity. The colon is resident to large numbers of both commensal bacteria and immune populations, and interplay between the microbiota, immune system and the epithelial barrier is likely involved in repair. Whether the induction of Sca-1 in regenerative colonic crypts is downstream of IFN signaling as we identified, and the contribution of immune pathways to repair will be interesting to contrast between our two studies.

All in all, our two studies strongly complement each other and independently validate that the regenerating epithelium after diverse damage is reprogrammed into a fetal-like state.

4.4 Future Directions and Outstanding Questions

While our work has identified novel phenomena in injury repair in the intestine, our study was largely descriptive, and several questions remain to be answered.

4.4.1 Upstream regulators of the GC state

One open question emanating from our study was that we were not able to conclusively identify what signals control many aspects of the GC phenotype. While we showed that IFNγ signaling was responsible for the induction of Sca-1 and many other IFN target genes in GCs, we IFNγ was not singularly responsible for repressing $Lgr5^+$ ISCs, or hyper-proliferation in GCs. IFNγ deficiency had no effect on the effect of $Lgr5$ expression in GCs, demonstrating that other factors were involved in the repression of the stem cells. While IFNγ treatment of organoids did repress stem cell markers, suggesting IFNγ may contribute to the repression of $Lgr5^+$ ISCs, is not the solely critical factor *in vivo*.

Similarly, we did not note an effect on proliferation in GCs in IFNγ-deficient mice. IFNγ has been linked to epithelial proliferation in parasitic infection[176], but we did not note a reduction in GC proliferation in mice lacking IFNγ, suggesting IFNγ was not involved in Hp induced proliferation. Like repression of the $Lgr5^+$ ISCs, other factors may control GC hyper-proliferation.

These lines of evidence suggest that IFNγ is not a major upstream regulator of the GC phenotype beyond induction of IFN targets such as Sca-1. It remains unclear what signals repress $Lgr5^+$ ISCs and stimulate GC proliferation. Our GSEA analysis points to some candidate

pathways, including mTOR, TNFa, and IL-6 (**Table 3.4**). Gene targets of these pathways were enriched in the granuloma crypt dataset, suggesting these pathways may be activated in GCs, but whether these pathways are truly activated in GCs requires experimental testing. mTOR is important in crypt regeneration after irradiation injuries[306], as was as generally for growth factor fueled cell growth and proliferation[307], suggesting there could be a potential role for mTOR signaling in GCs. IL-6 is of particular interest as an immune cytokine that has been previously implicated in intestinal repair, intriguingly linked to YAP-TAZ signaling[148,238].

Furthermore, *H. polygyrus* itself is a potent modulator of its external environment. *H. polygyrus* has been shown to secrete factors mimicking mammalian cytokines and growth factors to reshape its niche and the immune response[250,308]. In this vein, the GC phenotype may be worm-induced response that is beneficial for completion of parasitic lifecycle.

Another potential upstream inducer of the GC phenotype is the disruption of the ISC niche. We found that Paneth cells are disrupted in GCs, and as an important member of the ISC niche, the loss of Paneth cells could have deleterious effects on ISCs. Additionally, the influx of immune cells, and even the worm itself could disrupt stromal components of the ISC niche. Stromal cells, including telocytes, supply ISCs with critical growth factors, such as Wnts and Rspondins[94,108,309]. The physical disruption or displacement of these cells due to the formation of the granuloma could disrupt niche signaling to the ISCs, and cause loss of ISCs. This is difficult to test experimentally, but it would intriguing to see if known stromal niche cells are lost near GCs.

Finally, the signals upstream of the induction of the fetal program remain unknown in GCs. The colitis study from Yui and colleagues suggest that mechanical signals and YAP/TAZ signaling may play a role, but we did not test the contribution of Hippo signaling. Presumably,

the granulomatous reaction to Hp, and indeed even the worm itself, would have dramatic effects on the mechanical environment near GCs. Fibrosis is a major aspect of granulomatous reactions[310], so it is possible that the stromal environment near GCs could be remodeled in a way to induce fetal reprogramming via the YAP/TAZ mechanism described by Yui and colleagues. IL-6, implicated in our GSEA analysis and linked with YAP-TAZ signaling, could also play a role. As above, querying candidate pathways should hopefully lead to the identification of pathways involved in the induction of the fetal state.

Identification of the upstream regulators of fetal reprogramming would enable another critical line of inquiry – namely what the biological function of the adaptation of a fetal state is. We speculate that reprogramming unlocks a proliferative capacity that is restricted during homeostasis, but a lack functional testing precludes proving this hypothesis. If the upstream regulators of fetal reprogramming can be identified, whether Hippo signaling as hypothesized in Yui *et al*. or another pathway, then blocking that pathway through pharmacologic or genetic means would allow the assessment of what this pathway is doing.

4.4.2 Identity of fetal-like cells

We identified that a subpopulation of cells within GCs (Cluster 12) were enriched for fetal transcripts, suggesting that these cells underpinned the fetal signature and produced spheroids in culture. We did not characterize these cells beyond identifying them via clustering in single cell RNAseq. If these cells can be further isolated from the larger pool of Sca-1$^+$ GC cells, several new avenues for study can be undertaken. Candidate marker genes may be identified from our single cell RNAseq data, which may enable isolation of these cells through antibody staining or genetic labeling. If specific markers of the Cluster 12 cells are found, for

example - *Anxa1,* which was enriched in the fetal signature, cluster 12, and described in Yui *et al*. as a reprogrammed cell marker, then these cells can be isolated and further characterized.

Specific markers that discern Cluster 12 cells from the larger Sca-1$^+$ population could lead to the development of a suite of tools to track how they behave and what their function is. One could develop genetic reporter or lineage tracing tools based on cluster 12 specific marker genes. By creating an inducible Cre recombinase allele under the control of a Cluster 12 specific promotor, one could track, isolate, and functionally test the Cluster 12 cells.

Isolation by flow cytometry of the presumptive fetal-like cells would enable the transcriptional identity of the fetal subpopulation relative to the larger GC pool to be uncovered, which would give greater resolution of the reprogrammed cell state. Additionally, by sorting and culturing the fetal subpopulation, one could test their ability to form spheroids. It is intuitive that the Cluster 12 cells are the cells of origin of spheroids, yet this needs to experimentally proven by isolation and *in vitro* culture.

It would also be of interest to see what the clonogenic potential of these cells is *in vivo*. We suspect that fetal-like cells are highly proliferative and maintain the crypt, which could be proven through lineage tracing. Comparing the linage tracing capacity of Cluster 12 cells with non-fetal GC cells would prove that the fetal population is critical for GC proliferation.

Finally, and critically, by crossing mice expressing a Cluster 12 specific Cre driver to Rosa26 *loxP* flanked STOP diphtheria toxin fragment A (Rosa26-DTA) mice, one could assess the functional role of the fetal subpopulation. Such a mouse would allow the inducible ablation of the cluster 12 fetal cells. It would be of great interest to see if the loss of fetal cells prevents proper injury repair.

4.4.3 Precursors of fetal cells

If specific markers of cluster 12 cells can be uncovered, it would be intriguing to identify which homeostatic precursors gave rise to this population. Is it a specific population, for instance the *Lgr5*^{+} ISCs, or another progenitor cell type - such as enterocyte progenitors? Or can any crypt cell be reprogrammed into a fetal cell? Lineage tracing of homeostatic cell populations should provide an answer to this question, and would be especially simple to do in simpler short-term injury models such as irradiation, pending whether fetal reprogramming is a feature of those injuries. Coupling established de-differentiation experiments, such as those done with enterocyte, secretory, and Paneth cell precursors with assessment of induction of the fetal program should be easily accomplished.

It is becoming clear that the lineage hierarchy between intestinal cell populations is not as linear as once thought, and identifying which cells are capable of de-differentiation or reprogramming, and which are not, would facilitate understanding of how cellular plasticity and injury repair are mechanistically controlled.

4.4.4 Conservation in other injuries

An immediate and obvious avenue of study is to ask whether intestinal responses to irradiation, T-cell stimulated inflammation, and stem cell depletion feature activation of the fetal program as Hp and DSS do. We chose to focus on natural infections and did not extend our study of fetal reversion to models other than Hp. While irradiation, anti-TCRβ, and *Lgr5*^{+} stem cell depletion all featured many similarities with GCs, we did not probe whether Sca-1^{+} cells in those contexts formed fetal-like spheroids, or conduct whole crypt or single cell RNAseq experiments to assess induction of the fetal signature. Our study, complemented with Yui *et al*., certainly

suggests that fetal reprogramming may be a widely conserved injury response, and would have important implications.

Uncovering the role of reprogramming in other injuries would give insight in to how de-differentiation occurs, since ablation of *Lgr5*^{+} cells and irradiation are the most commonly used model for that work. It would have relevance for human patients. Injuries to intestine in human patients are common in autoimmune disorders such as Crohn's disease and ulcerative colitis, graft versus host disease after hematopoietic stem cell transplant, or as a side effect of irradiation during cancer treatments[311–313]. The pathogenesis of these conditions more closely resembles anti-TCRβ and irradiation than Hp infection, although parasitic infection is certainly relevant for human patients as well.

4.4.5 Return to homeostasis

Finally, after resolution of infection, we presume that GCs return to homeostasis, Sca-1 is silenced, the adult program is re-established, and the Lgr5+ ISCs return. To prove that Sca-1^{+} cells return to homeostasis though, we would have to conduct a long-term lineage tracing study with an inducible Cre recombinase under control of a GC-specific promotor. Sca-1 itself would be an ideal candidate for this, or a Cluster 12 specific fetal marker gene. Unfortunately, these tools are not available at this time. With such a tool however, one could conduct a long-term lineage tracing study from Sca-1 or a cluster 12 marker, and assess the ability of these populations to ultimately re-derive the homeostatic crypt and the adult *Lgr5*^{+} cell population.

Without such tools, we cannot formally prove that Sca-1+ GCs re-establish a homeostatic program. However, it is likely that they do. We know that homeostasis is re-established after the other intestinal injuries that induce a GC-like state throughout the intestine, such as irradiation

124

and anti-TCRβ, and so it follows that the GCs in Hp infection ultimately return to homeostasis after the granuloma is cleared.
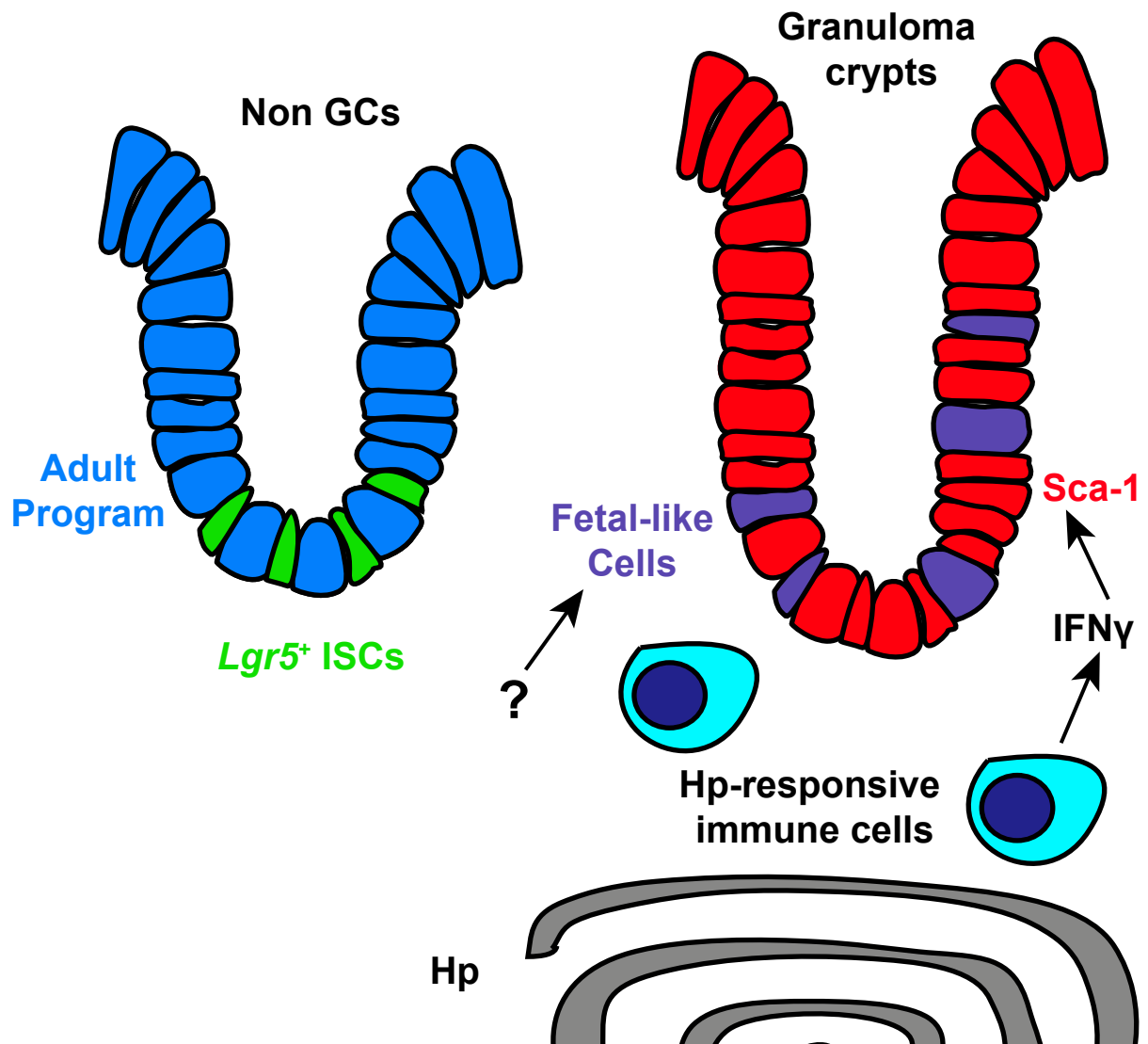
Figure 4 | Summary Model

Crypts overlying granulomas repress *Lgr5*^{+} ISCs, while adopting a hyper-proliferative state. Immune cells responding to Hp infection signal to GCs through IFNγ, driving the expression of Sca-1 on regenerating *Lgr5*^{-} crypts. Within Sca-1^{+} crypt cells, a novel subset adopted a fetal-like state.

References

1. Wells, J. M. & Watt, F. M. Diverse mechanisms for endogenous regeneration and repair in mammalian organs. 2–8 (2018). doi:10.1038/s41586-018-0073-7

2. Karin, M. & Clevers, H. Reparative inflammation takes charge of tissue regeneration. *Nature* **529,** 307–315 (2016).

3. Huber-Lang, M., Lambris, J. D. & Ward, P. A. Innate immune responses to trauma. *Nat. Immunol.* **19,** 327–341 (2018).

4. Schäfer, M. & Werner, S. Cancer as an overhealing wound: An old hypothesis revisited. *Nat. Rev. Mol. Cell Biol.* **9,** 628–638 (2008).

5. Morrison, S. J. & Spradling, A. C. Stem Cells and Niches: Mechanisms That Promote Stem Cell Maintenance throughout Life. *Cell* **132,** 598–611 (2008).

6. Tannishtha, R., Morrison, S. J., Clarke, M. F. & Weissman, I. L. Stem Cells, Cancer, and Cancer Stem Cells. *Nature* **414,** 105–111 (2001).

7. Cotsarelis, G., Sun, T. T. & Lavker, R. M. Label-retaining cells reside in the bulge area of pilosebaceous unit: Implications for follicular stem cells, hair cycle, and skin carcinogenesis. *Cell* **61,** 1329–1337 (1990).

8. Snippert, H. J. & Clevers, H. Tracking adult stem cells. *EMBO Reports* **12,** 113–122 (2011).

9. Wilson, A. *et al.* Hematopoietic Stem Cells Reversibly Switch from Dormancy to Self-Renewal during Homeostasis and Repair. *Cell* **135,** 1118–1129 (2008).

10. Foudi, A. *et al.* Analysis of histone 2B-GFP retention reveals slowly cycling hematopoietic stem cells. *Nat. Biotechnol.* **27,** 84–90 (2009).

11.   Klein, A. M., Nakagawa, T., Ichikawa, R., Yoshida, S. & Simons, B. D. Mouse germ line stem cells undergo rapid and stochastic turnover. *Cell Stem Cell* **7,** 214–224 (2010).

12.   Jones, K. B. & Klein, O. D. Oral epithelial stem cells in tissue maintenance and disease: The first steps in a long journey. *International Journal of Oral Science* **5,** 121–129 (2013).

13.   Reynolds, B. A. & Weiss, S. Generation of neurons and astrocytes from isolated cells of the adult mammalian central nervous system. *Science* **255,** 1707–10 (1992).

14.   Dexter, T. M., Allen, T. D. & Lajtha, L. G. Conditions controlling the proliferation of haemopoietic stem cells in vitro. *J. Cell. Physiol.* **91,** 335–344 (1977).

15.   Rheinwald, J. G. & Green, H. Serial Cultivation of Strains of Human Epidermal Keratinocytes: the Formation of Keratinizing Colonies from Single Cells. *Cell* **6,** 331–344 (1975).

16.   Sato, T. *et al.* Single Lgr5 stem cells build crypt-villus structures in vitro without a mesenchymal niche. *Nature* **459,** 262–265 (2009).

17.   Pastrana, E., Silva-Vargas, V. & Doetsch, F. Eyes wide open: A critical review of sphere-formation as an assay for stem cells. *Cell Stem Cell* **8,** 486–498 (2011).

18.   Wilson, N. K. *et al.* Combined Single-Cell Functional and Gene Expression Analysis Resolves Heterogeneity within Stem Cell Populations. *Cell Stem Cell* **16,** 712–724 (2015).

19.   Spangrude, G. J., Heimfeld, S. & Weissman, I. L. Purification and characterization of mouse hematopoietic stem cells. *Science (80-.).* **241,** 58–62 (1988).

20.   Shackleton, M. *et al.* Generation of a functional mammary gland from a single stem cell. *Nature* **439,** 84–88 (2006).

21.   Stingl, J. *et al.* Purification and unique properties of mammary epithelial stem cells. *Nature* **439,** 993–997 (2006).

22.	Sun, J. *et al.* Clonal dynamics of native haematopoiesis. *Nature* **514,** 322–327 (2014).

23.	Busch, K. *et al.* Fundamental properties of unperturbed haematopoiesis from stem cells in vivo. *Nature* (2015). doi:10.1038/nature14242

24.	Van Keymeulen, A. *et al.* Distinct stem cells contribute to mammary gland development and maintenance. *Nature* **479,** 189–193 (2011).

25.	Van Amerongen, R., Bowman, A. N. & Nusse, R. Developmental stage and time dictate the fate of Wnt/β-catenin- responsive stem cells in the mammary gland. *Cell Stem Cell* **11,** 387–400 (2012).

26.	Visvader, J. E. & Stingl, J. Mammary stem cells and the differentiation hierarchy: Current status and perspectives. *Genes Dev.* **28,** 1143–1158 (2014).

27.	Kretzschmar, K. & Watt, F. M. Lineage tracing. *Cell* **148,** 33–45 (2012).

28.	Buckingham, M. E. & Meilhac, S. M. Tracing cells for tracking cell lineage and clonal behavior. *Dev. Cell* **21,** 394–409 (2011).

29.	Barker, N. *et al.* Identification of stem cells in small intestine and colon by marker gene Lgr5. *Nature* **449,** 1003–1007 (2007).

30.	Morris, R. J. *et al.* Capturing and profiling adult hair follicle stem cells. *Nat. Biotechnol.* **22,** 411–417 (2004).

31.	Wang, B., Zhao, L., Fish, M., Logan, C. Y. & Nusse, R. Self-renewing diploid Axin2 + cells fuel homeostatic renewal of the liver. *Nature* **524,** 180–185 (2015).

32.	Barker, N., Van Oudenaarden, A. & Clevers, H. Identifying the stem cell of the intestinal crypt: Strategies and pitfalls. *Cell Stem Cell* **11,** 452–460 (2012).

33.	Joseph, C. *et al.* Deciphering Hematopoietic Stem Cells in Their Niches: A Critical Appraisal of Genetic Models, Lineage Tracing, and Imaging Strategies. *Cell Stem Cell* **13,**

520–533 (2013).

34.   Hirrlinger, J. *et al.* Split-Cre complementation indicates coincident activity of different genes in vivo. *PLoS One* **4,** (2009).

35.   He, L. *et al.* Enhancing the precision of genetic lineage tracing using dual recombinases. *Nat. Med.* **23,** 1488–1498 (2017).

36.   Nusse, Y. M. & Klein, O. D. If a stem cell dies in the crypt, and no one is around to see it... *Cell Stem Cell* **12,** 389–390 (2013).

37.   Savage, D. C. Microbial ecology of the gastrointestinal tract. *Annu Rev Microbiol* **31,** 107–133 (1977).

38.   Williams, J. M. *et al.* Epithelial Cell Shedding and Barrier Function: A Matter of Life and Death at the Small Intestinal Villus Tip. *Vet. Pathol.* **52,** 445–455 (2015).

39.   Peterson, L. W. & Artis, D. Intestinal epithelial cells: Regulators of barrier function and immune homeostasis. *Nat. Rev. Immunol.* **14,** 141–153 (2014).

40.   Gerbe, F. *et al.* Intestinal epithelial tuft cells initiate type 2 mucosal immunity to helminth parasites. *Nature* **529,** 226–230 (2016).

41.   Von Moltke, J., Ji, M., Liang, H. E. & Locksley, R. M. Tuft-cell-derived IL-25 regulates an intestinal ILC2-epithelial response circuit. *Nature* **529,** 221–225 (2016).

42.   Gerbe, F. *et al.* Distinct ATOH1 and Neurog3 requirements define tuft cells as a new secretory cell type in the intestinal epithelium. *J. Cell Biol.* **192,** 767–780 (2011).

43.   Worthington, J. J., Reimann, F. & Gribble, F. M. Enteroendocrine cells-sensory sentinels of the intestinal environment and orchestrators of mucosal immunity. *Mucosal Immunology* **11,** 3–20 (2018).

44.   Clevers, H. C. & Bevins, C. L. Paneth Cells: Maestros of the Small Intestinal Crypts.

Annu. Rev. Physiol. **75,** 289–311 (2013).

45.   Garabedian, E. M., Roberts, L. J. J., McNevin, M. S. & Gordon, J. I. Examining the role of Paneth cells in the small intestine by lineage ablation in transgenic mice. *J. Biol. Chem.* **272,** 23729–23740 (1997).

46.   Bevins, C. L. & Salzman, N. H. Paneth cells, antimicrobial peptides and maintenance of intestinal homeostasis. *Nat. Rev. Microbiol.* **9,** 356–368 (2011).

47.   Adolph, T. E. *et al.* Paneth cells as a site of origin for intestinal inflammation. *Nature* (2013). doi:10.1038/nature12599

48.   Haramis, A. P. G. *et al.* De Novo Crypt Formation and Juvenile Polyposis on BMP Inhibition in Mouse Intestine. *Science (80-.).* **303,** 1684–1686 (2004).

49.   Batts, L. E., Polk, D. B., Dubois, R. N. & Kulessa, H. Bmp signaling is required for intestinal growth and morphogenesis. *Dev. Dyn.* **235,** 1563–1570 (2006).

50.   Walton, K. D. *et al.* Hedgehog-responsive mesenchymal clusters direct patterning and emergence of intestinal villi. *Proc. Natl. Acad. Sci.* **109,** 15817–15822 (2012).

51.   Shyer, A. E. *et al.* Villification: How the gut gets its villi. *Science (80-.).* **342,** 212–218 (2013).

52.   Sumigray, K. D., Terwilliger, M. & Lechler, T. Morphogenesis and Compartmentalization of the Intestinal Crypt. *Dev. Cell* **45,** 183–197.e5 (2018).

53.   Gregorieff, A. & Clevers, H. Wnt signaling in the intestinal epithelium: From endoderm to cancer. *Genes Dev.* **19,** 877–890 (2005).

54.   Bry, L. *et al.* Paneth cell differentiation in the developing intestine of normal and transgenic mice. *Proc. Natl. Acad. Sci. U. S. A.* **91,** 10335–10339 (1994).

55.   Perdigoto, C. N. & Bardin, A. J. Sending the right signal: Notch and stem cells. *Biochim.*

Biophys. Acta - Gen. Subj. **1830,** 2307–2322 (2013).

56.   Zecchini, V., Domaschenz, R., Winton, D. & Jones, P. Notch signaling regulates the differentiation of post-mitotic intestinal epithelial cells. *Genes Dev.* **19,** 1686–1691 (2005).

57.   Noah, T. K. & Shroyer, N. F. Notch in the Intestine: Regulation of Homeostasis and Pathogenesis. *Annu. Rev. Physiol* **75,** 263–88 (2013).

58.   Fre, S. *et al.* Notch signals control the fate of immature progenitor cells in the intestine. *Nature* **435,** 964–968 (2005).

59.   Van Es, J. H. *et al.* Notch/γ-secretase inhibition turns proliferative cells in intestinal crypts and adenomas into goblet cells. *Nature* **435,** 959–963 (2005).

60.   Ponder, B. A. J. *et al.* Derivation of mouse intestinal crypts from single progenitor cells. *Nature* **313,** 689–691 (1985).

61.   Schmidt, G. H., Winton, D. J. & Ponder, B. a. Development of the pattern of cell renewal in the crypt-villus unit of chimaeric mouse small intestine. *Development* **103,** 785–790 (1988).

62.   Potten, C. S., Gandara, R., Mahida, Y. R., Loeffler, M. & Wright, N. A. The stem cells of small intestinal crypts: Where are they? *Cell Prolif.* **42,** 731–750 (2009).

63.   Cheng, H. & Leblond, C. P. Origin, differentiation and renewal of the four main epithelial cell types in the mouse small intestine V. Unitarian theory of the origin of the four epithelial cell types. *Am. J. Anat.* **141,** 537–561 (1974).

64.   Drost, J. & Clevers, H. Organoids in cancer research. *Nat. Rev. Cancer* 1 (2018). doi:10.1038/s41568-018-0007-6

65.   Clevers, H. Modeling Development and Disease with Organoids. *Cell* **165,** 1586–1597

(2016).

66.   van der Flier, L. G. *et al.* Transcription Factor Achaete Scute-Like 2 Controls Intestinal
        Stem Cell Fate. *Cell* **136,** 903–912 (2009).

67.   van der Flier, L. G., Haegebarth, A., Stange, D. E., van de Wetering, M. & Clevers, H.
        OLFM4 Is a Robust Marker for Stem Cells in Human Intestine and Marks a Subset of
        Colorectal Cancer Cells. *Gastroenterology* **137,** 15–17 (2009).

68.   Muñoz, J. *et al.* The Lgr5 intestinal stem cell signature: Robust expression of proposed
        quiescent ′ +4′ cell markers. *EMBO J.* **31,** 3079–3091 (2012).

69.   Ritsma, L. *et al.* Intestinal crypt homeostasis revealed at single-stem-cell level by in vivo
        live imaging. *Nature* **507,** 362–365 (2014).

70.   Grün, D. *et al.* De Novo Prediction of Stem Cell Identity using Single-Cell Transcriptome
        Data. *Cell Stem Cell* **19,** 266–277 (2016).

71.   Dalerba, P. *et al.* Single-cell dissection of transcriptional heterogeneity in human colon
        tumors. *Nat. Biotechnol.* **29,** 1120–1127 (2011).

72.   Haber, A. L. *et al.* A single-cell survey of the small intestinal epithelium. *Nature* **551,**
        333–339 (2017).

73.   Kester, L. & Oudenaarden, A. Van. Single-Cell Transcriptomics Meets Lineage Tracing.
        Celll Stem Cell 1–14 (2018). doi:10.1016/j.stem.2018.04.014

74.   Al-Hajj, M., Becker, M. W., Wicha, M., Weissman, I. & Clarke, M. F. Therapeutic
        implications of cancer stem cells. *Curr. Opin. Genet. Dev.* **14,** 43–47 (2004).

75.   Li, L. & Clevers, H. Coexistence of quiescent and active adult stem cells in mammals.
        Science **327,** 542–545 (2010).

76.   Dean, M., Fojo, T. & Bates, S. Tumour stem cells and drug resistance. *Nature Reviews*

Cancer **5,** 275–284 (2005).

77. Weissman, I. L. Stem cells: units of development, units of regeneration, and units in evolution. *Cell* **100,** 157–168 (2000).

78. Arai, F. *et al.* Tie2/angiopoietin-1 signaling regulates hematopoietic stem cell quiescence in the bone marrow niche. *Cell* **118,** 149–161 (2004).

79. Winton, D. J. & Ponder, B. A. J. Stem-Cell Organization in Mouse Small Intestine. *Proc. R. Soc.* **241,** 13–18 (1990).

80. Potten, C. S. Extreme sensitivity of some intestinal crypt cells to X and γ irradiation. *Nature* **269,** 518–521 (1977).

81. Sangiorgi, E. & Capecchi, M. R. Bmi1 is expressed in vivo in intestinal stem cells. *Nat. Genet.* **40,** 915–920 (2008).

82. Stern, C. E. *et al.* Interconversion Between Intestinal Stem Cell Populations in Distinct Niches. *Science (80-.).* **334,** 1420–1424 (2011).

83. Montgomery, R. K. *et al.* Mouse telomerase reverse transcriptase (mTert) expression marks slowly cycling intestinal stem cells. *Proc. Natl. Acad. Sci.* **108,** 179–184 (2011).

84. Powell, A. E. *et al.* The pan-ErbB negative regulator lrig1 is an intestinal stem cell marker that functions as a tumor suppressor. *Cell* **149,** 146–158 (2012).

85. Itzkovitz, S. *et al.* Single-molecule transcript counting of stem-cell markers in the mouse intestine. *Nat. Cell Biol.* **14,** 106–114 (2012).

86. Yan, K. S. *et al.* Intestinal Enteroendocrine Lineage Cells Possess Homeostatic and Injury-Inducible Stem Cell Activity. *Cell Stem Cell* **21,** 78–90.e6 (2017).

87. Fuchs, E. & Horsley, V. Ferreting out stem cells from their niches. *Nat. Cell Biol.* **13,** 513–518 (2011).

88. Wagers, A. J. The stem cell niche in regenerative medicine. *Cell Stem Cell* **10,** 362–369 (2012).

89. Sato, T. *et al.* Paneth cells constitute the niche for Lgr5 stem cells in intestinal crypts. *Nature* **469,** 415–418 (2011).

90. Sasaki, N. *et al.* Reg4+ deep crypt secretory cells function as epithelial niche for Lgr5+ stem cells in colon. *Proc. Natl. Acad. Sci.* **113,** E5399–E5407 (2016).

91. Rothenberg, M. E. *et al.* Identification of a cKit+colonic crypt base secretory cell that supports Lgr5+stem cells in mice. *Gastroenterology* **142,** 1195–1205.e6 (2012).

92. Kim, T.-H., Escudero, S. & Shivdasani, R. A. Intact function of Lgr5 receptor-expressing intestinal stem cells in the absence of Paneth cells. *Proc. Natl. Acad. Sci.* **109,** 3932–3937 (2012).

93. Kabiri, Z. *et al.* Stroma provides an intestinal stem cell niche in the absence of epithelial Wnts. *Development* **141,** 2206–2215 (2014).

94. Shoshkes-carmel, M., Wang, Y. J., Wangensteen, K. J., Itzkovitz, S. & Kaestner, K. H. Subepithelial telocytes are the source of Wnts that support intestinal crypts. *Nature* (2018). doi:10.1038/s41586-018-0084-4

95. San Roman, A. K., Jayewickreme, C. D., Murtaugh, L. C. & Shivdasani, R. A. Wnt secretion from epithelial cells and subepithelial myofibroblasts is not required in the mouse intestinal stem cell niche in vivo. *Stem Cell Reports* **2,** 127–134 (2014).

96. Greicius, G. *et al. PDGFRα* $^+$ pericryptal stromal cells are the critical source of Wnts and RSPO3 for murine intestinal stem cells in vivo. *Proc. Natl. Acad. Sci.* 201713510 (2018). doi:10.1073/pnas.1713510115

97. Beumer, J. & Clevers, H. Regulation and plasticity of intestinal stem cells during

homeostasis and regeneration. *Development* **143,** 3639–3649 (2016).

98.   Clevers, H. & Nusse, R. Wnt/β-catenin signaling and disease. *Cell* **149,** 1192–1205 (2012).

99.   Fevr, T., Robine, S., Louvard, D. & Huelsken, J. Wnt/ -Catenin Is Essential for Intestinal Homeostasis and Maintenance of Intestinal Stem Cells. *Mol. Cell. Biol.* **27,** 7551–7559 (2007).

100.   van Es, J. H. *et al.* A Critical Role for the Wnt Effector Tcf4 in Adult Intestinal Homeostatic Self-Renewal. *Mol. Cell. Biol.* **32,** 1918–1927 (2012).

101.   Su, L. *et al.* Multiple intestinal neoplasia caused by a mutation in the murine homolog of the APC gene. *Science (80-.).* **256,** 668–670 (1992).

102.   Pinto, D. & Clevers, H. Wnt, stem cells and cancer in the intestine. *Biol. Cell* **97,** 185–196 (2005).

103.   Morin, P. J. *et al.* Activation of β-catenin-Tcf signaling in colon cancer by mutations in β-catenin or APC. *Science (80-.).* **275,** 1787–1790 (1997).

104.   Polakis, P. The adenomatous polyposis coil (APC) tumor suppressor. *Biochim. Biophys. Acta - Rev. Cancer* **1332,** F127–F147 (1997).

105.   Lustig, B. *et al.* Negative feedback loop of Wnt signaling through upregulation of conductin/axin2 in colorectal and liver tumors. *Mol. Cell. Biol.* **22,** 1184–93 (2002).

106.   Farin, H. F., Van Es, J. H. & Clevers, H. Redundant sources of Wnt regulate intestinal stem cells and promote formation of paneth cells. *Gastroenterology* **143,** 1518–1529.e7 (2012).

107.   Farin, H. F. *et al.* Visualization of a short-range Wnt gradient in the intestinal stem-cell niche. *Nature* **530,** 340–343 (2016).

108. Aoki, R. *et al.* Foxl1-Expressing Mesenchymal Cells Constitute the Intestinal Stem Cell Niche. *Cell. Mol. Gastroenterol. Hepatol.* **2,** 175–188 (2016).

109. Schuijers, J. *et al.* Ascl2 acts as an R-spondin/wnt-responsive switch to control stemness in intestinal crypts. *Cell Stem Cell* **16,** 158–170 (2015).

110. Van der Flier, L. G. *et al.* The Intestinal Wnt/TCF Signature. *Gastroenterology* **132,** 628–632 (2007).

111. de Lau, W., Peng, W. C., Gros, P. & Clevers, H. The R-spondin/Lgr5/Rnf43 module: Regulator of Wnt signal strength. *Genes Dev.* **28,** 305–316 (2014).

112. De Lau, W. *et al.* Lgr5 homologues associate with Wnt receptors and mediate R-spondin signalling. *Nature* **476,** 293–297 (2011).

113. Hao, H. X. *et al.* ZNRF3 promotes Wnt receptor turnover in an R-spondin-sensitive manner. *Nature* **485,** 195–202 (2012).

114. Xie, Y. *et al.* Interaction with both ZNRF3 and LGR4 is required for the signalling activity of R-spondin. *EMBO Rep.* **14,** 1120–1126 (2013).

115. Carmon, K. S., Gong, X., Lin, Q., Thomas, A. & Liu, Q. R-spondins function as ligands of the orphan receptors LGR4 and LGR5 to regulate Wnt/ -catenin signaling. *Proc. Natl. Acad. Sci.* **108,** 11452–11457 (2011).

116. Sato, T. & Clevers, H. Growing self-organizing mini-guts from a single intestinal stem cell: Mechanism and applications. *Science (80-.).* **340,** 1190–1194 (2013).

117. Ootani, A. *et al.* Sustained in vitro intestinal epithelial culture within a Wnt-dependent stem cell niche. *Nat. Med.* **15,** 701–706 (2009).

118. Kim, K. A. *et al.* Mitogenic influence of human R-spondin1 on the intestinal epithelium. *Science (80-.).* **309,** 1256–1259 (2005).

119. Yan, K. S. *et al.* Non-equivalence of Wnt and R-spondin ligands during Lgr5 + intestinal stem-cell self-renewal. *Nature* **545,** 238–242 (2017).

120. Storm, E. E. *et al.* Targeting PTPRK-RSPO3 colon tumours promotes differentiation and loss of stem-cell function. *Nature* **529,** 97–100 (2016).

121. Kinzel, B. *et al.* Functional roles of Lgr4 and Lgr5 in embryonic gut, kidney and skin development in mice. *Dev. Biol.* **390,** 181–190 (2014).

122. Kang, E., Yousefi, M. & Gruenheid, S. R-spondins are expressed by the intestinal stroma and are differentially regulated during Citrobacter rodentium- and dssinduced colitis in mice. *PLoS One* **11,** (2016).

123. Stzepourginski, I. *et al.* CD34 [+] mesenchymal cells are a major component of the intestinal stem cells niche at homeostasis and after injury. *Proc. Natl. Acad. Sci.* **114,** E506–E513 (2017).

124. Wilson, A. & Radtke, F. Multiple functions of Notch signaling in self-renewing organs and cancer. *FEBS Lett.* **580,** 2860–2868 (2006).

125. Stanger, B. Z., Datar, R., Murtaugh, L. C. & Melton, D. A. Direct regulation of intestinal fate by Notch. *Proc. Natl. Acad. Sci.* **102,** 12443–12448 (2005).

126. Stamataki, D. *et al.* Delta1 expression, cell cycle exit, and commitment to a specific secretory fate coincide within a few hours in the mouse intestinal stem cell system. *PLoS One* **6,** (2011).

127. van Es, J. H. *et al.* Dll1 + secretory progenitor cells revert to stem cells upon crypt damage. *Nat. Cell Biol.* **14,** 1099–1104 (2012).

128. van Es, J. H., de Geest, N., van de Born, M., Clevers, H. & Hassan, B. A. Intestinal stem cells lacking the Math1 tumour suppressor are refractory to Notch inhibitors. *Nat.*

Commun. **1,** 1–5 (2010).

129. Pellegrinet, L. *et al.* Dll1- and Dll4-mediated notch signaling are required for homeostasis of intestinal stem cells. *Gastroenterology* **140,** 1230–1240 (2011).

130. Riccio, O. *et al.* Loss of intestinal crypt progenitor cells owing to inactivation of both Notch1 and Notch2 is accompanied by derepression of CDK inhibitors p27Kip1 and p57Kip2. *EMBO Rep.* **9,** 377–383 (2008).

131. VanDussen, K. L. *et al.* Notch signaling modulates proliferation and differentiation of intestinal crypt base columnar stem cells. *Development* **139,** 488–497 (2012).

132. Mahé, M. M. *et al.* Establishment of gastrointestinal epithelial organoids. *Curr Protoc Mouse Biol* **3,** 217–240 (2014).

133. Tian, H. *et al.* Opposing activities of notch and wnt signaling regulate intestinal stem cells and gut homeostasis. *Cell Rep.* **11,** 33–42 (2015).

134. Kwon, C. *et al.* Notch post-translationally regulates β-catenin protein in stem and progenitor cells. *Nat. Cell Biol.* **13,** 1244–1251 (2011).

135. Marchbank, T., Goodlad, R. A., Lee, C. Y. & Playford, R. J. Luminal epidermal growth factor is trophic to the small intestine of parenterally fed rats. *Clin. Sci.* **89,** 117–120 (1995).

136. Miettinen, P. J. *et al.* Epithelial immaturity and multiorgan failure in mice lacking epidermal growth factor receptor. *Nature* **376,** 337–41 (1995).

137. He, X. C. *et al.* BMP signaling inhibits intestinal stem cell self-renewal through suppression of Wnt–β-catenin signaling. *Nat. Genet.* **36,** 1117–1121 (2004).

138. Qi, Z. *et al.* BMP restricts stemness of intestinal Lgr5 + stem cells by directly suppressing their signature genes. *Nat. Commun.* **8,** 1–14 (2017).

139. Hardwick, J. C. H. *et al.* Bone Morphogenetic Protein 2 Is Expressed by, and Acts Upon, Mature Epithelial Cells in the Colon. *Gastroenterology* **126,** 111–121 (2004).

140. Kosinski, C. *et al.* Gene expression patterns of human colon tops and basal crypts and BMP antagonists as intestinal stem cell niche factors. *Proc. Natl. Acad. Sci.* **104,** 15418–15423 (2007).

141. Yu, F.-X., Meng, Z., Plouffe, S. W. & Guan, K.-L. Hippo Pathway Regulation of Gastrointestinal Tissues. *Annu. Rev. Physiol.* **77,** 201–227 (2015).

142. Piccolo, S. & Cordenonsi, M. Regulation of YAP and TAZ by epithelial plasticity. in *The Hippo Signaling Pathway and Cancer* **9781461462,** 89–113 (2013).

143. Yu, F. X. & Guan, K. L. The Hippo pathway: Regulators and regulations. *Genes Dev.* **27,** 355–371 (2013).

144. Meng, Z., Moroishi, T. & Guan, K. Mechanisms of Hippo pathway regulation. *Genes Dev.* **30,** 1–17 (2016).

145. Cai, J. *et al.* The Hippo signaling pathway restricts the oncogenic potential of an intestinal regeneration program. *Genes Dev.* **24,** 2383–2388 (2010).

146. Azzolin, L. *et al.* YAP/TAZ incorporation in the β-catenin destruction complex orchestrates the Wnt response. *Cell* **158,** 157–170 (2014).

147. Gregorieff, A., Liu, Y., Inanlou, M. R., Khomchuk, Y. & Wrana, J. L. Yap-dependent reprogramming of Lgr5+ stem cells drives intestinal regeneration and cancer. *Nature* **526,** 715–718 (2015).

148. Taniguchi, K. *et al.* A gp130-Src-YAP module links inflammation to epithelial regeneration. *Nature* **519,** 57–62 (2015).

149. Tian, H. *et al.* A reserve stem cell population in small intestine renders Lgr5-positive cells

dispensable. *Nature* **478,** 255–259 (2011).

150. Buczacki, S. J. A. *et al.* Intestinal label-retaining cells are secretory precursors expressing Lgr5. *Nature* **495,** 65–69 (2013).

151. Tetteh, P. W. *et al.* Replacement of Lost Lgr5-Positive Stem Cells through Plasticity of Their Enterocyte-Lineage Daughters. *Cell Stem Cell* **18,** 203–213 (2016).

152. Jadhav, U. *et al.* Dynamic Reorganization of Chromatin Accessibility Signatures during Dedifferentiation of Secretory Precursors into Lgr5+ Intestinal Stem Cells. *Cell Stem Cell* **21,** 65–77.e5 (2017).

153. De Sousa E Melo, F. *et al.* A distinct role for Lgr5 + stem cells in primary and metastatic colon cancer. *Nature* **543,** 676–680 (2017).

154. Schwitalla, S. *et al.* Intestinal tumorigenesis initiated by dedifferentiation and acquisition of stem-cell-like properties. *Cell* **152,** 25–38 (2013).

155. Klein, A. M. & Simons, B. D. Universal patterns of stem cell fate in cycling adult tissues. *Development* **138,** 3103–3111 (2011).

156. Klein, A. M., Doupé, D. P., Jones, P. H. & Simons, B. D. Kinetics of cell division in epidermal maintenance. *Phys. Rev. E - Stat. Nonlinear, Soft Matter Phys.* **76,** 021910 (2007).

157. Snippert, H. J. *et al.* Intestinal crypt homeostasis results from neutral competition between symmetrically dividing Lgr5 stem cells. *Cell* **143,** 134–144 (2010).

158. Lopez-Garcia, C., Klein, A. M., Simons, B. D. & Winton, D. J. Intestinal stem cell replacement follows a pattern of neutral drift. *Science (80-.).* **330,** 822–825 (2010).

159. Potten, C. S. The Epidermal Proliferative Unit: the Possible Role of the Central Basal Cell. *Cell Prolif.* **7,** 77–88 (1974).

160. Doupé, D. P., Klein, A. M., Simons, B. D. & Jones, P. H. The Ordered Architecture of Murine Ear Epidermis Is Maintained by Progenitor Cells with Random Fate. *Dev. Cell* **18,** 317–323 (2010).

161. Clayton, E. *et al.* A single type of progenitor cell maintains normal epidermis. *Nature* **446,** 185–189 (2007).

162. Gadani, S. P., Walsh, J. T., Lukens, J. R. & Kipnis, J. Dealing with Danger in the CNS: The Response of the Immune System to Injury. *Neuron* **87,** 47–62 (2015).

163. Niethammer, P. The early wound signals. *Curr. Opin. Genet. Dev.* **40,** 17–22 (2016).

164. Rider, P., Voronov, E., Dinarello, C. A., Apte, R. N. & Cohen, I. Alarmins: Feel the Stress. *J. Immunol.* **198,** 1395–1402 (2017).

165. Kubes, P. & Mehal, W. Z. Sterile Inflammation in the Liver. *Gastroenterology* **143,** 1158–1172 (2012).

166. Takeuchi, O. & Akira, S. Pattern Recognition Receptors and Inflammation. *Cell* **140,** 805–820 (2010).

167. Chen, G. Y. & Nuñez, G. Sterile inflammation: Sensing and reacting to damage. *Nat. Rev. Immunol.* **10,** 826–837 (2010).

168. Ivashkiv, L. B. & Donlin, L. T. Regulation of type i interferon responses. *Nat. Rev. Immunol.* **14,** 36–49 (2014).

169. Platanias, L. C. Mechanisms of type-I- and type-II-interferon-mediated signalling. *Nat. Rev. Immunol.* **5,** 375–386 (2005).

170. Valente, G. *et al.* Distribution of interferon-γ receptor in human tissues. *Eur. J. Immunol.* **22,** 2403–2412 (1992).

171. Stark, G. R. & Darnell, J. E. The JAK-STAT Pathway at Twenty. *Immunity* **36,** 503–514

(2012).

172. Schneider, W. M., Chevillotte, M. D. & Rice, C. M. Interferon-Stimulated Genes: A Complex Web of Host Defenses. *Annu. Rev. Immunol.* **32,** 513–545 (2014).

173. Essers, M. A. G. *et al.* IFNα activates dormant haematopoietic stem cells in vivo. *Nature* **458,** 904–908 (2009).

174. Baldridge, M. T., King, K. Y., Boles, N. C., Weksberg, D. C. & Goodell, M. A. Quiescent haematopoietic stem cells are activated by IFN-?? in response to chronic infection. *Nature* **465,** 793–797 (2010).

175. Sun, L. *et al.* Type i interferons link viral infection to enhanced epithelial turnover and repair. *Cell Host Microbe* **17,** 85–97 (2015).

176. Artis, D., Potten, C. S., Else, K. J., Finkelman, F. D. & Grencis, R. K. Trichuris muris: Host Intestinal Epithelial Cell Hyperproliferation during Chronic Infection Is Regulated by Interferon-$\upgamma$. *Exp. Parasitol.* **92,** 144–153 (1999).

177. Tidball, J. G. Regulation of muscle growth and regeneration by the immune system. *Nat. Rev. Immunol.* **17,** 165–178 (2017).

178. Brack, A. S. & Rando, T. A. Tissue-specific stem cells: Lessons from the skeletal muscle satellite cell. *Cell Stem Cell* **10,** 504–514 (2012).

179. Mauro, A. Satellite cell of skeletal muscle fibers. *J. Biophys. Biochem. Cytol.* **9,** 493–495 (1961).

180. Sambasivan, R. *et al.* Pax7-expressing satellite cells are indispensable for adult skeletal muscle regeneration. *Development* **138,** 4333–4333 (2011).

181. Lepper, C., Partridge, T. A. & Fan, C.-M. An absolute requirement for Pax7-positive satellite cells in acute injury-induced skeletal muscle regeneration. *Development* **138,**

3639–3646 (2011).

182. Dziki, J. L., Velayutham, M., Hussey, G. S. & Turnquist, H. R. Cytokine networks in immune-mediated muscle regeneration. *J. Immunol. Regen. Med.* **1,** 32–44 (2018).

183. Deng, B., Wehling-Henricks, M., Villalta, S. A., Wang, Y. & Tidball, J. G. IL-10 Triggers Changes in Macrophage Phenotype That Promote Muscle Growth and Regeneration. *J. Immunol.* **189,** 3669–3680 (2012).

184. Chazaud, B. *et al.* Satellite cells attract monocytes and use macrophages as a support to escape apoptosis and enhance muscle growth. *J. Cell Biol.* **163,** 1133–1143 (2003).

185. Saclier, M. *et al.* Differentially activated macrophages orchestrate myogenic precursor cell fate during human skeletal muscle regeneration. *Stem Cells* **31,** 384–396 (2013).

186. Lu, H., Huang, D., Ransohoff, R. M. & Zhou, L. Acute skeletal muscle injury: CCL2 expression by both monocytes and injured muscle is required for repair. *FASEB J.* **25,** 3344–3355 (2011).

187. Londhe, P. & Davie, J. K. Interferon-γ resets muscle cell fate by stimulating the sequential recruitment of JARID2 and PRC2 to promoters to repress myogenesis. *Sci. Signal.* **6,** (2013).

188. Londhe, P. & Davie, J. K. Gamma interferon modulates myogenesis through the major histocompatibility complex class II transactivator, CIITA. *Mol. Cell. Biol.* **31,** 2854–2866 (2011).

189. LANGEN, R. C. J. Tumor necrosis factor-alpha inhibits myogenic differentiation through MyoD protein destabilization. *FASEB J.* **18,** 227–237 (2004).

190. Tonkin, J. *et al.* Monocyte/macrophage-derived IGF-1 orchestrates murine skeletal muscle regeneration and modulates autocrine polarization. *Mol. Ther.* **23,** 1189–1200 (2015).

191. Burzyn, D. *et al.* A Special Population of regulatory T Cells Potentiates muscle repair. *Cell* **155,** 1282–1295 (2013).

192. Duncan, A. W., Dorrell, C. & Grompe, M. Stem Cells and Liver Regeneration. *Gastroenterology* **137,** 466–481 (2009).

193. Stanger, B. Z. Cellular Homeostasis and Repair in the Mammalian Liver. *Annu. Rev. Physiol.* **77,** 179–200 (2015).

194. Huch, M. *et al.* In vitro expansion of single Lgr5 + liver stem cells induced by Wnt-driven regeneration. *Nature* **494,** 247–250 (2013).

195. Lu, W. Y. *et al.* Hepatic progenitor cells of biliary origin with liver repopulation capacity. *Nat. Cell Biol.* **17,** 973–983 (2015).

196. Yanger, K. *et al.* Adult hepatocytes are generated by self-duplication rather than stem cell differentiation. *Cell Stem Cell* **15,** 340–349 (2014).

197. Schaub, J. R., Malato, Y., Gormond, C. & Willenbring, H. Evidence against a stem cell origin of new hepatocytes in a common mouse model of chronic liver injury. *Cell Rep.* **8,** 933–939 (2014).

198. Lin, S. *et al.* Distributed hepatocytes expressing telomerase repopulate the liver in homeostasis and injury. *Nature* **556,** 244–248 (2018).

199. Rountree, C. B., Mishra, L. & Willenbring, H. Stem cells in liver diseases and cancer: Recent advances on the path to new therapies. *Hepatology* **55,** 298–306 (2012).

200. Fausto, N. Liver regeneration and repair: Hepatocytes, progenitor cells, and stem cells. *Hepatology* **39,** 1477–1487 (2004).

201. Bird, T. G., Lorenzini, S. & Forbes, S. J. Activation of stem cells in hepatic diseases. *Cell Tissue Res.* **331,** 283–300 (2008).

202. Michalopoulos, G. K. Phenotypic fidelity (or not?) of epithelial cells in the liver. *Hepatology* **55,** 2024–2027 (2012).

203. Yimlamai, D. *et al.* Hippo pathway activity influences liver cell fate. *Cell* **157,** 1324–1338 (2014).

204. Markose, D., Kirkland, P., Ramachandran, P. & Henderson, N. C. Immune cell regulation of liver regeneration and repair. *J. Immunol. Regen. Med.* (2018). doi:10.1016/j.regen.2018.03.003

205. Kubes, P. & Jenne, C. Immune Responses in the Liver. *Annu. Rev. Immunol. Annu. Rev. Immunol* **36,** 1–931 (2018).

206. Szabo, G. & Petrasek, J. Inflammasome activation and function in liver disease. *Nat. Rev. Gastroenterol. Hepatol.* **12,** 387–400 (2015).

207. Pittman, K. & Kubes, P. Damage-associated molecular patterns control neutrophil recruitment. *Journal of Innate Immunity* **5,** 315–323 (2013).

208. Wang, J. & Kubes, P. A Reservoir of Mature Cavity Macrophages that Can Rapidly Invade Visceral Organs to Affect Tissue Repair. *Cell* **165,** 668–678 (2016).

209. Wang, J. *et al.* Visualizing the function and fate of neutrophils in sterile injury and repair. *Science (80-.).* **358,** 111–116 (2017).

210. Dal-Secco, D. *et al.* A dynamic spectrum of monocytes arising from the in situ reprogramming of CCR2 $^{+}$ monocytes at a site of sterile injury. *J. Exp. Med.* **212,** 447–456 (2015).

211. Duffield, J. S. *et al.* Selective depletion of macrophages reveals distinct, opposing roles during liver injury and repair. *J. Clin. Invest.* **115,** 56–65 (2005).

212. Ramachandran, P. *et al.* Differential Ly-6C expression identifies the recruited macrophage

phenotype, which orchestrates the regression of murine liver fibrosis. *Proc. Natl. Acad. Sci.* **109,** E3186–E3195 (2012).

213. Boulter, L. *et al.* Macrophage-derived Wnt opposes Notch signaling to specify hepatic progenitor cell fate in chronic liver disease. *Nat. Med.* **18,** 572–579 (2012).

214. Goh, Y. P. S. *et al.* Eosinophils secrete IL-4 to facilitate liver regeneration. *Proc. Natl. Acad. Sci.* **110,** 9914–9919 (2013).

215. Liew, P. X., Lee, W. Y. & Kubes, P. iNKT Cells Orchestrate a Switch from Inflammation to Resolution of Sterile Liver Injury. *Immunity* **47,** 752–765.e5 (2017).

216. Blanpain, C., Mohrin, M., Sotiropoulou, P. A. & Passegué, E. DNA-damage response in tissue-specific and cancer stem cells. *Cell Stem Cell* **8,** 16–29 (2011).

217. Booth, C., Tudor, G., Tonge, N., Shea-Donohue, T. & MacVittie, T. J. Acute gastrointestinal syndrome in high-dose irradiated mice. *Health Phys.* **103,** 400–410 (2012).

218. Qiu, W. *et al.* PUMA Regulates Intestinal Progenitor Cell Radiosensitivity and Gastrointestinal Syndrome. *Cell Stem Cell* **2,** 576–583 (2008).

219. Merritt, A. J. *et al.* The Role of p53 in Spontaneous and Radiation-induced Apoptosis in the Gastrointestinal TVact of Normal and p53-deficient Mice. *Cancer Res.* **54,** 614–617 (1994).

220. Wilson, J. W., Pritchard, D. M., Hickman, J. A. & Potten, C. S. Radiation-Induced p53 and p21WAF–1/CIP1 Expression in the Murine Intestinal Epithelium. *Am. J. Pathol.* **153,** 899–909 (1998).

221. Potten, C. A. & Hendry, J. H. Differential regeneration of intestinal proliferative cells and cryptogenic cells after irradiation. *Int. J. Radiat. Biol.* **27,** 413–424 (1975).

222. Yan, K. S. *et al.* The intestinal stem cell markers Bmi1 and Lgr5 identify two functionally distinct populations. *Proc. Natl. Acad. Sci. U. S. A.* **109,** 466–471 (2012).

223. Tao, S. *et al.* Wnt activity and basal niche position sensitize intestinal stem and progenitor cells to DNA damage. *EMBO J.* **36,** 2920–2921 (2017).

224. Metcalfe, C., Kljavin, N. M., Ybarra, R. & De Sauvage, F. J. Lgr5+ stem cells are indispensable for radiation-induced intestinal regeneration. *Cell Stem Cell* **14,** 149–159 (2014).

225. Liu, T.-C. & Stappenbeck, T. S. Genetics and Pathogenesis of Inflammatory Bowel Disease. *Annu. Rev. Pathol. Mech. Dis.* **11,** 127–148 (2016).

226. Neurath, M. F. New targets for mucosal healing and therapy in inflammatory bowel diseases. *Mucosal Immunology* **7,** 6–19 (2014).

227. Elson, C. O. *et al.* Experimental models of inflammatory bowel disease reveal innate, adaptive, and regulatory mechanisms of host dialogue with the microbiota. *Immunol. Rev.* **206,** 260–276 (2005).

228. Kiesler, P., Fuss, I. J. & Strober, W. Experimental Models of Inflammatory Bowel Diseases. *C. Cell. Mol. Gastroenterol. Hepatol.* **1,** 154–170 (2015).

229. Boismenu, R. & Chen, Y. Insights from mouse models of colitis. *J. Leukoc. Biol* **67,** 267–278 (2000).

230. Dieleman, L. A. *et al.* Dextran sulfate sodium-induced colitis occurs in severe combined immunodeficient mice. *Gastroenterology* **107,** 1643–52 (1994).

231. Pull, S. L., Doherty, J. M., Mills, J. C., Gordon, J. I. & Stappenbeck, T. S. Activated macrophages are an adaptive element of the colonic epithelial progenitor niche necessary for regenerative responses to injury. *Proc. Natl. Acad. Sci.* **102,** 99–104 (2005).

232. Rakoff-Nahoum, S., Paglino, J., Eslami-Varzaneh, F., Edberg, S. & Medzhitov, R. Recognition of commensal microflora by toll-like receptors is required for intestinal homeostasis. *Cell* **118,** 229–241 (2004).

233. Cario, E., Gerken, G. & Podolsky, D. K. Toll-Like Receptor 2 Controls Mucosal Inflammation by Regulating Epithelial Barrier Function. *Gastroenterology* **132,** 1359–1374 (2007).

234. Scheeren, F. A. *et al.* A cell-intrinsic role for TLR2-MYD88 in intestinal and breast epithelia and oncogenesis. *Nat. Cell Biol.* **16,** 1238–1248 (2014).

235. Malvin, N. P., Seno, H. & Stappenbeck, T. S. Colonic epithelial response to injury requires Myd88 signaling in myeloid cells. *Mucosal Immunol.* **5,** 194–206 (2012).

236. Seno, H. *et al.* Efficient colonic mucosal wound repair requires Trem2 signaling. *Proc. Natl. Acad. Sci.* **106,** 256–261 (2009).

237. Lin, Y. *et al.* Chemerin aggravates DSS-induced colitis by suppressing M2 macrophage polarization. *Cell. Mol. Immunol.* **11,** 355–366 (2014).

238. Kuhn, K. A., Manieri, N. A., Liu, T. C. & Stappenbeck, T. S. IL-6 stimulates intestinal epithelial proliferation and repair after injury. *PLoS One* **9,** 1–18 (2014).

239. Miyoshi, H., Ajima, R., Luo, C. T., Yamaguchi, T. P. & Stappenbeck, T. S. Wnt5a potentiates TGF-β signaling to promote colonic crypt regeneration after tissue injury. *Science (80-.).* **338,** 108–113 (2012).

240. Davidson, L. A. *et al.* Alteration of colonic stem cell gene signatures during the regenerative response to injury. *Biochim. Biophys. Acta - Mol. Basis Dis.* **1822,** 1600–1607 (2012).

241. Shlomchik, W. D. Graft-versus-host disease. *Nat Rev Immunol* **7,** 340–352 (2007).

242. Takashima, S. *et al.* The Wnt agonist R-spondin1 regulates systemic graft-versus-host disease by protecting intestinal stem cells. *J. Exp. Med.* **208,** 285–294 (2011).

243. Hanash, A. M. *et al.* Interleukin-22 Protects Intestinal Stem Cells from Immune-Mediated Tissue Damage and Regulates Sensitivity to Graft versus Host Disease. *Immunity* **37,** 339–350 (2012).

244. Sonnenberg, G. F. & Artis, D. Innate lymphoid cells in the initiation, regulation and resolution of inflammation. *Nature Medicine* **21,** 698–708 (2015).

245. Dudakov, J. A., Hanash, A. M. & van den Brink, M. R. M. Interleukin-22: Immunobiology and Pathology. *Annu. Rev. Immunol.* **33,** 747–785 (2015).

246. Zenewicz, L. A. *et al.* Interleukin-22 but Not Interleukin-17 Provides Protection to Hepatocytes during Acute Liver Inflammation. *Immunity* **27,** 647–659 (2007).

247. Lindemans, C. A. *et al.* Interleukin-22 promotes intestinal-stem-cell-mediated epithelial regeneration. *Nature* **528,** 560–564 (2015).

248. Grainger, J. R. *et al.* Helminth secretions induce de novo T cell Foxp3 expression and regulatory function through the TGF-β pathway. *J. Exp. Med.* **207,** 2331–2341 (2010).

249. Grencis, R. K. Immunity to Helminths: Resistance, Regulation, and Susceptibility to Gastrointestinal Nematodes. *Annu. Rev. Immunol.* **33,** 201–225 (2015).

250. Buck, A. H. *et al.* Exosomes secreted by nematode parasites transfer small RNAs to mammalian cells and modulate innate immunity. *Nat. Commun.* **5,** 1–11 (2014).

251. Reynolds, L. A., Filbey, K. J. & Maizels, R. M. Immunity to the model intestinal helminth parasite Heligmosomoides polygyrus. *Semin. Immunopathol.* **34,** 829–846 (2012).

252. Else, K. J., Finkelman, F. D., Maliszewski, C. R. & Grencis, R. K. Cytokine-mediated regulation of chronic intestinal helminth infection. *J. Exp. Med.* **179,** 347–51 (1994).

253. Anthony, R. M. *et al.* Memory TH2 cells induce alternatively activated macrophages to mediate protection against nematode parasites. *Nat. Med.* **12,** 955–960 (2006).

254. Allen, J. E. & Maizels, R. M. Diversity and dialogue in immunity to helminths. *Nat. Rev. Immunol.* **11,** 375–388 (2011).

255. Artis, D. & Grencis, R. K. The intestinal epithelium: Sensors to effectors in nematode infection. *Mucosal Immunol.* **1,** 252–264 (2008).

256. Hashimoto, K. *et al.* Depleted intestinal goblet cells and severe pathological changes in SCID mice infected with Heligmosomoides polygyrus. *Parasite Immunol.* **31,** 457–465 (2009).

257. Behnke, J. M., Lowe, A., Clifford, S. & Wakelin, D. Cellular and serological responses in resistant and susceptible mice exposed to repeated infection with Heligmosomoides polygyrus bakeri. *Parasite Immunol.* **25,** 333–340 (2003).

258. Artis, D. *et al.* RELM /FIZZ2 is a goblet cell-specific immune-effector molecule in the gastrointestinal tract. *Proc. Natl. Acad. Sci.* **101,** 13596–13600 (2004).

259. Herbert, D. R. *et al.* Intestinal epithelial cell secretion of RELM-β protects against gastrointestinal worm infection. *J. Exp. Med.* **206,** 2947–2957 (2009).

260. McDermott, J. R. *et al.* Mast cells disrupt epithelial barrier function during enteric nematode infection. *Proc. Natl. Acad. Sci.* **100,** 7761–7766 (2003).

261. Cliffe, L. J. *et al.* Immunology - Accelerated intestinal epithelial cell turnover: A new mechanism of parasite expulsion. *Science (80-.).* **308,** 1463–1465 (2005).

262. Turner, J. E., Stockinger, B. & Helmby, H. IL-22 Mediates Goblet Cell Hyperplasia and Worm Expulsion in Intestinal Helminth Infection. *PLoS Pathog.* **9,** 1–7 (2013).

263. Maizels, R. M. *et al.* Immune modulation and modulators in Heligmosomoides polygyrus

infection. *Exp. Parasitol.* **132,** 76–89 (2012).

264. Morimoto, M. *et al.* Peripheral CD4 T Cells Rapidly Accumulate at the Host:Parasite Interface during an Inflammatory Th2 Memory Response. *J. Immunol.* **172,** 2424–2430 (2004).

265. Patel, N., Kreider, T., Urban, J. F. & Gause, W. C. Characterisation of effector mechanisms at the host:parasite interface during the immune response to tissue-dwelling intestinal nematode parasites. *Int. J. Parasitol.* **39,** 13–21 (2009).

266. Filbey, K. J. *et al.* Innate and adaptive type 2 immune cell responses in genetically controlled resistance to intestinal helminth infection. *Immunol. Cell Biol.* **92,** 436–448 (2014).

267. Reynolds, L. A. *et al.* MyD88 Signaling Inhibits Protective Immunity to the Gastrointestinal Helminth Parasite *Heligmosomoides polygyrus*. *J. Immunol.* **193,** 2984–2993 (2014).

268. Helmby, H. Human helminth therapy to treat inflammatory disorders- where do we stand? *BMC Immunology* **16,** (2015).

269. Clevers, H. The intestinal crypt, a prototype stem cell compartment. *Cell* **154,** 274–284 (2013).

270. Zhu, Y., Huang, Y. F., Kek, C. & Bulavin, D. V. Apoptosis differently affects lineage tracing of lgr5 and bmi1 intestinal stem cell populations. *Cell Stem Cell* **12,** 298–303 (2013).

271. Goodyear, A. W., Kumar, A., Dow, S. & Ryan, E. P. Optimization of murine small intestine leukocyte isolation for global immune phenotype analysis. *J. Immunol. Methods* **405,** 97–108 (2014).

272. Gregorieff, A. & Clevers, H. In situ hybridization to identify gut stem cells. *Curr. Protoc. Stem Cell Biol.* **2015,** 2F.1.1-2F.1.10 (2015).

273. Subramanian, A. *et al.* Gene set enrichment analysis: A knowledge-based approach for interpreting genome-wide expression profiles. *Proc. Natl. Acad. Sci.* **102,** 15545–15550 (2005).

274. Liberzon, A. *et al.* The Molecular Signatures Database Hallmark Gene Set Collection. *Cell Syst.* **1,** 417–425 (2015).

275. Mustata, R. C. *et al.* Identification of Lgr5-Independent Spheroid-Generating Progenitors of the Mouse Fetal Intestinal Epithelium. *Cell Rep.* **5,** 421–432 (2013).

276. Macosko, E. *et al.* Highly Parallel Genome-wide Expression Profiling of Individual Cells Using Nanoliter Droplets. *Cell* **161,** 1202–1214 (2015).

277. Satija, R., Farrell, J. A., Gennert, D., Schier, A. F. & Regev, A. Spatial reconstruction of single-cell gene expression data. *Nat. Biotechnol.* **33,** 495–502 (2015).

278. Halbritter, F., Vaidya, H. J. & Tomlinson, S. R. GeneProf: Analysis of high-throughput sequencing experiments. *Nature Methods* **9,** 7–8 (2012).

279. Ferguson, A. & Jarrett, E. E. Hypersensitivity reactions in small intestine. I Thymus dependence of experimental 'partial villous atrophy'. *Gut* **16,** 114–117 (1975).

280. Kamal, M., Dehlawi, M. S., Brunet, L. R. & Wakelin, D. Paneth and intermediate cell hyperplasia induced in mice by helminth infections. *Parasitology* **125,** 275–281 (2002).

281. Flanagan, K. *et al.* Intestinal Epithelial Cell Up-Regulation of LY6 Molecules during Colitis Results in Enhanced Chemokine Secretion. *J. Immunol.* **180,** 3874–3881 (2008).

282. Amulic, B., Cazalet, C., Hayes, G. L., Metzler, K. D. & Zychlinsky, A. Neutrophil Function: From Mechanisms to Disease. *Annu. Rev. Immunol.* **30,** 459–489 (2012).

283. Miura, N. *et al.* Anti-CD3 induces bi-phasic apoptosis in murine intestinal epithelial cells: Possible involvement of the Fas/Fas ligand system in different T cell compartments. *Int. Immunol.* **17,** 513–522 (2005).

284. Sollid, L. M. & Jabri, B. Triggers and drivers of autoimmunity: lessons from coeliac disease. *Nat. Rev. Immunol.* **13,** 294–302 (2013).

285. Zhou, P., Streutker, C., Borojevic, R., Wang, Y. & Croitoru, K. IL-10 modulates intestinal damage and epithelial cell apoptosis in T cell-mediated enteropathy. *Am. J. Physiol. Gastrointest. Liver Physiol.* **287,** G599-604 (2004).

286. Fordham, R. P. *et al.* Transplantation of Expanded Fetal Intestinal Progenitors Contributes to Colon Regeneration after Injury. *Cell Stem Cell* **13,** 734–744 (2013).

287. Asfaha, S. *et al.* Krt19+/Lgr5- Cells Are Radioresistant Cancer-Initiating Stem Cells in the Colon and Intestine. *Cell Stem Cell* **16,** 627–638 (2015).

288. Fernandez Vallone, V. *et al.* Trop2 marks transient gastric fetal epithelium and adult regenerating cells after epithelial damage. *Development* **143,** 1452–1463 (2016).

289. Gadye, L. *et al.* Injury Activates Transient Olfactory Stem Cell States with Diverse Lineage Capacities. *Cell Stem Cell* **21,** 775–790.e9 (2017).

290. Lin, B. *et al.* Injury Induces Endogenous Reprogramming and Dedifferentiation of Neuronal Progenitors to Multipotency. *Cell Stem Cell* **21,** 761–774.e5 (2017).

291. Yui, S. *et al.* YAP/TAZ-Dependent Reprogramming of Colonic Epithelium Links ECM Remodeling to Tissue Regeneration. *Cell Stem Cell* **22,** 35–49.e7 (2018).

292. Holmes, C. & Stanford, W. L. Concise Review: Stem Cell Antigen-1: Expression, Function, and Enigma. *Stem Cells* **25,** 1339–1347 (2007).

293. Allen, J. E. & Sutherland, T. E. Host protective roles of type 2 immunity: Parasite killing

and tissue repair, flip sides of the same coin. *Semin. Immunol.* **26,** 329–340 (2014).

294.   Clevers, H., Loh, K. M. & Nusse, R. An integral program for tissue renewal and regeneration: Wnt signaling and stem cell control. *Science (80-.).* **346,** (2014).

295.   Yu, S. *et al.* Paneth Cell Multipotency Induced by Notch Activation following Injury. *Cell Stem Cell* 1–14 (2018). doi:10.1016/j.stem.2018.05.002

296.   Rajagopal, J. & Stanger, B. Z. Plasticity in the Adult: How Should the Waddington Diagram Be Applied to Regenerating Tissues? *Dev. Cell* **36,** 133–137 (2016).

297.   Srivastava, D. & DeWitt, N. In Vivo Cellular Reprogramming: The Next Generation. *Cell* **166,** 1386–1396 (2016).

298.   Jopling, C., Boue, S. & Belmonte, J. C. I. Dedifferentiation, transdifferentiation and reprogramming: Three routes to regeneration. *Nat. Rev. Mol. Cell Biol.* **12,** 79–89 (2011).

299.   Nacu, E. & Tanaka, E. M. Limb Regeneration: A New Development? *Annu. Rev. Cell Dev. Biol.* **27,** 409–440 (2011).

300.   McCusker, C., Bryant, S. V. & Gardiner, D. M. The axolotl limb blastema: cellular and molecular mechanisms driving blastema formation and limb regeneration in tetrapods. *Regeneration* **2,** 54–71 (2015).

301.   Rompolas, P., Mesa, K. R. & Greco, V. Spatial organization within a niche as a determinant of stem-cell fate. *Nature* **502,** 513–518 (2013).

302.   Tata, P. R. *et al.* Dedifferentiation of committed epithelial cells into stem cells in vivo. *Nature* **503,** 218–223 (2013).

303.   Arthur-Farraj, P. J. *et al.* c-Jun Reprograms Schwann Cells of Injured Nerves to Generate a Repair Cell Essential for Regeneration. *Neuron* **75,** 633–647 (2012).

304.   Donati, G. *et al.* Wounding induces dedifferentiation of epidermal Gata6 + cells and

acquisition of stem cell properties. *Nat. Cell Biol.* **19,** 603–613 (2017).

305. Sato, T. *et al.* Long-term expansion of epithelial organoids from human colon, adenoma, adenocarcinoma, and Barrett's epithelium. *Gastroenterology* **141,** 1762–1772 (2011).

306. Sampson, L. L., Davis, A. K., Grogg, M. W. & Zheng, Y. MTOR disruption causes intestinal epithelial cell defects and intestinal atrophy postinjury in mice. *FASEB J.* **30,** 1263–1275 (2016).

307. Laplante, M. & Sabatini, D. M. MTOR signaling in growth control and disease. *Cell* **149,** 274–293 (2012).

308. Smyth, D. J. *et al.* TGF-β mimic proteins form an extended gene family in the murine parasite Heligmosomoides polygyrus. *Int. J. Parasitol.* (2018). doi:10.1016/j.ijpara.2017.12.004

309. Lahar, N. *et al.* Intestinal subepithelial myofibroblasts support in vitro and in vivo growth of human small intestinal epithelium. *PLoS One* **6,** 1–9 (2011).

310. Chiaramonte, M. G., Donaldson, D. D., Cheever, A. W. & Wynn, T. A. An IL-13 inhibitor blocks the development of hepatic fibrosis during a T-helper type 2-dominated inflammatory response. *J. Clin. Invest.* **104,** 777–785 (1999).

311. Ross, W. a & Couriel, D. Colonic graft-versus-host disease. *Curr. Opin. Gastroenterol.* **21,** 64–69 (2005).

312. Burisch, J. & Munkholm, P. Inflammatory bowel disease epidemiology. *Curr. Opin. Gastroenterol.* **29,** 357–362 (2013).

313. Shadad, A. K., Sullivan, F. J., Martin, J. D. & Egan, L. J. Gastrointestinal radiation injury: symptoms, risk factors and mechanisms. *World J. Gastroenterol.* **19,** 185–198 (2013).

Publishing Agreement

It is the policy of the University to encourage the distribution of all theses, dissertations, and manuscripts. Copies of all UCSF theses, dissertations, and manuscripts will be routed to the library via the Graduate Division. The library will make all theses, dissertations, and manuscripts accessible to the public and will preserve these to the best of their abilities, in perpetuity.

I hereby grant permission to the Graduate Division of the University of California, San Francisco to release copies of my thesis, dissertation, or manuscript to the Campus Library to provide access and preservation, in whole or in part, in perpetuity.

Author Signature _____ Date ___July 9, 2018___